Implications of Indian Summer Monsoon on various coupled air-sea processes in the North Indian Ocean

A thesis submitted during 2023 to the University of Hyderabad in partial fulfillment of the award of a Ph.D. degree in

Earth, Ocean and Atmospheric Sciences

By

Vikas Kumar Kushwaha (18ESPE04)



Under the supervision of

Prof. Karumuri Ashok

Centre for Earth, Ocean and Atmospheric Sciences,
School of Physics,
University of Hyderabad
(P.O.) Central University, Gachibowli,
Hyderabad – 500 046
Telangana

India

DECLARATION

I hereby declare that this thesis entitled "Implications of Indian Summer Monsoon on various

coupled air-sea processes in the North Indian Ocean" is the result of an investigation carried out

by me in the Centre for Earth, Ocean and Atmospheric Sciences, School of Physics, University of

Hyderabad under the guidance and supervision of Prof. Karumuri Ashok. This work is a bonafide

research work and free from plagiarism. I also declare that the thesis has not been submitted

previously in part or in full to this or any other University or Institution for the award of any degree

or diploma.

A report on the plagiarism statistics from the University of Hyderabad librarian is enclosed.

Place: University of Hyderabad, Hyderabad.

Date:

Vikas Kumar Kushwaha

Regd No.: 18ESPE04

CEOAS, School of Physics

University of Hyderabad

Gachibowli

Hyderabad, PIN-500046



This is to certify that the thesis entitled "Implications of Indian Summer Monsoon on various coupled air-sea processes in the North Indian Ocean" submitted by Mr. Vikas Kumar Kushwaha bearing Registration Number 18ESPE04 in partial fulfilment of the requirements for award of Doctor of Philosophy in the Centre for Earth, Ocean and Atmospheric Sciences (CEOAS), School of Physics, University of Hyderabad is a bonafide work carried out by him under my supervision. This thesis is free from Plagiarism and has not been submitted previously in part or in full to this or any other University or Institution for award of any degree or diploma.

Further, the student has the following publications before submission of the thesis for adjudication:

- 1. **Kushwaha, V.K.**, Kumar, S.P., Feba, F., Ashok, K. "Findlater jet induced summer monsoon memory in the Arabian Sea", Sci Rep 12, 13037 (2022). https://doi.org/10.1038/s41598-022-17025-1
- 2. **Kushwaha, V.K.**, Ashok, K., Feba, F., Lakshmi, R.S., Chatterjee, A., Kumar, S.P., "A modeling approach to ascertain the memory induced by Findlater Jet in the Arabian Sea" Under review in *Geophysical Research letters*
- 3. Feba, F., **Kushwaha, V.K.**, Ashok, K., "Impact of Indian Summer Monsoon on the post-monsoon Tropical Cyclones in the North Indian Ocean" Under review in *Climate Dynamics*

Conferences/Symposiums

- 1. **Kushwaha, V.K.**, Kumar, S.P., Feba, F., Ashok, K., *'Findlater jet induced summer monsoon memory in the Arabian Sea.'* International Geographical Union (IGU)- Union Geographique Internationale (UGI), Paris, France from 18 22 July 2022 (**Poster Presentation**)
- 2. **Kushwaha, V.K.**, Feba, F., Ashok, K., 'Impact of fresh water discharge into the Bay of Bengal on the monsoon onset' TERI NORCE Research School on Global Climate

Anomalies, Teleconnections and Regional Implications" at the TERI from 4-9 August, 2019. (Oral Presentation)

- 3. **Kushwaha, V.K.**, Kumar, S.P., Feba, F., Ashok, K., *'Findlater jet induced summer monsoon memory in the Arabian Sea.'* National Symposium TROPMET-2022 organised by the Indian Meteorological Society on "Advances in Weather and Climate Prediction and Climate Change Projection over South Asia: Applications in Water and Agriculture Sectors" from 29 November 02 December 2022 at the Indian Institute of Science Education and Research Bhopal (IISERB). (**Poster Presentation**)
- 4. Feba, F., **Kushwaha, V.K.,** Ashok, K., 'Impact of Indian Summer Monsoon on the post-monsoon Tropical Cyclones in the North Indian Ocean' National Ocean Workshop- 2018, 14-16 November, at INCOIS, Hyderabad. (**Poster Presentations**)

Further, the student has passed the following courses towards fulfilment of coursework requirement for Ph.D. :

Course Code	Course Name	Credits I	Pass/Fail
1. ES801	EARTH SYSTEM SCIENCES	4	Pass
2. ES805	RESEARCH METHODOLOGY	3	Pass
3. ES806	MATHEMATICS FOR EARTH SCIENCES	4	Pass
4. AP811	SPECIAL PAPER ON A SPECIFIED RESEARCH TOPIC	2	Pass
5. ES807	INTERDISCIPLINARY COURSE	4	Pass

Supervisor

Prof. KARUMURI ASHOK
Centre for Earth, Ocean & Atmospheric Sciences
University of Hyderabad
Hyderabad-500 046, INDIA.

Head

entre for Earth, Ocean & Atmospheric Sciences
University of Hyderabad
Hyderabad-500 046, INDIA
HoD, CEOAS

Dr. K.S.Krishna, FNA, FASc, FNASc Professor & Head Centre for Earth, Ocean and Atmospheric Sciences University of Hyderabad Hyderabad-500 046, Telangana. India Dean, Sop Dean

DEAN (L/C)
School of Physics
University of Hyderabac
HYDERABAD - 500 046

Contents

Acknowledgements	1
List of figures	iii
List of tables	\mathbf{v}
List of abbreviations	vi
Abstract	vii
Chapter 1 Introduction	1
1.1 Indian Monsoons	1
1.1.1 Indian Summer Monsoon	1
1.1.2 Indian Winter Monsoon	5
1.2 Surface forcing and its oceanic response in the tropical India ocean	6
1.2.1 Indian summer monsoon and the Arabian sea	7
1.2.2 Indian winter monsoon and the Arabian sea	8
1.2.3 Wave Propogation	9
1.3 Modelling Efforts	10
1.4 Tropical cyclones in the north Indian ocean	10
1.5 Ocean heat content and the Tropical cyclones	14
1.6 Aims and Objectives	14
Chapter 2 Data and Methods	16
2.1 Data	16
2.1.1 Gridded observational and reanalysis datasets	16
2.1.1.1 Precipitation dataset	16
2.1.1.2 Ocean Temperature and Sea Level Anomaly	17
2.1.1.3 Atmospheric Datasets	18
2.1.1.4 Cyclone Frequency Data	18
2.2 Statistical Methods	18
2.2.1 Statistical Composite Analysis	19
2.2.2 The Linear Correlation	19
2.2.3 Calculation of Statistical Significance	20
2.2.4 Analysis of Empirical Orthogonal Function (EOF)	21

2.3 Mathematical Expressions used in computing relevant Dynamical and physical	22
parameters	
2.3.1 Wind Stress Curl	22
2.3.2 Upper Ocean Heat Content	22
2.3.3 Cyclogenesis Potential	23
Chapter 3 Findlater jet induced Indian summer monsoon memory in the Arabian sea	24
3.1 Annual Cycle	24
3.1.1 Wind Forcing	24
3.1.2 Mixed Layer Depth	26
3.1.3 Upper Ocean Heat Content	29
3.1.4 Wave Propagation	31
3.2 Dynamics	32
3.3 Conclusion	39
Chapter 4 A modelling approach to ascertain the memory induced by Findlater jet in the	40
Arabian Sea	
4.1 Model simulations	40
4.1.1 Model Setup	40
4.1.2 Model Sensitivity Experiments	41
4.2 Validation of MOM5 output	43
4.3 Wind Forcing during ISM in two distinct years	45
4.4 Mixed layer depth during ISM in two distinct years	46
4.5 Difference of oceanic parameters between two distinct years	47
4.5.1 Mixed layer depth	47
4.5.2 Upper ocean heat content	49
4.5.3 Rossby wave	51
4.6 Conclusion	54
Chapter 5 Impact of Indian summer monsoon on the frequency of post-monsoon tropical	I
cyclones in the north Indian ocean	56
5.1 Tropical Cyclone frequency of the post-monsoon season in the NIO	56
5.2 The cyclogenesis parameters in the NIO	57
5.3 Cyclogenesis Potential in the Bay of Bengal	62
5.4 Conclusion	64

Chapter 6 Conclusions and Future Scope	65
6.1 Summary	65
6.2 Future Scope	68
References	70
Plagiarism Report	89

Acknowledgements

During my thesis work, I have been supported, encouraged, and motivated by many people. It is my pleasure to convey wholehearted gratitude to all of them.

This work would not have been possible without the support and guidance of individuals at the University of Hyderabad at Hyderabad. First and foremost, I am grateful to my supervisor **Prof. Karumuri Ashok**. His knowledge, motivation as a teacher, and integral view of high-quality research have made a deep impression on me. He has always motivated and taught me to work hard, think, critically evaluate my work, develop a scientific temperament, and the importance of using every opportunity. I am indebted to him for his patient guidance and support, which helped me to overcome difficulties throughout my Ph.D. work. I also want to thank my co-author **Dr. S. Prasanna Kumar**, Retd. Director, National Institute of Oceanography, Goa, for his continuous encouragement and support throughout my Ph.D. duration. I also acknowledge the contributions from my collaborators, **Dr. Abhisek Chatterjee and Dr. Lakshmi Shenoy**, for their technical help regarding modelling and use of data, and answering all my technical questions with patience.

I am grateful to my Ph.D. doctoral committee members, **Dr. S. Maqbool Ahmed**, Principal Scientific Officer and Head of Central Instruments Laboratory, UoH, **Dr. S. Sri Lakshmi**, Assistant Professor, CEOAS and **Dr. Vijay P. Kanawade**, Assistant Professor, CEOAS, UoH, for their valuable suggestions/comments, encouragement, and thought-provoking questions which greatly enhanced the quality of my research.

I am also grateful to **Prof. K. S. Krishna**, Head of the department, CEOAS, UoH, and former Head of the department, **Prof. M. Jayananda**, for the facilities made available to me for my research work. Thanks to **Prof. V. Chakravarthi** and **Prof. A. C. Narayana** for their constant encouragement since my master's days here at University. I also sincerely thank the other faculty of CEOAS, **Dr. T. Devleena Mani, Prof. Sreenivas** and **Dr. Aliba**, for their encouragement.

I gratefully acknowledge the Council of Scientific and Industrial Research and University Grants Commission National Eligibility Test for funding me during my Ph.D. I would also like to acknowledge the support from various funding agencies and coordinators of the conference/workshop I attended during my Ph.D.

I want to give special thanks to **Dr. Feba Francis**; my stay at the University of Hyderabad would not be possible without her. She was the one who always encouraged, motivated, and entertained me throughout my Ph.D. She gave me confidence and supported me during my worst phase. I always look forward to her as my mentor.

I thank my labmates and friends, **Dr. Charan Teja Tejavath**, **Dr. Hemadri Bhusan Amat**, **Dr. Sreejith**, **Mathew Sebastian**, **Dr. Stella**, **Dr. Abin Thomas**, **Dr. Yagnesh Raghava Yakkala**, **Dr. Boyaj Alugula**, **Dr. S. Bidyabati**, **Dr. D. Govardhan**, for sharing ideas, constructive criticisms, long scientific debates and discussions, and enjoying the Ph.D. days together at the CEOAS. Few of them actually helped me financially and emotionally during my Ph.D. I want to warmly thank all my other research scholars and non-teaching staff of the CEOAS. Apart from them, I also want to thank my childhood and Masters's friends, HPL and CCL University cricket league friends, and Basketball Cricket Teammates.

I also thank and acknowledge various data analysis tools, GrADS, ferret, NCL, CDO, NCO, and python. With these data analysis tools completing this was possible.

Finally, thanks go to my family; firstly to Mumma (Urmila Devi) and Papa (Laxman Prasad Singh), who always encouraged me to do well in life and their belief in me; to my eldest brother Naveen for letting me know I could find my way wherever and however I wished; to Anil for his encouragement and all the comic stories which he had narrated and made me laugh through all these years; to my sister Anita and for her discovery of my inner comic and also to my sister in law for sharing same kind of sense of madness with me. I want to dedicate this thesis to them.

Thank you,

Vikas Kumar Kushwaha

List of Figures

		Page No
Chapter 1		
Figure 1.1	Monthly means of rainfall over India	2
Figure 1.2	A Schematic representation of the Semi-permanent features	3
	of the Indian summer monsoon	
Figure 1.3	The interannual variability of the Indian summer rainfall	4
Figure 1.4	The number of depressions, cyclonic storms and severe	13
	cyclonic storms in the Bay of Bengal in post monsoon.	
Chapter 3		
Figure 3.1	Climatological mean zonal wind during June to September	25
	in the Arabian Sea.	
Figure 3.2	Vertical structure of monthly mean climatology of zonal wind	26
Figure 3.3	Annual cycle of climatology of WSC during (a) JJAS (b) ON,	27
	(c) DJF, and (d) MAM.	
Figure 3.4	Annual cycle of climatology of MLD during (a) JJAS (b) ON,	28
	(c) DJF, and (d) MAM.	
Figure 3.5	Annual cycle of climatology of UOHC during (a) JJAS (b) ON,	30
	(c) DJF, and (d) MAM.	
Figure 3.6	Hovmöller plot of climatology of monthly mean sea level anomaly	31
Figure 3.7	Correlation of WSC and UOHC in the Arabian Sea	32
Figure 3.8	(a) The PC 1 and (b) PC 2 of the EOF of the UOHC during ON	34
Figure 3.8	Correlation of WSC and WICR	35
Figure 3.8	Correlation of WICR and UOHC in the Arabian Sea	37

Chapter 4		
Figure 4.1	Climatology of MLD in MOM5 during (a) JJAS, (b) ON,	42
	(c) DJF and (d) MAM.	
Figure 4.2	Climatology of MLD in MOM5 during (a) JJAS, (b) ON,	43
	(c) DJF and (d) MAM.	
Figure 4.3	Climatology of MLD in MOM5 during (a) JJAS, (b) ON,	44
	(c) DJF and (d) MAM.	
Figure 4.4	Climatology of MLD in MOM5 during (a) JJAS, (b) ON,	45
	(c) DJF and (d) MAM.	
Figure 4.5	Wind stress curl in MOM5 during a) 1988, b) 2002	46
Figure 4.6	Difference in MLD between 1998 and 2002 during (a) JJAS,	48
	(b) ON, (c) DJF and (d) MAM.	
Figure 4.7	Difference in UOHC between 1998 and 2002 during (a) JJAS,	50
	(b) ON, (c) DJF and (d) MAM.	
Figure 4.8	Time Series of dUOHC averaged over the box	51
Figure 4.9	Hovmöller plot of D_{20} isotherm during a) 1988, b) 2002	52
Figure 4.10	Difference in UOHC between 1998 and 2002 during (a) JJAS,	53
	(b) ON, (c) DJF and (d) MAM in SODA datasets.	
Figure 4.11	Difference in UOHC between 1994 and 2014 during (a) JJAS,	54
	(b) ON, (c) DJF and (d) MAM in SODA datasets.	
Chapter 5		
Figure 5.1	Composites of vertical shear of winds during ON for drought years,	58
	flood years and their differences in columns respectively	

Figure 5.2	Composites of SST during ON for a) drought years, b) flood years,	59
	and c) all years	
Figure 5.3	Composites of TCHP during ON for a) drought years, b) flood years,	60
	and c) all years	
Figure 5.4	Composites of anomalous vorticity during ON for drought years,	61
	flood years and their differences in columns respectively.	
Figure 5.5	Composites of mid-tropospheric humidity during ON for drought years,	61
	flood years and their differences in columns respectively.	
Figure 5.6	Composites of Potential temperature during ON for drought years,	62
	flood years and their differences in columns respectively.	
Figure 5.7	Cyclogenesis Potential Parameter (GPP) over NIO during flood	63
	and drought year	

List of Tables

Chapter 2

Table 5.1 The frequency of TCs in the North Indian Ocean during ON 57 over the period 130 years from 1891 to 2021.

Abbreviations

AISMR All India Summer Monsoon Rainfall

ISM Indian Summer Monsoon

WM Indian Winter Monsoon

AS Arabian Sea

BoB Bay of Bengal

NIO North Indian Ocean

ENSO El Niño Southern Oscillation

DJF December, January, February

MAM March, April and May

Hadley Centre Sea Ice and Sea Surface Temperature dataset

IMD India Meteorological Department

IOD Indian Ocean Dipole

ITCZ Inter-Tropical Convergence Zone

JJAS June, July, August and September

MOM5 Modular Ocean Model, Version 5

ON October and November

SLA Sea-level Anomaly

SODA Simple Ocean Data Assimilation Reanalysis 3.1.1 dataset

UOHC Upper Ocean Heat content

SST Sea Surface Temperature

MLD Mixed Layer Depth

WICR West Indian coastal rainfall

Abstract

By analyzing various observations-based and reanalysis gridded data sets primarily for the 1980-2015 period, we show that a cross-equatorial low-level wind over the Arabian Sea (AS) during the summer monsoon (June to September), known as Findlater Jet (FJ), modulates the thermocline in the Arabian Sea (AS). Our analysis shows that the FJ signal gets 'trapped' in the AS in the form of upper ocean heat content till the following winter months (December to February). This 'memory' is apparently a consequence of the combined effect of FJ-induced wind stress curl and the annual downwelling Rossby waves in the AS. Briefly, during the summer monsoon months, the strong low-level westerly winds cause a negative wind stress curl in the south of the FJ axis over the central AS, resulting in a deep thermocline and a high magnitude of heat being trapped. In winter monsoon months, though the wind stress curl is positive over large parts of the AS and thus expected to shoal the thermocline and reduce the upper ocean heat content in the central AS, this does not happen due to two reasons. Firstly, winds are weaker and spread over a larger area over the AS, making the magnitude of the wind stress curl low. Secondly, the westward propagating downwelling Rossby wave radiated from the eastern AS deepens the thermocline and prevents ventilation of the trapped heat. During the following spring, the collapse of the Rossby waves leads to the shoaling and mixing of underlying waters with surface waters, thereby resurfacing the trapped heat. The resurfacing of the trapped heat makes the AS a memory bank of the FJ-induced signal. To ascertain the above-proposed mechanism, we have carried out several sensitivity experiments with an ocean model. The experiments differ only in the monsoon wind forcing, mimicking strong and weak monsoonal seasonal atmospheric circulation over different years. From the differences between the good and bad monsoon years in the simulated mixed layer depth (dMLD) and upper ocean heat content (dUOHC), we show that these parameters are positive in the southern AS due to an increase in the strength of FJ-induced wind stress curl in the southern AS during the good summer monsoon. This results in a deeper thermocline, and increased heat

retention in the following fall through spring seasons due to inherent seasonality. The simulations confirm the proposed mechanisms.

Tropical Cyclones (TCs) in the North Indian Ocean (NIO) are modulated by several factors. By examining Gray's parameters for cyclogenesis, we show that the frequency of TCs during the Post-Monsoon (ON) is increased in the Bay of Bengal and AS after a good monsoon. Moreover, a deficit rainfall leads to a decrease in the frequency of TCs in the BoB but a slight increase in the AS. My analysis shows that the consequence of the combined effect of several Sikka-Gray parameters. Specifically, during the drought year, the mid-tropospheric humidity, low-level vorticity, and Tropical Cyclone Heat Potential (TCHP) are lower than in normal years, and the vertical shear is higher over most of the NIO. These factors lead to the reduced cyclonic frequency in the BoB and vice versa. Whereas, for the AS, the TCHP and low-level vorticity are slightly higher in the southeastern AS, contributing to a slight increase of cyclones even in the drought years.

Chapter 1

Introduction

The Indian Ocean is a dynamically and physically complex basin. The key feature that makes the Indian Ocean so unique is the seasonal reversal of winds and currents caused by the monsoons (Schott & McCreary, 2001). The Indian monsoon system is a strongly coupled air-sea-land system consisting of two monsoons, the winter monsoon that occurs from December to February (DJF) and the southwest monsoon that occurs during June to September (JJAS) over the Indian continent. These monsoons dominate Indian Ocean dynamics, especially in the northern Indian Ocean (Schott & McCreary, 2001).

1.1 Indian Monsoons

1.1.1 Indian Summer Monsoon

Sailors and traders have travelled through the Arabian Sea for many years with a thorough knowledge of the seasonal reversal of winds (Rawlinson et al., 1916). The Arabic name for "season" mausam, which eventually became known as the monsoon, was used to describe this seasonal reversal that was accompanied by precipitation. The contrast between continents and seas is reflected in the monsoon's overall features and regional variations. As a result of the difference in temperature between land and water, the ocean-land pressure difference develops. Wind seasonality in conjunction with heavy precipitation provides the solution to this discrepancy (Ramage, 1971; Rao, 1976).

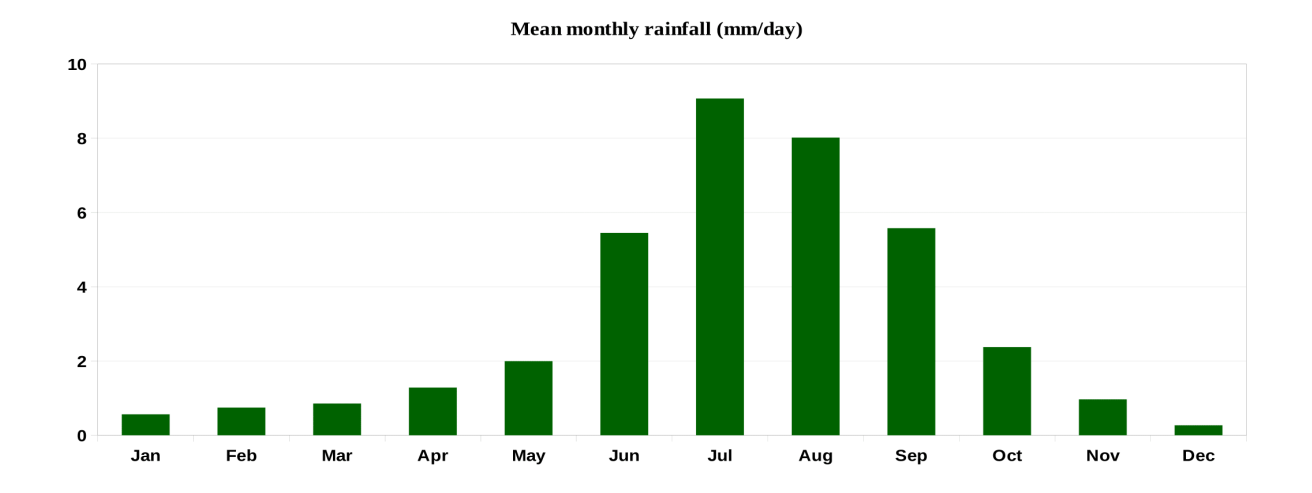


Figure 1.1: Monthly climatology of all India rainfall for the 1901-2019 period.

The Indian Summer Monsoon (ISM), also known as the southwest monsoon, is a prominent oceanatmospheric phenomenon characterized by organized southwesterly winds and enhanced rainfall
that becomes active from June to September. It affects the livelihood of the people of the Indian
subcontinent. The ISM accounts for 70% of annual precipitation over India (Figure 1.1) and 60% of
agriculture sector jobs (Webster, 1998; Gadgil et al., 2006; Ashok et al., 2022). ISM winds reach
mainland India from two sides. In the pre-monsoon season of March-May, a cross equatorial
pressure difference develops from the Mascarene to the Indian subcontinent. This pressure gradient
ensues due to the thermal contrast caused by the differential temperature gradient between land and
sea. In these months, trade winds flowing along the equatorial Indian Ocean blow from the Somali
coast as southwesterly winds towards India due to pressure gradients. On June 1, this southwesterly
portion of ISM winds, with standard deviations of eight to nine days, reached the Indian
subcontinent around the Kerala coast (IMD, 1943; Joseph et al., 1994). After then, India
experiences a four-month rainy season that lasts until September.

Meanwhile, the easterly component of summer monsoon winds reach the Andaman and Nicobar Islands on May 20 and then encompasses the whole Bay of Bengal. The ISM moves rapidly in a

north-south direction till around 23 0N after the onset of ISM over the Kerala coast. Above 23 ^oN, the ISM progresses around the monsoon trough and then flows from southeast to southwest. In summary, within twenty days of onset, the ISM reaches most of the Indian subcontinent (Figure not shown). The ISM is maintained once it has been established by the release of latent heat by its own water vapour. Potential energy creates a heat source in the mid atmosphere and sustains the pressure gradient as the Indian subcontinent land starts to cool down (Webster et al., 1998; Goswami et al., 2017; Gadgil et al., 2018).

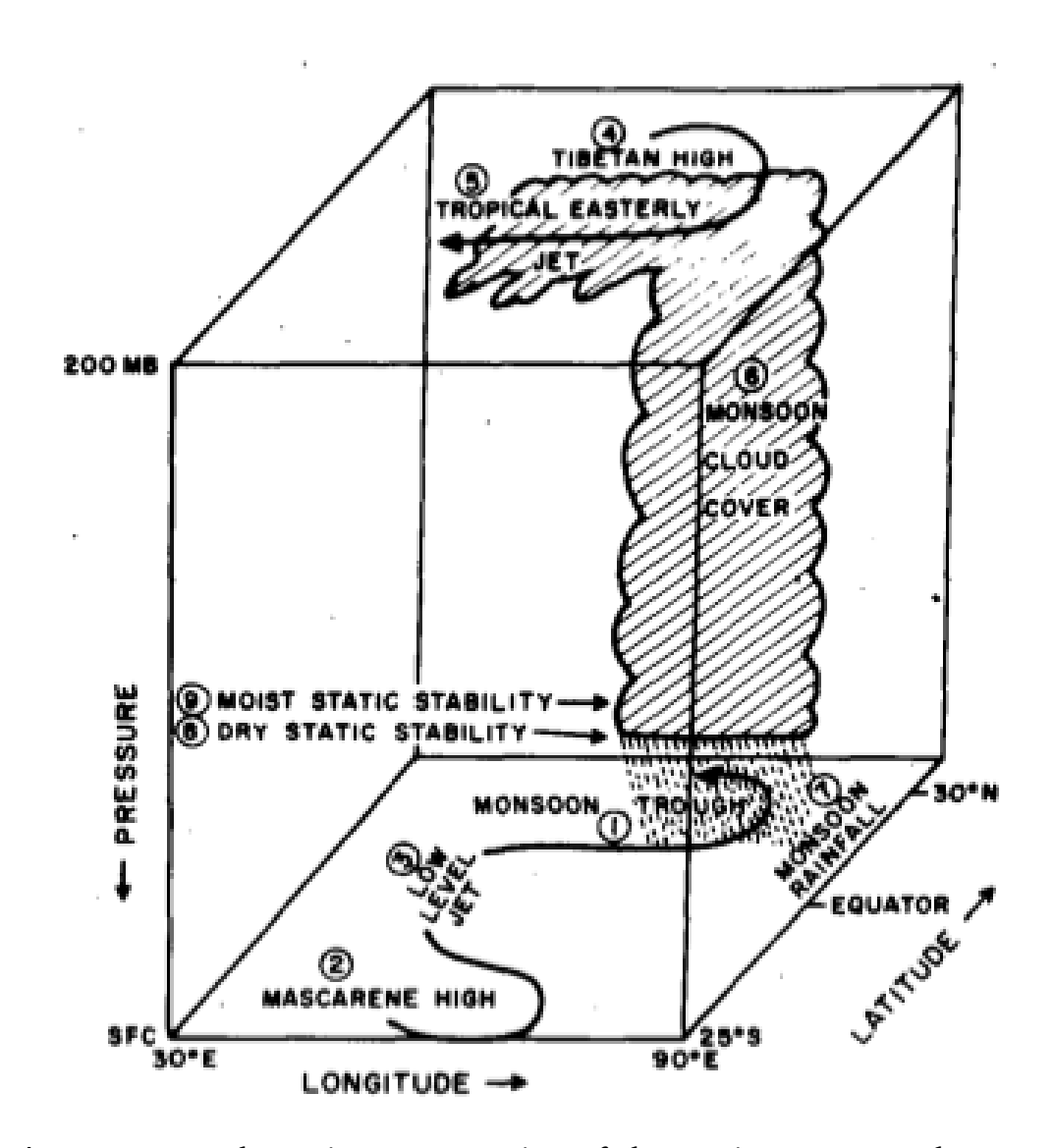


Figure 1.2: A schematic representation of the semi permanent characteristics of the ISM taken from Krishnamurti and Bhalme, (1976).

Dynamic ISM systems have some semi-permanent characteristic patterns. They exist at different locations and intensities on different scales during the summer monsoon season. The distinctive topographical and geological aspects of the land determine these coherent patterns. The primary semi-permanent components of the ISM include the Mascarene High, Monsoon Trough, Low-Level Jet, Tibetan High, Heat Low, and Tropical Easterly Jet. Figure 1.2 shows a schematic representation of these characteristics (Krishnamurthy & Bhalme, 1976).

The variability of each feature influences and is closely related to the spatial and temporal distribution of monsoon circulation strength and precipitation. The intraseasonal to interannual fluctuation in ISM is linked to the variability of these features. See monsoon monograph series, Rao, (1976), and Pant and Kumar, (1997) for further information (Tyagi et al., 2012).

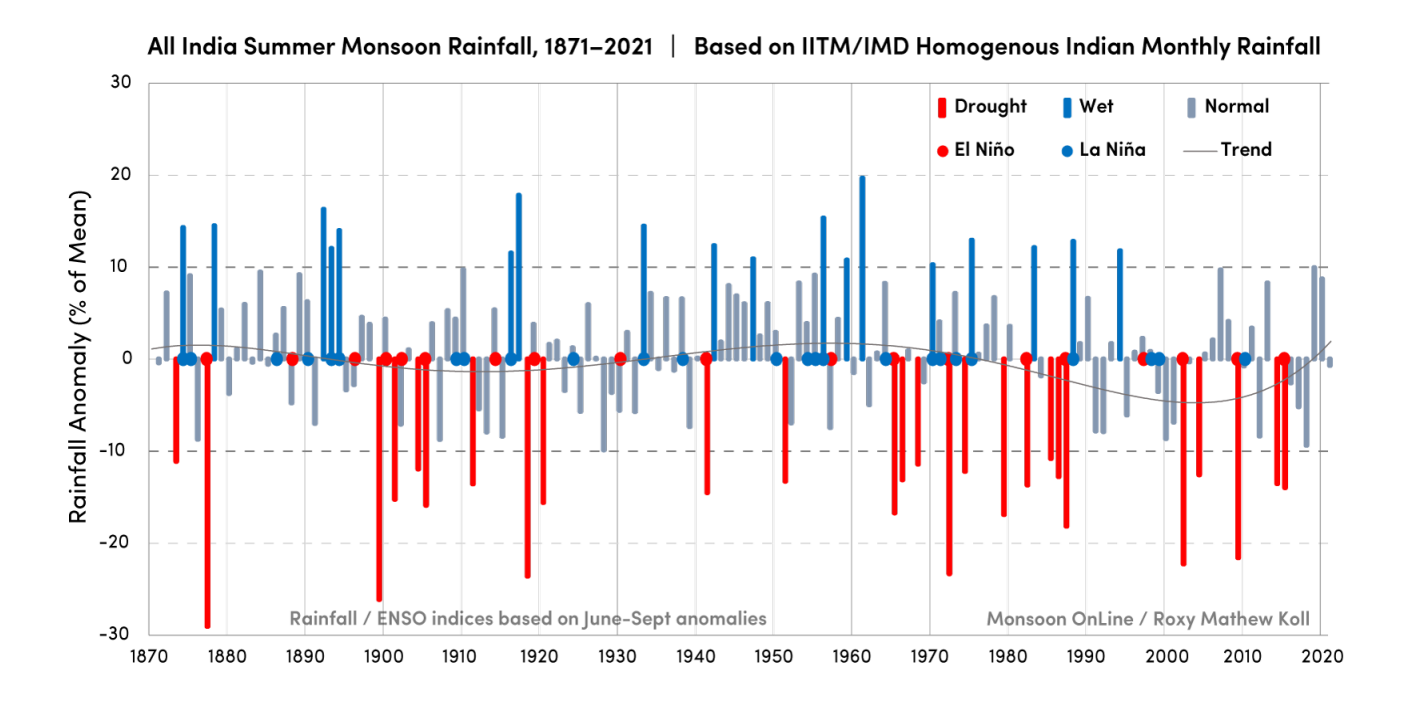


Figure 1.3: Interannual variations of all India ISM rainfall during the 1871-2021 period. (Source- https://mol.tropmet.res.in/monsoon-interannual-timeseries/)

Though the interannual variability (Figure 1.3) in the ISM rainfall is small, with a standard deviation of about 10%, it can severely affect the economy of this region which is primarily based on rain-fed agriculture and industry based on agriculture. Understanding the effects of environmental change on ISM rainfall and its spatial patterns present a crucial research challenge with huge ramifications on water resources and management policies. It is also known that the ISM impacts the dynamics and biogeochemistry of the surrounding water bodies, the Arabian Sea (AS) and the Bay of Bengal (BoB), making their regional oceanography contrastingly different (Prasanna Kumar et al., 2009).

1.1.2 Indian Winter Monsoon

The other important part of the seasonally changing system which impact the Indian subcontinent is the Indian winter monsoon (WM). During boreal winter, the pressure gradient is reversed relative to that during the ISM. The monsoonal winds connect the tropics to higher northern latitudes, and from the Siberian High the cold air masses travel southward (Wang et al. 2003, 2012). On the other hand, during this season, due to the movement of the subtropical Jetstream equatorward as compared to summer, the Western Disturbance (WD) transports water from the Mediterranean to Central Asia, feeding rivers and glaciers in northern India (Dimri et al. 2015 and refs.). The winter precipitation gradient increases from the southern thar desert to the northwestern Himalayas. It also contributes significantly to mean annual rainfall in the Himalayan region (Dimri, 2013) and southern India (Bhanu Kumar et al., 2004). In addition, the Arabian Sea winter temperatures are suggested to be with subsequent ISM precipitation (Clark et al., 2000). Also, the hydrography of the surface water is related with evaporative cooling, convective deepening of the mixed layer, and the nutrient influx into the photic zone in the northeastern AS (Prasanna Kumar & Prasad, 1999; Barber et al., 2001), which are associated with cold and dry WM winds.

To understand the response of these monsoon system on the ocean circulations in the north Indian ocean, we need to understand how and what forcing mechanisms are driving the upper oceans.

1.2 Surface forcing and its oceanic response in the tropical India ocean

The dynamic response of the North Indian Ocean (NIO) to the seasonally reversing monsoon winds is one of the most explored components of the NIO (Lighthill et al., 1969; Hsiung, 1985; Schott et al., 2002; Schott et al., 2004, 2009; Miyama et al., 2003; Horii et al., 2013). Numerous observational and modelling studies, such as those by Schott et al. (2001), Wiggert et al. (2002), McCreary et al. (1996), and Winguth et al. (1994) have concentrated not only on the dynamics of monsoon circulations but also on the biogeochemistry, thermodynamics and the ecosystem of the NIO. The role of tropical Indian ocean in the variability of monsoon has been a hot topic since early studies, but no agreement has been reached (Annamalai et al., 2004, Shukla et al., 1977, Weare et al., 1979). The NIO surface warming in recent decades also raises questions about NIO's response caused from anthropogenic activity and its influence on climate variability globally (Charles et al., 1997; Levitus et al., 2000; Giannini et al., 2003; Hoerling & Kumar, 2003). Although the role of NIO sea surface temperature (SST) in the variability of the monsoon perhaps to be not well understood, the Arabian Sea response to the variability of the monsoon due to increased surface cooling during the strong monsoons is relatively well understood (Shukla & Misra, 1977; Weare, 1979). Meteorologists suspected increased evaporative cooling due to stronger southwesterly, but oceanographers have often conjured up more increased inshore and offshore upwellings along the Arabian Peninsula (Jung et al., 2002; Altabet et al., 2002; Anderson et al., 2002; Ivanochko et al., 2005). Several studies have focused on the effect of the strength of the southwesterly on the AS cooling and argued that the southwesterly strength is more critical than the precipitation over the

Indian subcontinent (e.g., Duing and Leetma, 1980; Molinari et al., 1986; McCreary & Kundu, 1989; Vinaychandran et al., 2004).

1.2.1 Indian summer monsoon and the Arabian sea

The cross-equatorial atmospheric flow (south-westerlies) from the East African coast towards India develops by the end of May, intensifies into a low-level jet during July, and collapses by the end of September (Joseph et al., 1966; Anderson et al., 1976). This low-level atmospheric jet, known as Findlater Jet (FJ) (Findlater, (1969)), attains a speed as high as 100 knots near the East African coast (Hoskins et al., 1995; Boos et al., 2009). The axis of the FJ is represented by the region of maximum wind speed at the height of 850 millibars (hPa) (shown in Figure `1.3) and extends from the Horn of Africa to the coast of Gujarat in India. The FJ plays a vital role in the spatiotemporal variability of the ISM rainfall. For example, Webster et al. (1998) and Pushpanjali et al. (2013) found that the SM rainfall positively correlates with the strength of FJ. In general, strong FJs are associated with more active spells of ISM rainfall, while weak FJs are associated with breaks in the rainfall. The characteristics of the FJ and its variability range from diurnal (Ardanuy, 1979; Nair et al., 2014), intraseasonal (Joseph et al., 2004; Pushpanjali et al., 2020), and interannual time (Pushpanjali et al., 2010; Narayanan et al., 2016; Vizy et al., 2020) scales have been well-researched. There are also studies on the long-term trends of FJ (Archer et al., 2008; Iqbal et al., 2017).

It is known that the FJ has some influence on the upper ocean through wind stress. During the ISM season, the cyclonic wind stress curl north of the axis of the FJ induces local Ekman suction and open-ocean upwelling, while the anticyclone wind stress south of the axis leads to Ekman pumping and open ocean downwelling there (Bauer et al., 1991; Prasanna Kumar et al., 2001). This results in

the modulation of mixed layer depth on either side of the axis of the FJ (McCreary et al., 1993; Weller et al., 2002; Prasanna Kumar et al., 2005). Murtugude et al. (2007) found that the stronger FJ intensified coastal upwelling, crediting the interpretation of paleo records collected in coastal and coastal caves. However, the processes in the open Arabian Sea are likely to be more complicated. Stronger FJ are associated with positive wind stress curl and negative wind stress curl, therefore leading to deeper thermoclines, but stronger in magnitude winds also results to a deep mixed layer and the cooling by entrainment (Bauer et al., 1991; Prasanna Kumar et al., 2001). Subsequently, the total heat transport to the ocean from the atmosphere is increased, indicating that the ocean firmly controls the air-sea interaction. Ekman pumping related to the stronger FJ leads to convergence and surface warming (Weller et al., 2002). However, the mixed layer deepening in the central AS is marked by increased entrainment and cooler water convergence. Warming occured due to convergence can be observed deep in the thermocline below about 100m (Murtugude et al., 2007).

1.2.2 Indian winter monsoon and the Arabian sea

During the boreal winter, the southern Indian ocean heats as the Eurasian continent cools. The ensuing higher surface pressure in the region of Arabian Peninsula and lower surface pressure below the Intertropical Convergence Zone at around 10 °S causes the Indian Winter Monsoon, which is marked by northeasterly surface winds in the AS. WM is known to have a profound influence on the NIO biogeochemistry and its ecosystems (e.g., Smith & Madhupratap, 2005). Due to the cold, dry air flowing off the continent, substantial evaporative heat loss occurs in the atmosphere of the northern AS. This, along with mechanical agitation from northeasterly surface winds, leads to the mixed layer to deepening, resulting in winter blooms in the northern part of the Arabian sea (Banse & McClain, 1986; Madhupratap et al., 1996; Morrison et al., 1999). This bloom adds considerably to AS's overall annual primary production (Madhupratap et al., 1996; Marra et al., 2005) and it starts when ocean conditions in the winter are more supportive for fishing activities

as compare to the summer, resulting a large amount of fish catches (Madhupratap et al., 2001). Moreover, during WM, the northeast monsoon current (NMC) turns north at 70 0E into the West Indian Coastal Current after flowing westward into the South India Basin. A Lakshadweep eddy, a large anticyclone (Shetye et al., 1998), emerges offshore from MNC and off the western tip of India. Drifter climatology also indicates a branch of the NMC leading westward, as previously reported by Molinari et al. (1990). On the western boundary, the Somalia Current (SC) flows southward between latitudes 10 °N and 3 °S and flows into the eastern South Equatorial Counter Current (SECC). As already shown in the model study by McCreary et al. (1993), in particle trajectory modeling studies (Song et al., 2004), and also in the SODA-POP 2.0.3 reanalysis, the SECC is a year-round feature, except that it is subsurface during the summer monsoon and overlying westward ones Ekman currents is obscured. The NMC flows west through the basin during this season, carrying fresher water from the Bay of Bengal to the Arabian Sea. Water from the Bay of Bengal was also transported across the equator into the eastern basin this season, as model studies have already reported (Han & McCreary, 2001; Jensen, 2003).

1.2.3 Wave Propogation

There is a cyclonic circulation between latitudes 5 °N and 10 °N in the AS adjacent to the boundary of the Indian subcontinent (Chelton et al., 1998). It appears to be fed by water from the NMC, which then flows into the Somali Current and eventually crosses the equator. During the WM, though the north-easterly winds are weak, the convective cooling and associated mixing deepen the mixed layer in the northern AS. The other dominant factor influencing the upper ocean, including the mixed layer in the AS, is the annual Rossby waves (Prasanna Kumar et al., 2005; Brandt et al., 2002; Jury et al., 2004). They are the dominating patterns of sea surface height (SSH) variability, especially all through the inter-monsoon period. The westward propagation of first and second-

mode annual Rossby waves explains 87% of the seasonal, mid-basin hydrographic variance below 100 m along 8°N (Brandt et al., 2002).

1.3 Modelling Efforts

The fundamental characteristics and response of significant ocean currents and temperature fluctuations are captured by Arabian Sea and north Indian ocean circulation predictive models using the monthly average climate force fields (McCreary et al., 1993; Bruce et al., 1998; Murtugudde et al., 1998; Chirokova & Webster, 2006; Pérez-Hernández et al., 2012; Rao et al., 2016). Several modeling studies mainly focus on heat transport and meridional overturning circulation in the Indian Ocean (Garternicht et al., 1997; Wacogne et al., 1996; Pérez-Hernández et al., 2012; Rao et al., 2016; Lee et al., 1997; Lee et al., 1998; Naguraet al., 2008, 2010a, 2010b). In every case, the southward annual mean of the Ekman drift at the surface in the NIO is driven by strong ISM winds and is the essential part of the north-south heat fluxes. This southward warm water transport is replaced by upwelled water by a shallow northward flow in the thermocline of the NIO.

There are also modeling studies by (Keen et al., 1997; Young et al., 1994) which indicated that offshore upwelling advection is major process in the AS and contributes considerably to primary productivity in the central AS. However, no study has used the ocean model to capture the signal induced by ISM winds in the AS.

1.4 Tropical cyclones in the north Indian ocean

The genesis of tropical cyclones (TCs) mainly occurs in the oceanic regions where the sea surface temperature (SST) is above 26 °C, the vertical wind shear is low, and the mid-tropospheric humidity is high (Gray & Sikka, 1968). TCs activity get fueled through the transfer of latent heat fluxes and

sensible heat fluxes from the ocean (Emanuel, 1986; Ooyama, 1969; Vinod et al., 2014). The atmospheric boundary layer becomes more moistened as a result of the increase fluxes of latent heat from ocean to atmosphere, which favourably affects cyclogenesis and subsequent intensification (Gao & Chiu, 2010; Gao et al., 2016; Gao et al., 2019; ; Jaimes et al., 2015; Lin et al., 2014). SST modulates the ocean-atmosphere heat transport in two different ways. The intensity of TCs increases along with the increased SST, which enhances heat transport to the atmosphere from the ocean. Contrarily, when cyclones move over the ocean, SST drops, which slows down the transfer of heat between the ocean and atmosphere and reduces the strength of TCs (DeMaria et al., 1999; Cione et al., 2003; Lloyd et al., 2011). The size and structure of cyclones are negatively impacted by the cooling caused by ocean cyclones (Chen et al., 2010; Ma et al., 2013; Zhu et al., 2004). Previous research has shown the influence of ocean-cyclone interaction mechanisms on the propagation of TCs (Jullien et al., 2014; Subrahmanyam et al., 2005; Ogata et al., 2015).

TCs in the oceans depends on various ocean-atmosphere interaction processes, which depend on the seasonal variation of SSTs, Mixed Layer depth, Barrier layer depth, and salinity. The north Indian Ocean (NIO) has a substantial seasonal variation in all the above parameters. During the premonsoon months, the SST throughout the NIO is around 29- 30 °C. Whereas during the post monsoon (ON), the sea surface temperature is around 1 °C lesser. The salinity in the BoB also goes through seasonal variation. In the ON season, the salinity in the northwest BoB is very low compared to southwest BoB (Rao & Sivakumar, 2003). This decrease in salinity in the northwest BoB is primarily because of the precipitation over the oceans and the large amount of river influx in the ON season (Akhil et al., 2014; Sengupta et al., 2006; Shenoi, 2002; Chaitanya et al., 2014; v Shetye et al., 1996). The influx of freshwater in the northwest BoB leads to strong stratification, and the mixed layer becomes shallower, which in turn results in the formation of a strong barrier layer in the post-monsoon. The seasonal variability of the barrier layer is absent in the Arabian sea.

Moreover, the seasonal variation of the MLD is larger in the AS (Babu et al., 2004; Shenoi et al., 2002; Prasad et al., 2004; Narvekar et al., 2006). However, the seasonal variation of the MLD in the northwest BoB is little due to the presence of stratification, but it varies strongly in southern BoB. All these oceanic characteristics considerably impact the ocean-cyclones interaction in the NIO.

NIO accounts for 6% of all TCs worldwide (Neumann, 1993; Ali, 1999). Even though NIO is having comparatively lower frequency of TCs, this region is responsible for 80% of all fatalities from TCs worldwide, mainly due to storm surges (Beal et al., 2020). The BoB basin accounts for 4%, while the remaining 2% occurs in the AS (Alam et al., 2003). In NIO, the cyclone has two seasons a year, i.e., pre-monsoon (April- early June) and post-monsoon (October- December). These two TCs seasons are separated by the ISM season. Though the ISM separates the two cyclone seasons, very little has been studied about their possible association. So far, no study has indicated an association between ISM and the subsequent post-monsoon cyclonic activity. Nor has any study found any relation between ISM and post-monsoon BoB cyclones. Considering that the ISM and the cyclonic seasons are adjacent, it seems plausible that there could be a connection.

In addition to local ocean-cyclone interactions, cyclone frequency and intensity in the NIO are also influenced by interannual temporal changes in large-scale air-sea conditions such as El Niño Southern Oscillation (ENSO). Girishkumar et al. (2012) and Girishkumar et al. (2014) show the effect of ENSO on TCs in the ON season in BoB. They reported that the TCs are much more frequent during La Niña years as compare to the El Niño years. This is a result of the favourable atmospheric conditions brought on by La Niña, which include anomalously high relative humidity, anomalously low wind shear, and high relative vorticity in the BoB (Ng et al., 2012; Felton et al., 2013; Bhardwaj et al., 2019). The TCs frequency in NIO is also significantly effected by Indian Ocean Dipole (IOD) apart from ENSO (Yuan et al., 2013; Li et al., 2016). In negative IOD years, an

anomalous warm SST over tropical eastern India and conditions like high relative vorticity and increase in relative humidity in NIO atmosphere creates ideal conditions for TCs genesis in the BoB (Mahala et al., 2015; Li et al., 2016). A recent study by Roose et al. (2022) found that the influence of ENSO on the BoB TCs is limited to within the lower latitudes (5-10 °N latitudes). However, we found that the frequency of cyclones is much more above 10 °N (Figure 1.4) and indicates another factor at play besides ENSO. Therefore, we explore the post-monsoon TCs frequency in the BoB and the AS and the possible effects of ISM on it.

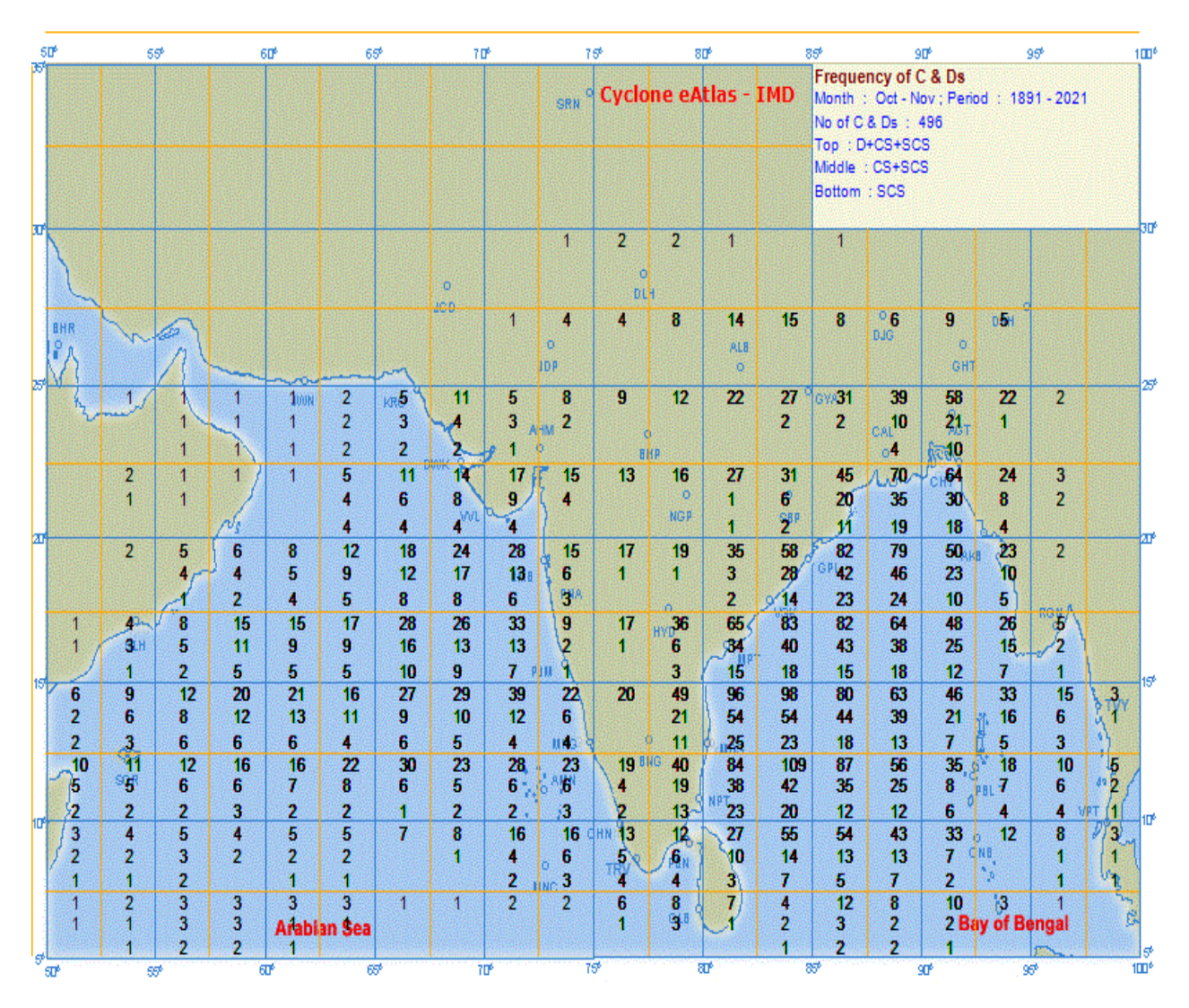


Figure 1.4: The number of depressions (D), cyclonic storms (CS) and severe cyclonic storms (SCS) in the Bay of Bengal for the period 1891 2021 during the post-monsoon season (October-November). (Source- IMD Cyclone eAtlas).

1.5 Ocean heat content and the Tropical cyclones

The intensity of TCs in the NIO is not only determined by the SST but also by the increase in the oceant heat and warm ocean subsurface. The upper ocean heat content (UOHC) is one of the important parameters and plays important part in controlling the intensity of the TCs along with the SSTs (Balaguru et al., 2013; Hallam et al., 2021; Wada et al., 2007; Trenberth et al., 2018;). A high UOHC indicates a warmer ocean surface, and the continuous influx of fluxes of latent and the sensible heat deriving out of the ocean supports or intensifies the TCs (Shay et al., 2000). In the two basins (i.e AS and BoB), the UOHC affects the cyclone's intensity differently in post and pre monsoon seasons (Vissa et al., 2013a). The UOHC difference between the two TCs seasons can be attributed to the differential average wind speed, barrier layer thickness, and the relative humidity in the two seasons. Studies have also quantified the effect of the Kelvin and Rossby waves propagation on UOHC in the NIO (Chowdhury et al., 2020b). However, we are not aware of any studies which have considered the effect of ISM on the UOHC in the post-monsoon season and its impact on tropical cyclones in the north Indian ocean.

1.6 Aims and Objectives

Though various studies focused on understanding the dynamics of circulation in the north Indian Ocean during different seasons (Shetye et al., 1998; Schott et al., 2001). However, the impact of FJ on the modulation of the upper waters in the AS during the ISM months has not been thoroughly studied (Bauer et al., 1991; Prasanna Kumar et al., 2001). Notably, no study has so far examined the impact of the FJ on the subsurface heat content in the AS beyond the ISM months during the seasons after the ISM. Also, the influence of ISM rainfall on the post-monsoon tropical cyclones in the NIO needs to be further studied and explored. This thesis is an endeavor to address these gaps. Therefore, I set the objectives of this thesis as follows:

- 1 To study the response of the Arabian sea to the Findlater Jet, and understand the dynamics behind the influence of Findlater Jet
- 2 A Modeling approach to ascertain the response of the Arabian Sea due to the influence of the Findlater Jet.
- 3 To study the impact of the Indian summer monsoon on the tropical cyclones during the postmonsoon in the north Indian ocean.

This entire thesis, including this introduction, is divided into six chapters. The data sources and methods are described in detail in Chapter 2. In Chapter 3, I present my findings of FJ-induced memory in the AS. The results of the modeling analysis of FJ impact in the AS are presented in Chapter 4. Chapter 5 shows the results of the impact of ISM on post-monsoon TCs. The last chapter, Chapter 6, provides a summary of the whole work as well as a brief outline of the scope of future study.

Chapter 2

Data and Methods

2.1 Data

In this thesis, I have reported results from the analysis of several aspects of ocean-atmospheric interaction processes in the north Indian ocean. The results presented in this work are based on analyses of various datasets covering different and well-defined time periods, as necessary. The non-uniformity of time periods is mainly owing to the limitations of the data availability. However, to avoid confusion, we have presented the results with explicit mention of the time period. Importantly, each analysis related to a particular aspect is carried out using multiple datasets covering a congruent period. Here, I'll be outlining the data sources and the statistical and data processing methods that were applied to the data.

2.1.1 Gridded observational and reanalysis datasets

2.1.1 Precipitation dataset

I used a gridded daily precipitation dataset with a longitude by latitude resolution of $0.25^{\circ} \times 0.25^{\circ}$ produced by the Indian Meteorological Department (IMD) (Pai et al., 2014) over the 1980-2021 period. This precipitation dataset was created using precipitation measurements from a network of 6995 rain gauge stations across 36 weather sub-divisional zones in India. Pai et al. (2014) also mention that the collected Data sets from the individual stations were interpolated using the two-dimensional interpolation method following Shepard (1968).

I also used the rain gauge data of All India Summer Monsoon Rainfall (AISMR) for the 1871–2021 time period from Parthasarathy et al. (1994) in this study. These data sets were produced utilising real time observations from a dispersed network of 306 rain gauges across India with the proper area weightings. The data can be accessed through IMD's Climate Data Service Portal (imdpune.gov.in).

2.1.2 Ocean Temperature and Sea Level Anomaly

The subsurface temperature (0 C) and wind stress (N/m²) data for the period 1980 to 2015 were downloaded from the Simple Ocean Data Assimilation Ocean/sea ice reanalysis (SODA) Version 3.3.1 (Carton et al., 2018). These data sets have a horizontal resolution of $0.25^{\circ} \times 0.25^{\circ}$, and are available from which (https://www2.atmos.umd.edu/~ocean/index_files/soda3.3.1_mn_download.htm). I have also used the Ocean Reanalysis System 4 (ORAS4; Balmaseda et al., 2013) from the European Centre for Medium-Range Weather Forecasts -ECMRWF, for the period from 1958 to 2015. These datasets have a horizontal resolution of 1° x 1° , and are available at 40 vertical levels.

I also use the sea surface temperature (SST) with a spatial resolution of 1° x 1° for the period of 1901- 2021 from Met Office Hadley Centre Sea Ice and Sea Surface Temperature dataset (HadISST; Rayner et al., 2003). This HadISST datasets have been extracted from the Met Office Marine Data Bank (MDB), the Comprehensive Ocean Atmospheric Data Set (COADS, now ICOADS), and the global telecommunication system (GTS). A Reduced Space Interpolation technique is used to make the gridded dataset (Kaplan et al., 1997). These sea surface temperature (SST) datasets are accessible to download from https://www.metoffice.gov.uk/hadobs/hadisst/data/download.html.

We also use Copernicus sea level anomaly (SLA) data sets for the period of 1993 to present. These data sets (https://resources.marine.copernicus.eu/) have a horizontal resolution of 0.25° X 0.25°.

2.1.3 Atmospheric Datasets

The zonal and meridional components of wind I use are taken from the National Centre for Medium Range Weather Forecast (NCMWRF) monthly reanalysis data product (Rani, et al., 2021). These are available at different pressure levels and at a horizontal resolution of 25 km over the 1980-2015 period.

We also used the zonal and meridional winds from the National Centers for Environmental Prediction (NCEP; Kalnay et al., 1996), available at 2.5° x 2.5° resolution and at 17 pressure levels. I also explore the potential temperature and relative humidity data sets from the National Centers for Environmental Prediction (NCEP; Kalnay et al., 1996). These datasets are reanalyzed gridded products available monthly from 1948 to the present.

2.1.4 Cyclone Frequency Data

I have used the cyclone frequency data available from the Regional Specialized Meteorological Centre for Tropical cyclones, India Meteorological Department. The datasets are available, at https://rsmcnewdelhi.imd.gov.in/uploads/climatology/cspos.pdf. This data set pertains to the frequency of all the cyclonic circulations that occurred with wind speeds greater than 34 knots in the NIO for the period 1891- 2021 and is inclusive of all severe cyclones, very severe cyclones, and super cyclones.

2.2 Statistical Methods

I have detrended all of the studied datasets in order to better understand the effects of the Findlater jet in the Arabian Sea (Chapter 3), as well as the effects of the Indian summer monsoon on the tropical cyclones during the post-monsoon in the NIO. This is done to exclude linear trends and solely highlight inter-annual variability. Contrarily, because it is known that the background signal does not exhibit linear trends, the observational and model output used to ascertain the Findlater jet-induced memory in the Arabian Sea (Chapter 4) have not been detrended. In general, I also employ a number of additional statistical methods, including linear regression analysis, composite analysis, and linear anomaly correlation analysis (Von Storch et al., 1999).

2.2.1 Statistical Composite Analysis

A composite analysis is a helpful tool used to determine some fundamental properties that are difficult to observe in overall averages. For studying climate or weather phenomena such as tropical cyclones (e.g., Ashok et al., 2000) or for studying the large-scale effects of teleconnection links on atmospheric variations such as El Niño (e.g., Ashok et al., 2004; Tejavath et al., 2018), composites are very useful. For tropical cyclone structures, it can be arranged by cyclone strength, vertical wind shear, or any other factors. Each composite brings out the common feature associated with a parameter, such as, the sea level pressure during a monsoon depression or anomalous rainfall over a region during El Niño. A related technique is the difference of means, which shows the distinctions between two groups.

2.2.2 The Linear Correlation

The method of linear correlation involves calculating the covariance of any two independent samples and looking for any possible linear correlations between them. I utilised the Pearson's correlation coefficient in this thesis. The correlation between two samples x and y with standard deviations s_x and s_y , respectively, is determined using the correlation coefficient (r) as follows:

$$r = \frac{\sum_{i=1}^{n} (x_i - \overline{x})(y_i - \overline{y})}{(n-1)s_x s_y}$$

$$\frac{\sum_{i=1}^{n} (x_i - \overline{x})(y_i - \overline{y})}{\sqrt{\sum_{i=1}^{n} (x_i - \overline{x})^2 \sum_{i=1}^{n} (y_i - \overline{y})^2}}$$

The value range of r is between -1 and +1. When r > 0, independent samples are regarded as being positively correlated. It is considered to be negatively correlated if r < 0 (Von Storch et al., 1999; Ross et al., 2020).

The method of correlation analysis also have some drawbacks. Correlation analysis doesnot assumes the causation for observed relationship. Correlations analysis also do not provide a quantitative assessment of how much which variables influence other variables. Additionally, outliers in the data tend to mislead the results. Most importantly, the series 'x' and 'y' in the equ. 2.1, by definition, are supposed to be independent. If not, the significance of the correlation coefficient is subject to the inherent autocorrelation in the timeseries.

2.2.3 Calculation of Statistical Significance

When interpreting statistics data, alternative hypotheses are tested against the initial (or null) hypothesis. A statistical test helps with decision-making by rejecting or maintaining this null hypothesis based on data samples. However, there is always a chance of mistake, where the genuine null hypothesis is rejected (type I error) or the false null hypothesis is accepted (type II error). Results are evaluated using statistical significance thresholds to minimise these mistakes.

The significance tests on the means in this thesis were conducted using the Student's t-test. The mean (\bar{x}) and standard deviation (s) of samples of size "n" are used to calculate the Student's t-test, which is typically applied to lower sample sizes.

$$t = \frac{\overline{x} - \mu}{s / \sqrt[n]{n}}$$

A one-tailed (degrees of freedom) or two-tailed (n-2 degrees of freedom) t-test is used, respectively, for unidirectional (n-1) or two-way (n-2 degrees of freedom) variation in the mean. This study employs a two-tailed t-test since the mean statistics of the variables I looked at can change in any direction.

2.2.4 Analysis of Empirical Orthogonal Function (EOF)

The Empirical Orthogonal Function (EOF), commonly known as principal component analysis, is a multivariate linear analytical tool for breaking down random vectors into orthogonal spatial patterns or empirically established basis functions. In order to examine the spatial pattern of climate variability and its temporal variation, the EOF technique is frequently employed in climate science. EOFs are orthogonal, linear patterns that vary in both space and time. These are obtained by calculating the spatially weighted anomalous covariance matrix's eigenvectors. The related eigenvalues quantify the proportion of variation that each spatial pattern contributes to. Each of the EOFs is independent of the others attributed to the fundamentals of orthogonality. Lower order EOFs can be seen as natural patterns of climate fluctuation, whereas higher order EOFs are often erratic and are hence referred to as "noise" in the observed system.

In the study of climate dynamics, the EOF technique methodology is commonly employed to comprehend the prevailing modes of long-term climate variability (e.g., Nicholls et al., 1989; Saji et al., 1999; Ashok et al., 2004; Yu et al., 2009; Marathe et al., 2015). At each of the EOFs, a covariant

spatial pattern may be seen. The EOF approach must be utilised with caution because it is sensitive to the selected time and space domain (Behera et al., 2003; Marathe et al., 2015, 2021).

2.3 Mathematical Expressions used in computing relevant Dynamical and physical parameters

2.3.1 Wind Stress Curl

Using the SODA Version 3.3.1 (Carton et al., 2018) over the period 1980 to 2015, I estimate the climatological monthly mean wind stress curl '*WSC*', area-averaged over the box 50°E to 70°E and 4°N to12°N in the central AS, through following the equation (Gill et al., 1982)

$$WSC = \frac{\partial \tau_y}{\partial x} - \frac{\partial \tau_x}{\partial y}$$

where τ_x and τ_y respectively denote the wind stress components along zonal and meridional directions.

2.3.2 Upper Ocean Heat Content

The SODA Version 3.3.1 subsurface temperature datasets were used for the determination of the monthly mean climatology of the depth of the 26 0 C isotherm (D₂₆). I also use these data sets in the estimation of the monthly mean climatology of tropical cyclone heat potential, which I refer to as Upper Ocean Heat Content (UOHC) for a more appropriate context, using the following equation (Leipper et al. (1972))

$$UOHC = \rho * Cp \int_{0}^{D26} [T(z) - 26] dz$$

Where T(z) is the temperature in degree Celsius at depth z (m), Cp is the specific heat (3850 J/kg 0 C), and ρ is the density (1024 kg/m 3) of seawater.

2.3.3 Cyclogenesis Potential

Tropical Cyclones are synoptic systems with a very short lifespan (~1-2 weeks). A low pressure system can intensify into a Super cyclone in a few days. Therefore, their early prediction beyond a few weeks is a herculean task. The easier and more plausible solution is to predict the potential for cyclogenesis.

The potential for cyclogenesis is defined by a measurable index called Genesis Potential Parameter (GPP; Kotal et al., 2009). The GPP considers all cyclogenesis parameters including the oceanic parameter.

$$GPP = \frac{\xi_{850} \times M \times I}{S} * \left(\frac{UOHC}{40} \right)$$

Where S represents vertical wind shear between 200hPa and 85hPa, ξ_{850} is the low-level vorticity at 850 hPa, 'I' is the temperature difference between 850hPa and 500hPa, a measure of mid-

tropospheric instability, and $M = \frac{[RH - 40]}{30}$, where RH is the relative humidity between 700hPa and 500hPa.

Chapter 3

Findlater jet induced Indian summer monsoon memory in the Arabian sea

In this chapter, I examine the impact of low-level Indian Summer Monsoon winds over the Arabian Sea, also known as the Findlater Jet (Findlater (1969)), on the local subsurface conditions. I analyze the surface winds and upper ocean heat content over the Arabian sea region and show that the Findlater jet stream during the ISM months is preserved in the southern Arabian sea subsurface 'through the subsequent winter seasons in the form of heat energy.

3.1 Annual Cycle

3.1.1 Wind Forcing

In order to understand the role of Findlater Jet (FJ) in regulating the Indian Summer Monsoon (ISM; June-September) rainfall, the climatological mean wind at 10 m above the sea surface for the study period during JJAS is shown in Figure 3.1 which shows the signature of the FJ as a core of strong southwesterly winds. The presence of the FJ can be identified by the climatological southwesterly winds seen over the central AS with a zonal wind speed in excess of 10 m/s.

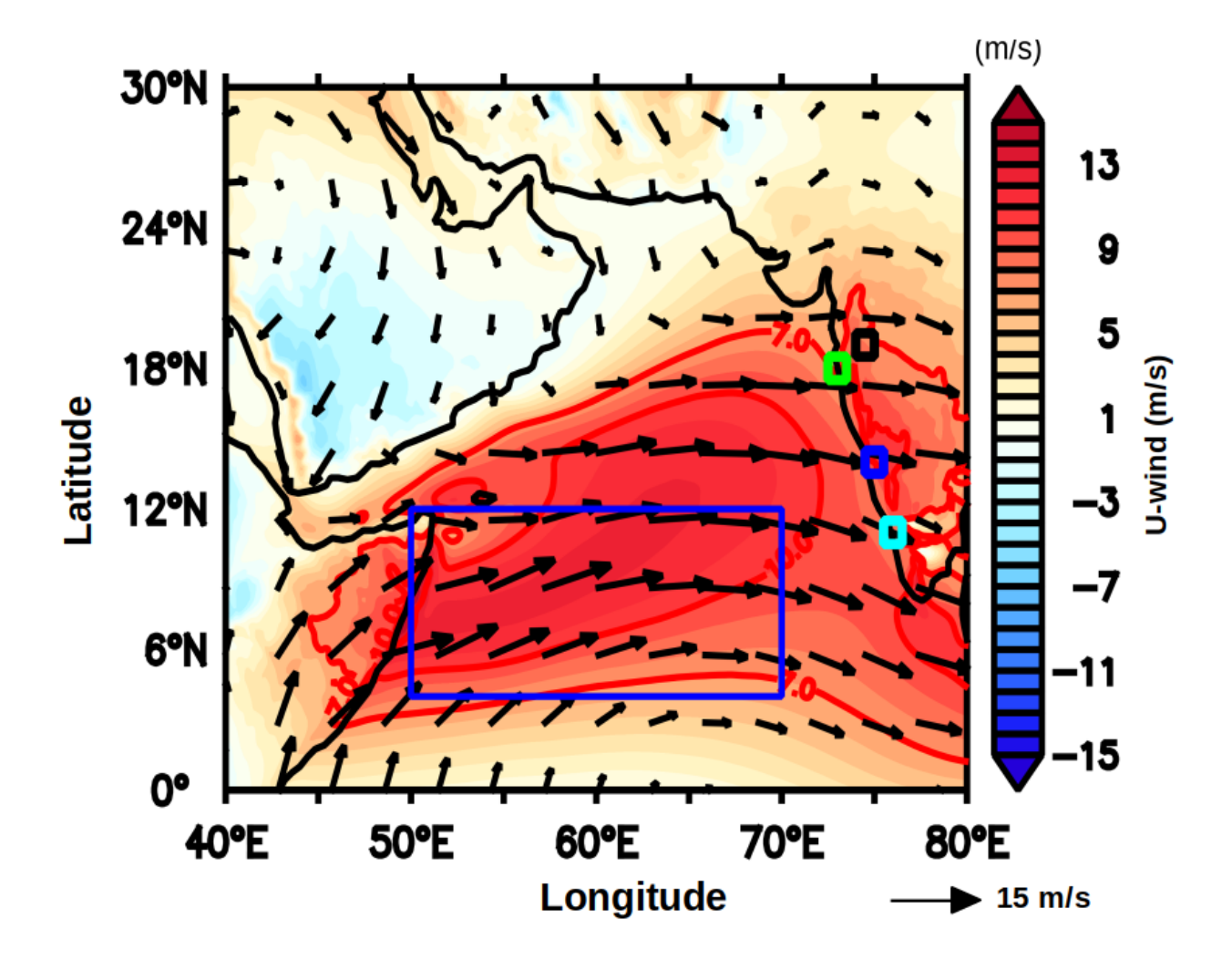


Figure 3.1: Climatological mean wind vector overlaid on zonal wind (u-wind, m/s) during

June to September (JJAS) at 850 hPa in the Arabian Sea. The blue box (50–70°E and 4–

12°N) represents the region within which parameters were averaged. Red solid lines indicate
the zonal wind speed contours of 7 m/s and 10 m/s. The different colour small squares
represent the location of subdivisonal stations, Madhya Maharashtra (black), Konkan (green),

Coastal Karnataka (blue), and Kerala (cyan).

Figure 3.2 shows the temporal and vertical structure of the wind vectors averaged over the box (Figure 3.1) located in the core region of the FJ in the central AS. During the ISM, the maximum intensity of the FJ is seen at 850 hPa. These winds are mostly westerly in direction up to 600 hPa,

and reverse to easterlies at greater heights with an increase in their magnitude. Just after the JJAS season, the ISM winds collapse, and the north-easterly winds start to prevail prominently between 1000 and 850 hPa indicating the winter monsoon conditions. Notice that the upper-level easterly winds between 200 to 300 hPa of the ISM also reverse to westerly winds during the winter monsoon.

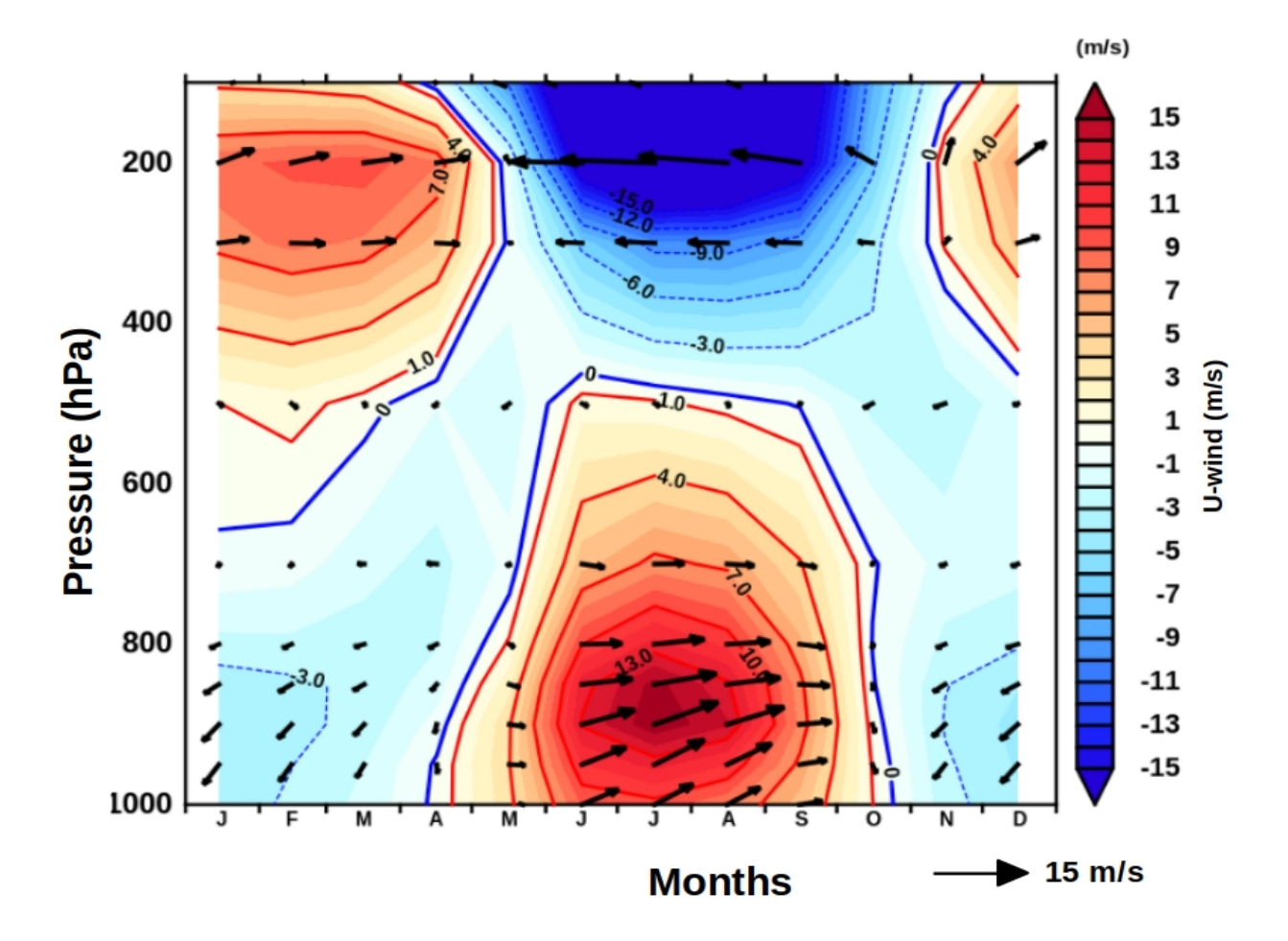


Figure 3.2: Vertical structure of monthly mean climatology of zonal wind (u-wind, m/s) averaged over the longitude 60°E to 70°E and latitude 6°N to 20°N overlaid with wind vectors.

3.1.2 Mixed Layer Depth

To decipher the impact of FJ on the upper ocean dynamics, the annual cycle of wind stress curl (Figure 3.3) and mixed layer depth (MLD) (Figure 3.4) were examined in the AS. The axis of the FJ is denoted by the zero wind stress curl (WSC) in Figure 3.3a during JJAS.

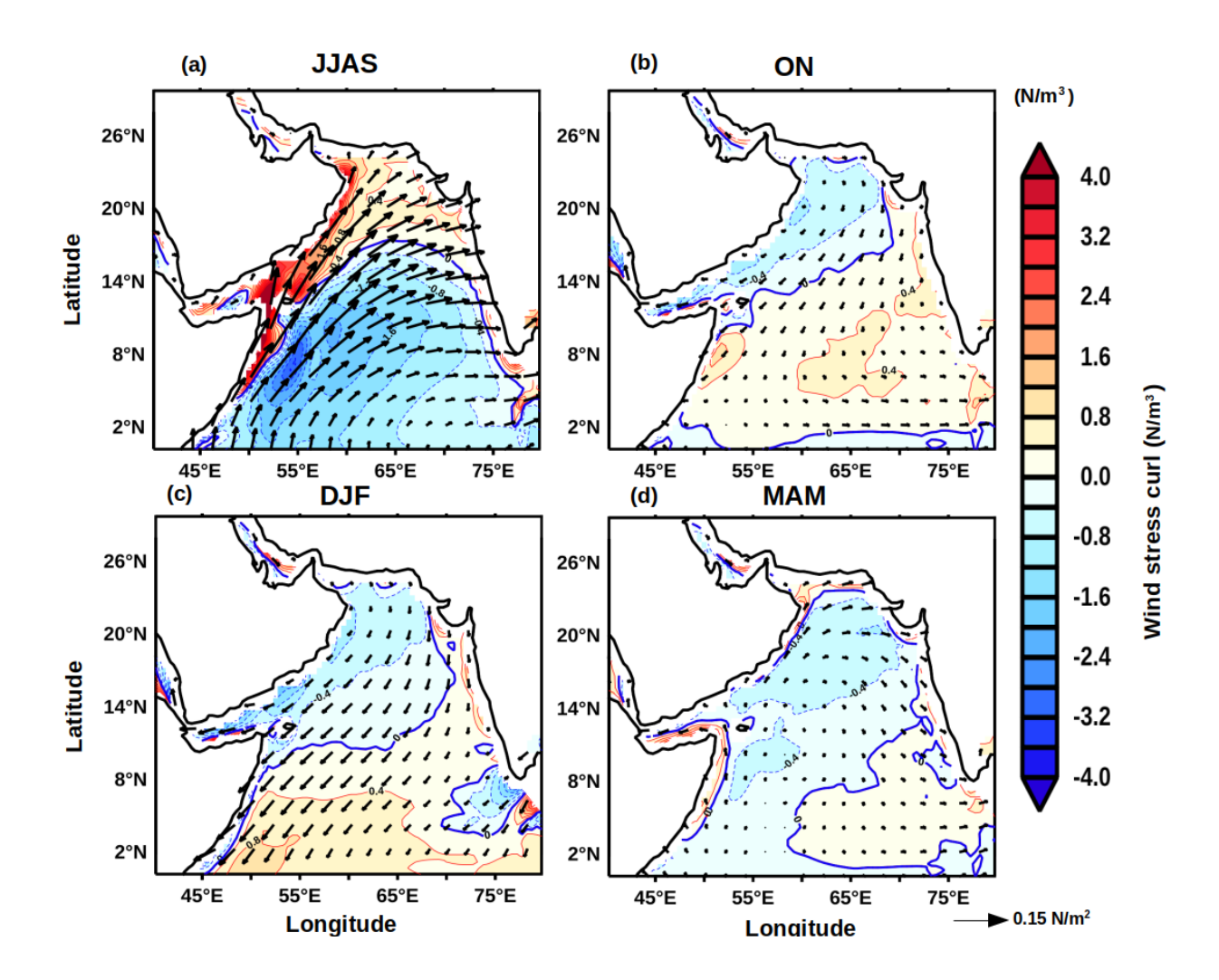


Figure 3.3: Annual cycle of climatology of wind stress curl (WSC, N/m³) during (a) JJAS, (b) ON, (c) DJF, and (d) MAM. Contour lines represent the magnitude of zero wind stress curl while the arrows represent the wind stress (N/m²) vector.

North of the axis of the FJ, the WSC was positive, which would induce an Ekman suction and support upwelling of subsurface waters. In contrast, south of the axis of the FJ the negative WSC would induce an Ekman pumping and support downwelling of surface waters. Indeed, such a

response of the wind forcing is seen clearly in the spatial distribution of MLD during JJAS (Figure 3.4a) which shows shallow mixed layer north of the axis of FJ and deep mixed layer south of it.

These results are consistent with earlier studies based on shipboard observation (Bauer et al., 1991; Prasanna Kumar et al., 2001) as well as mooring (Weller et al., 2002). As the season changes from ISM to post-monsoon (ON), the FJ collapses and disappears with weak WSC values over the entire AS (Figure 3.3b). Accordingly, the MLD also shows a decrease of 20–30 m (Figure 3.4b).

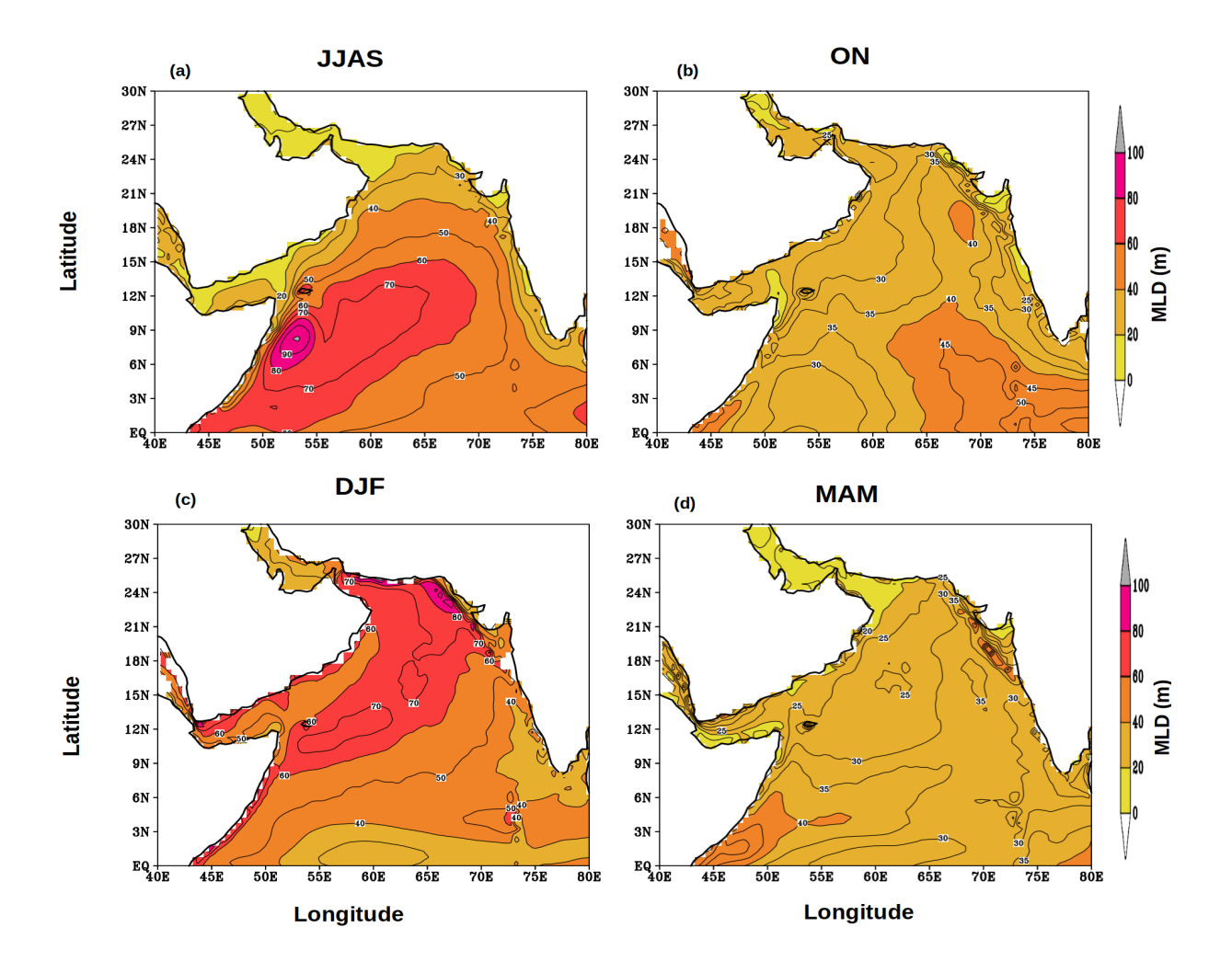


Figure 3.4: Annual cycle of climatology of mixed layer depth (MLD, m) during (a) JJAS, (b)
ON, (c) DJF, and (d) MAM.

In the winter season (DJF), under the prevailing easterly trade winds the WSC over the northwestern AS is weak and negative, on the other hand, it is weak and positive in the eastern and most of the southern AS (Figure 3.3c), suggesting a weak downwelling and upwelling in these locations, respectively. Consistent with the wind forcing, the basin-wide MLD in the AS is deep in the north and shallow in the south (Figure 3.4c). However, the deepening of MLD by 30 m in the north in comparison to post-monsoon is not entirely driven by wind as the WSC, though negative, is weak. The winter cooling and convective mixing that prevails in this season in the northern AS contributes to the deepening of MLD (Prasanna Kumar et al., 1996). The basin-wide WSC in the AS further weakens during the pre-monsoon (MAM) season (Figure 3.3d) as winds are weak and variable. This resulted in the occurrence of basin-wide shallow MLD (Figure 3.4d).

3.1.3 Upper Ocean Heat Content

Thus, FJ plays a crucial role in basin-scale modulation of mixed layer during ISM. As the FJ modulates the mixed layer, it is expected that the upper ocean heat content also will be impacted. The upper ocean heat content plays an important role in the generation of several atmospheric processes including tropical cyclone (Gray et al., 1979) and Indian summer monsoon (Venugopal et al., 2018) . The upper ocean thermal energy integrated from surface to the depth of 26 °C isotherm (D_{26}) is a commonly used metric for the Upper Ocean Heat Content (UOHC) and generally referred as the tropical cyclone heat potential. The seasonal cycle of UOHC (Figure 3.5) was examined to understand the role of FJ in modulating the upper ocean heat content. The basin-wide structure of UOHC during ISM (JJAS) shows that south of the axis of FJ, the UOHC is higher than 65×10^8 kJ/cm² and increases to 100×10^8 kJ/cm² towards the central AS, while towards the northwest and eastern parts of the AS it progressively decreases, reaching as low as 20×10^8 kJ/cm² (Figure 3.5a). The spatial distribution of D_{26} during ISM shows a pattern similar to that of UOHC (figure not shown) with values increasing form 65 m to 100 m south of the axis of the FJ, while towards the north and east it decreases. The lowest value is 20 m. Thus, the high values of UOHC are closely coupled to the deepening of D_{26} . The spatial pattern of both UOHC and D_{26} is consistent with that

of the WSC (Figure 3.3). The region of high UOHC and D_{26} shows a progressive shift towards the southeast in the post-monsoon (Figure 3.5b) and winter (Figure 3.5c) monsoons. However, the magnitude of both UOHC and D_{26} shows a marginal decrease during post-monsoon, which is linked to the weakening of the WSC.

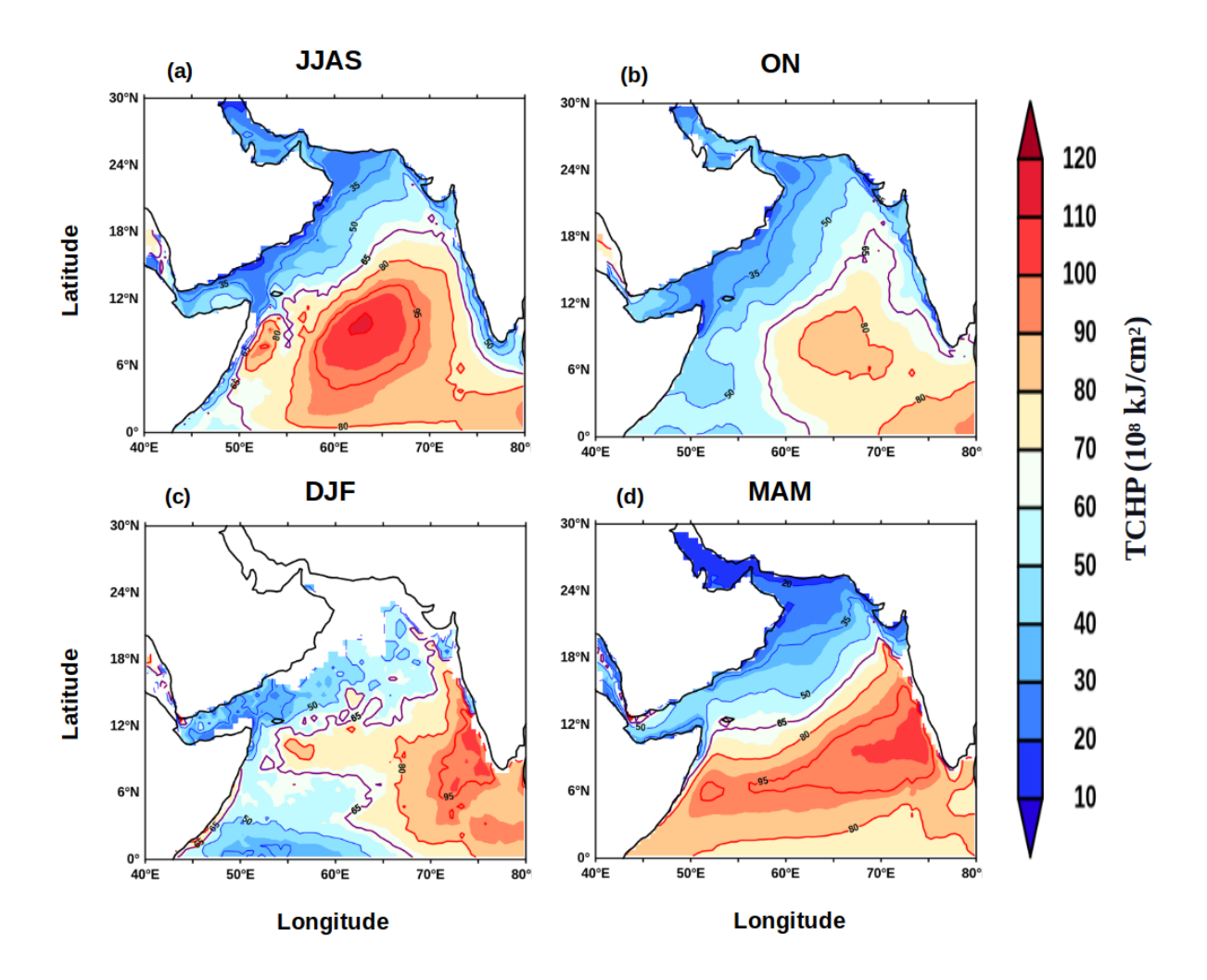


Figure 3.5: Annual cycle of climatology of Upper ocean heat content (UOHC, (10⁸ kJ/cm²) during (a) JJAS, (b) ON, (c) DJF and (d) MAM.

In contrast, the magnitude of both UOHC and D_{26} increases during winter (Figure 3.4d), though the WSC is positive. In the pre-monsoon season, both UOHC and D_{26} extend westward from their winter location and as a zonal band occupy the entire southern part of the AS.

3.1.4 Wave Propagation

The increasing magnitudes of both D_{26} and UOHC during winter and its westward expansion until the pre-monsoon is intriguing because of the weaker seasonal winds. A potential mechanism that could explain this anomaly is the propagation of Rossby waves.

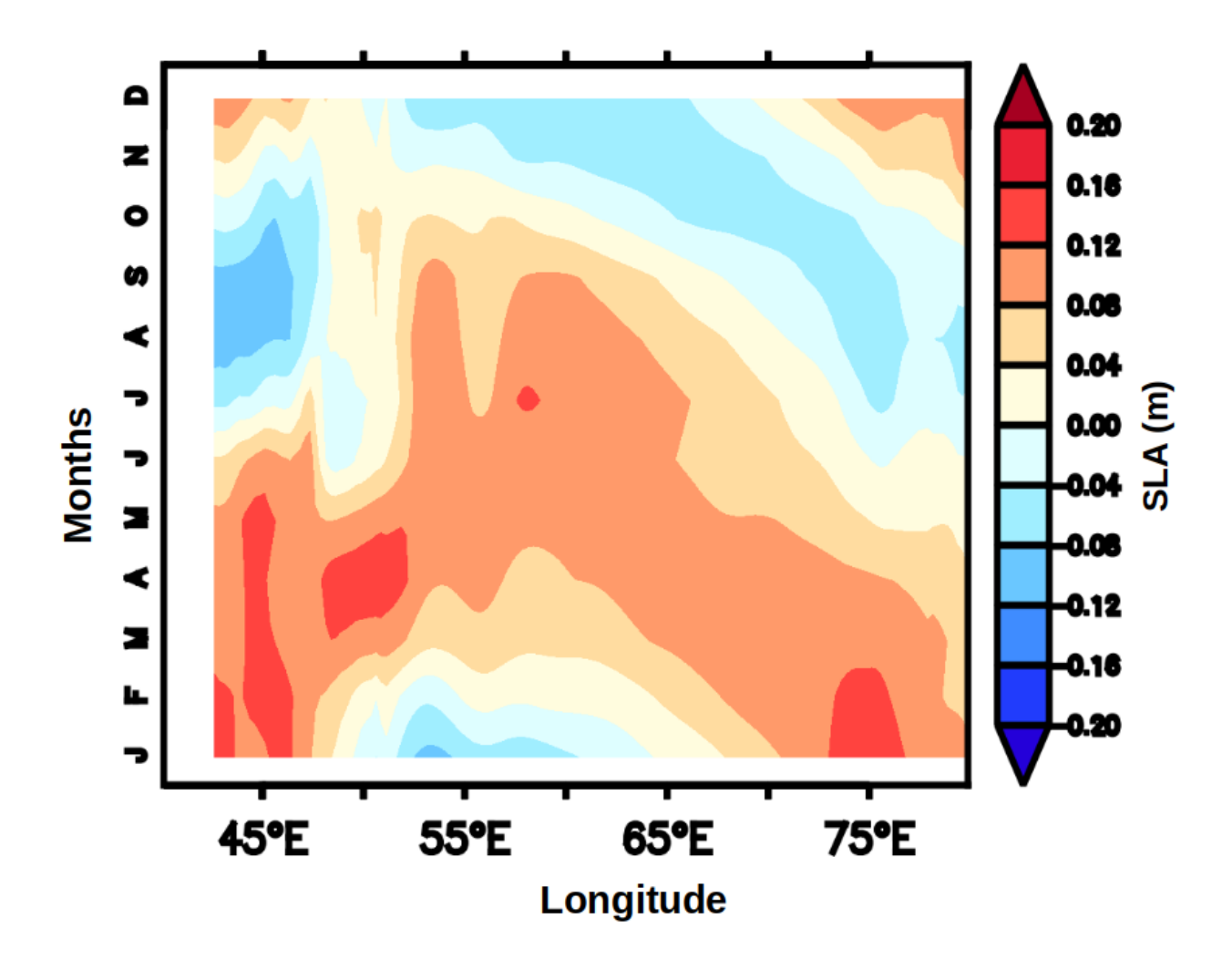


Figure 3.6: Hovmöller plot of climatology of monthly mean sea level anomaly (SLA, m) averaged over the latitudes from 4°N to 12°N in the Arabian Sea.

It is known that downwelling Rossby wave propagates from the west coast of India towards the coast of Somalia during each winter. This wave is generated by the coastally trapped Kelvin wave

traveling along the eastern boundary of the AS (McCreary et al., 1993). To explore this, I present a Hovmöller plot of SLA averaged over the latitudes 4° to 12° N (Figure 3.6), which clearly indicates a zonally sloping bands of SLAs. This is the signature of a westward propagating downwelling Rossby wave. Rossby waves are known to deepen the thermocline, and in the present case, it is manifested by the deepening of the D_{26} and associated increase in the ocean heat content.

3.2 Dynamics

The above discussion leads to the understanding that due to the WSC associated with the FJ during ISM, the southern part of the AS is able to store more thermal energy compared to its northern part.

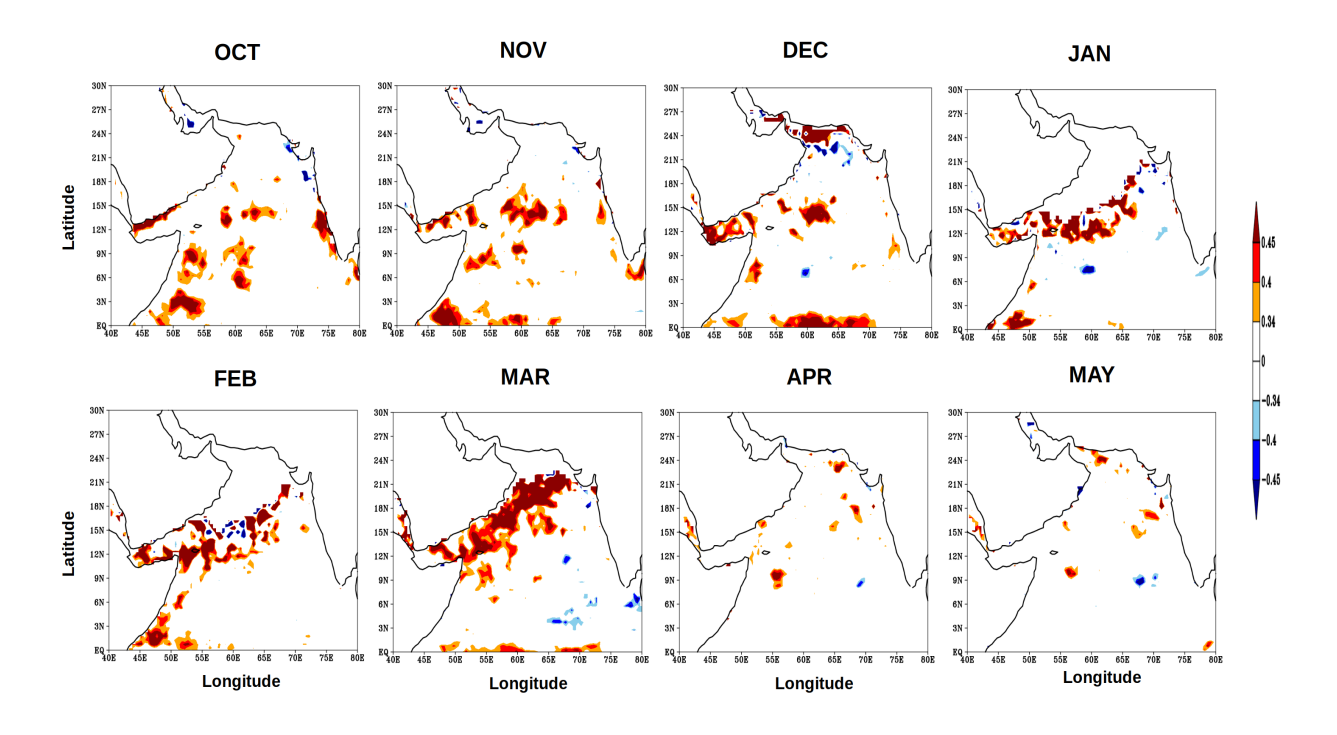


Figure 3.7: Monthly anomaly correlation of wind stress curl over the box region (50–70°E and 4–12°N, see Figure 3.1) of UOHC of the Arabian Sea from October to May for the period of 1980–2015. The red colour represent the positive correlation value and the blue colour represents the negative correlation value, both significant at 95% confidence.

To further understand this association, a box that essentially encompasses the region south of the axis of the FJ within the southern AS was selected, covering the 50-70°E and 4-12°N domain (Figure 3.1). Monthly spatial anomaly correlations were computed for each of the calendar months from October through May between the WSC within the box region and the leading UOHC in the AS during ISM in order to see how closely they were related. For this purpose, the monthly anomaly of the WSC was calculated by subtracting the JJAS-averaged WSC within the box from each calendar month. Similarly the monthly anomaly of UOHC was calculated by subtracting the JJAS-averaged UOHC at each grid point from each calendar month. Figure 3.7 shows the monthly spatial anomaly correlation from October to May in the AS. The UOHC anomaly from October to December south of the FJ was positively correlated to the WSC at 95% confidence level from a two-tailed Student's t-test. By the beginning of the subsequent year, i.e., during the following months of January and February, the region of significant positive correlations move closer to the FJ axis (Figure 3.7). From March to May, the correlation between the WSC and the UOHC anomaly in the southern AS is not significant any more (Figure 3.7). The result reiterates the role of FJ-induced Ekman dynamics in regulating the upper ocean heat content in the region south of the axis of the FJ during the post-monsoon and the winter monsoon.

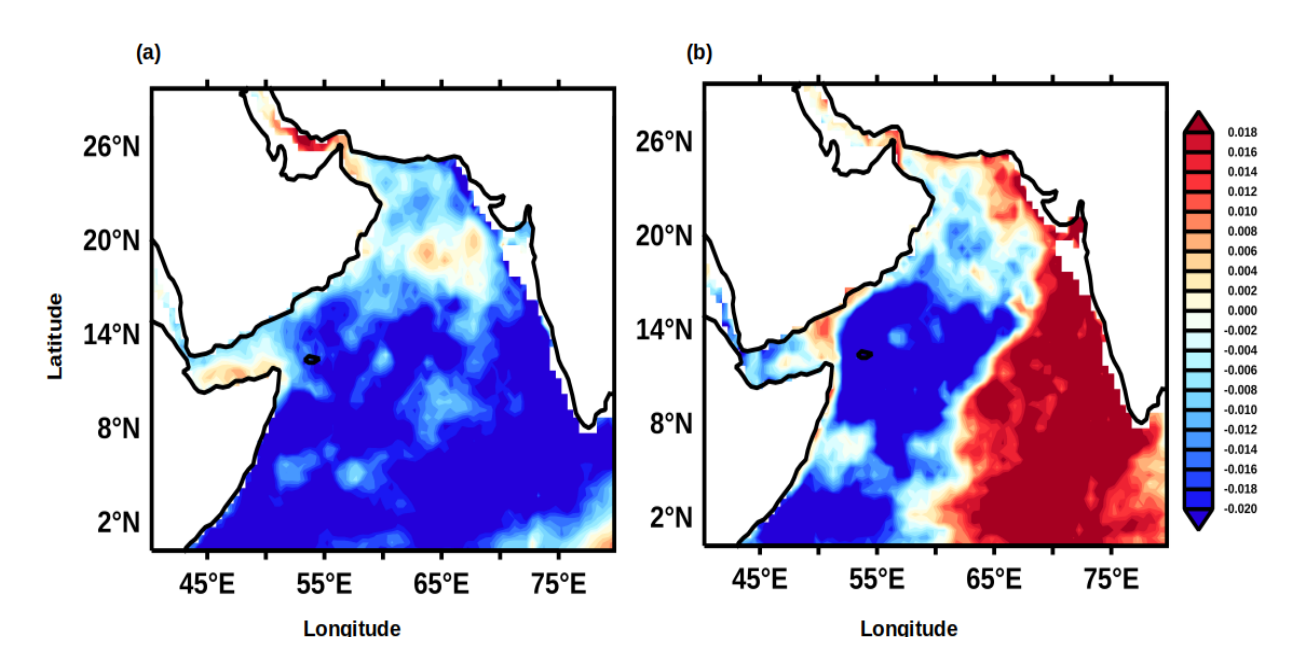


Figure 3.8: (a) The Principal Component 1 and (b) Principal component 2 of the EOF of the UOHC during ON.

To ensure the robustness of the above results, we have computed the variability of Empirical Orthogonal Function (EOF) for UOHC during ON months. Figure 3.8a,b shows the first and second principal components (PC) of the EOF. The variances of the first and second PCs of EOF for UOHC during ON months are 23.6% and 9.3% respectively. The second mode of EOF clearly brings out a pattern of spatial variability in the UOHC that is similar to that of the basin-wide pattern of WSC induced by the Findlater jet during ISM months (Figure not shown). The contrast between the northern and the southern sides of the FJ axis is quite distinctly visible in the second EOF (Figure 3.8b).

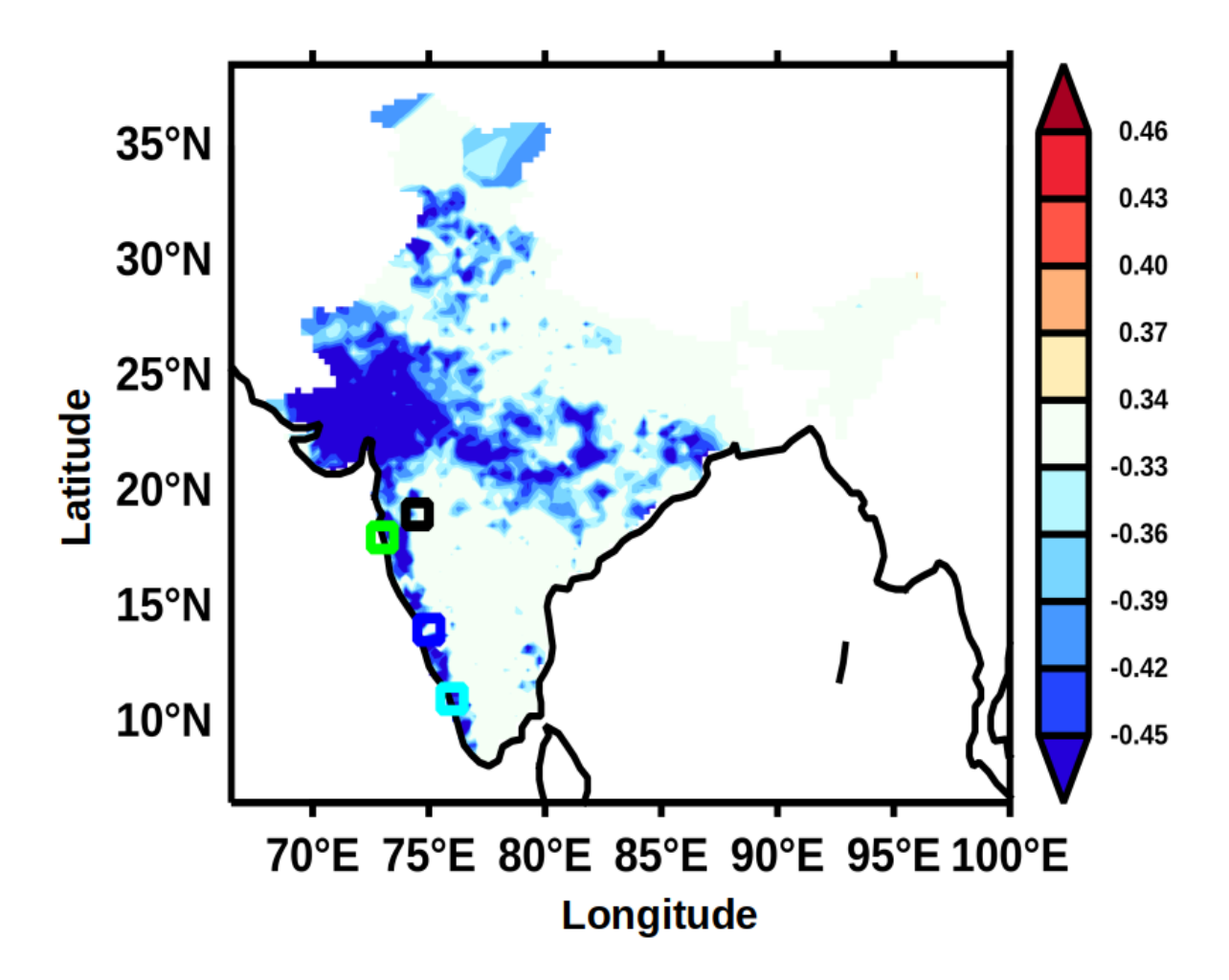


Figure 3.9: Anomaly correlation of climatology of WSC averaged during JJAS within the box region (50–70°E and 4–12°N, see Figure 3.1) with climatology of rainfall averaged for the same months in the Indian sub-continent. The blue colour represents the significant negative correlation value at 95% confidence. The different colour small squares of different colours represent the location of sub-divisonal stations, Madhya Maharashtra (black), Konkan (green), Coastal Karnataka (blue), and Kerala (cyan).

Having examined the relationship between the WSC within the box in the southern AS with UOHC over the AS, it is pertinent to show that the WSC within the box is indeed related to the rainfall over the Indian sub-continent. Figure 9 presents the spatial correlations of the WSC averaged over the

aforementioned box (shown in Figure 3.1) during June to September with concurrent rainfall distribution over the Indian sub-continent. The WSC over the box region is negatively correlated with local rainfall along the western, central and northern parts of India at 95% confidence level. This implies that a higher negative WSC is associated with an increase in the ISM rainfall. Mechanistically, this happens through increase in the UOHC via deepened D₂₆ .Finally, to address how the upper ocean heat content was related to the Indian summer monsoon, the June-September seasonal mean climatological rainfall at four locations along the west coast of India (see Figure 9 for locations), where summer monsoon signature is prominent, has been identified to represent west Indian coastal rainfall (WICR) variations. A lead correlation of WICR with UOHC in the AS were computed and presented in Figure 3.10. In the post-monsoon period (Figure 3.10a) the UOHC in the south-eastern part of the AS was positively and strongly correlated with WICR at 95% confidence level at all four stations. During the following winter months (DJF) (Figure 3.10b) the positive correlation of UOHC and WICR is spread over most part of the southern AS and along the west coast of India. Interestingly, the positive correlation of WICR and UOHC completely disappears in pre-monsoon period (Figure 3.10c).

The result from these lead correlations suggests that the UOHC in the southern part of the AS is anomalously higher during the seasons subsequent to Indian summer monsoon if the FJ is stronger (weaker) than normal and the rainfall over the WICR higher (lower) than the average. It emerges from the above results that the FJ signal is potentially 'memorized' in the sub-surface AS in the form of UOHC.

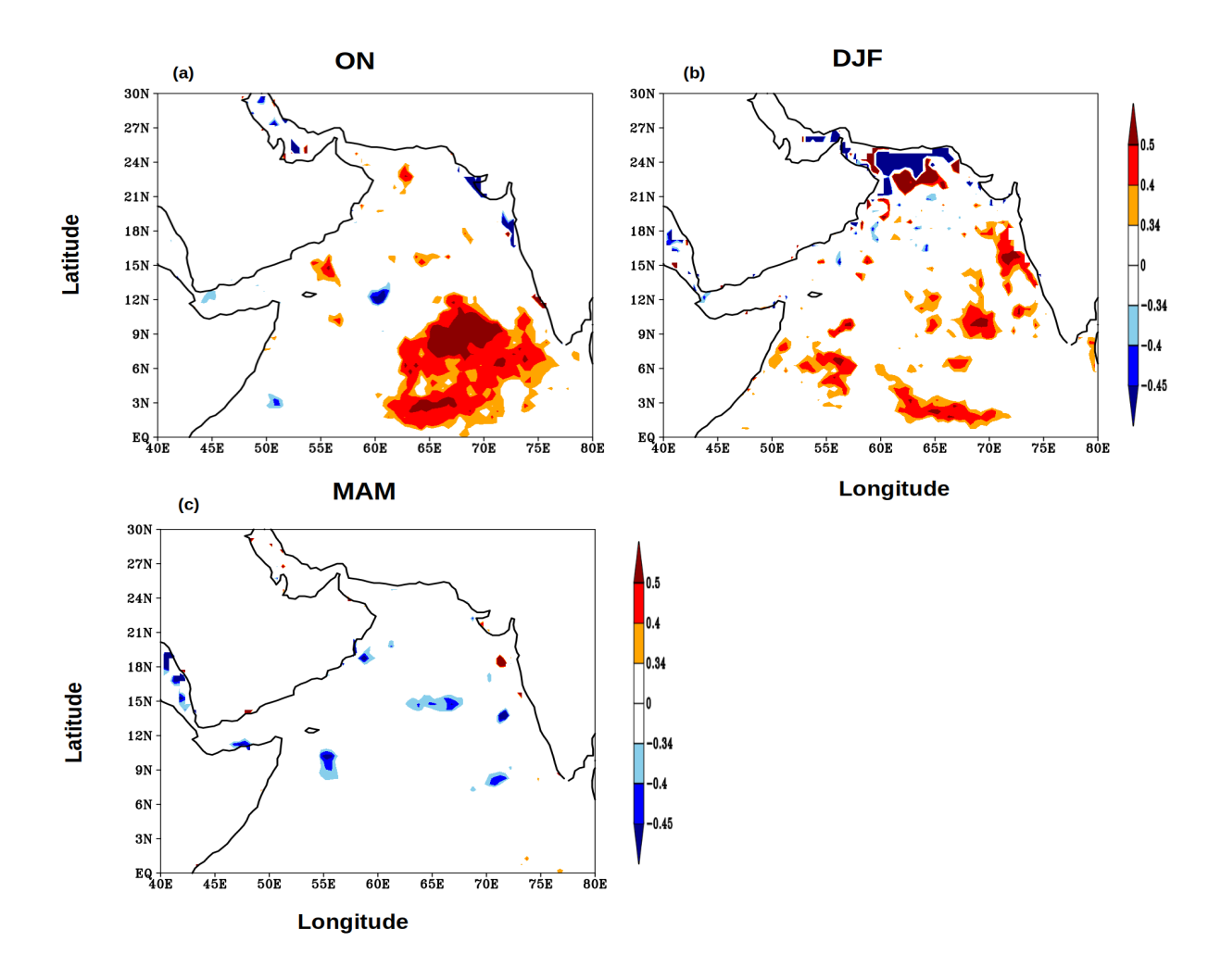


Figure 3.10: Monthly lead anomaly correlation of climatology of West Indian coastal rainfall (WICR) with climatology of UOHC in the Arabian Sea during (a) ON, (b) DJF, and (c) MAM for the period of 1980–2015. The red and blue colours represent the significant positive and negative correlation value respectively at 95% confidence.

It is also intriguing why the heat pumped in by the summer monsoon into the subsurface layer of the southern AS is not reduced or dissipated by mixing in the subsequent two seasons. In the next paragraphs, based on the results from the present study and existing understanding of the regional oceanography of the AS, we propose a potential mechanism, which facilitates the observed 'memorizing' of the FJ through the next two seasons in the subsurface of the AS. During the ISM period, the FJ produces a strong upper ocean convergence through the wind stress curl towards the

south of its axis. The resultant Ekman pumping leads to the downwelling of water to the south of the FJ axis. The downwelling of warm surface waters during June to September eventually builds up the heat content in the upper thermocline. A stronger FJ is known to leads to an increased Ekman pumping and deeper downwelling. This in turn deepens the D_{26} and results in the increase the upper ocean heat content during ISM. As the season changes from ISM to post-monsoon two processes co-occur in the AS: (1) the secondary heating and development of strong thermal stratification of the upper ocean, (2) the prevalence of weak and variable winds (Prasanna Kumar et al., 2009). Both of these processes curtail the mechanical mixing, and result in retaining most of the heat in the subsurface layers in the upper thermocline.

Why does not the subsurface heat stored during post-monsoon come up in the winter under winter convection? In winter, surface waters of the northern AS experience sensible heat loss due to reduced incoming solar radiation, and latent heat loss due to evaporative cooling under the prevailing dry north-easterly winds of continental origin. Both processes deepen the mixed layer In contrast, in the southern part of the AS, especially south of 15°N, does not experience winter cooling and convection. As the convective mixing is absent in this region, the heat stored in the subsurface does not dissipate. In addition, the westward propagating downwelling Rossby waves radiated from the eastern boundary of the AS deepen the upper thermocline. This will help to retain the warm waters below the surface during winter, as has been inferred from the UOHC and deep D₂₆ during winter (Figure 3.5). As the inherent strength of the winter monsoon winds over the AS is substantially weaker compared to the ISM, the wind-driven entrainment has very little effect on the subsurface warmer waters. We believe that all this constrains the FJ-induced heat to a deeper level during the post-monsoon and winter seasons. Once the propagation of Rossby wave from the eastern AS collapses towards the end of winter /beginning of the following pre-monsoon, i.e., the following spring season, the thermocline shoals up, and the heat that was stored in the previous

seasons in the subsurface layer becomes available in the upper ocean for subsequent ocean—atmosphere interaction.

3.3 Conclusion

The seasonal cycle of the AS is a net response to the Ekman dynamics associated with the local southwest and succeeding northeast monsoons, associated air-sea fluxes, and annual Rossby waves. Through an examination of various reanalysis/observational datasets for the period 1980–2015, we document a contiguous chain of inherent seasonal processes in the AS from boreal summer through the following year winter, which showed storage of the signature of the FJ in the form of heat energy in the sub-surface, represented by the UOHC for three consecutive seasons. Our study ascertains that the UOHC in the southern part of the AS during the winter monsoon was positively correlated with the WSC of the summer monsoon. Further, during a strong monsoon with strong FJ the UOHC in the southern AS was not only anomalously high, as expected, but continues to be so even during the subsequent boreal winter season in such years.

This UOHC signature of the previous year FJ stored in the AS is because of the seasonality of winds over the AS and the westward propagating Rossby wave radiated from the eastern boundary of AS. The modulation of the upper thermocline by the Rossby wave keeps the signal stored in the subsurface till the beginning of boreal spring and probably may pre-condition the local SST for the next monsoon. Exploring this aspect is beyond the scope of the present study. The proposed mechanism of subsurface storage of summer monsoon memory in our study is based only on the correlation analysis and needs further extensive modelling studies over the AS to further understand the interactions of FJ with the subsurface ocean. Nevertheless, findings from this study have great implications on the understanding of dynamics and thermodynamics of the upper ocean in the AS in the context of summer monsoon and its predictability.

Chapter 4

A modelling approach to ascertain the memory induced by Findlater jet in the Arabian Sea

In this chapter, I present results from sensitivity experiments we have carried out with the MOM5 model to ascertain the impact of Indian Summer Monsoon winds (i.e., Findlater Jet) on the subsurface Arabian sea. Two sensitivity experiments have been carried out. My analysis of the model results confirms that the heat which is induced by the Findlater jet during the Indian Summer Monsoon months is preserved in the southern Arabian sea till the subsequent spring season.

4.1 Model simulations

4.1.1 Model Setup

The model used in the present study is a regional adaptation of the Modular Ocean Model (MOM5, Griffies et al., 2012), which is a global ocean general circulation model. The version we use has been designed for the Indian Ocean with the domain 30 °S to 30 °N and 30 °E–120 °E with a resolution of 0.25° and has been used by several researchers to study various features of the Indian Ocean (Lakshmi et al., 2020, Chatterjee et al., 2013, 2019; Shankar et al., 2016, 2019). It is a hydrostatic, free surface, and z-coordinate model with forty vertical levels in which the 20 levels are for upper 120 m. The horizontal mixing scheme consists of a combination of Biharmonic and Laplacian schemes with Smagorinsky coefficients (Griffies & Hallberg, 2000), and the vertical

viscosity is based on Large et al. (1994), with the bulk Richardson number set to 0.3. The model bottom topography is based on Sindhu et al. (2007), with a minimum depth set to 15 m. To ensure the stability of the model, the horizontal friction is set to the lowest value.

The model has been forced using the daily climatological fields of radiative fluxes, momentum, and wind stresses taken from Tropflux (Praveen et al., 2012, 2013). The daily datasets for the years 1990 to 2016 were used to create the climatological fields. Within the 4-sponge layer at the open southern and eastern limits of the model, the temperature and salinity fields are relaxed to climatological values of the North Indian Ocean Atlas (NIOA; Chatterjee et al., 2012) using a temporal relaxation scale of 30 days. To prevent unrealistic currents, a climatological monthly river discharge (Vörösmarty et al., 1996; Papa et al., 2010) is specified across the top 15 m of the water column at river mouths and distributed over numerous grids. The Tropical Rainfall Measuring Mission provided the data on precipitation. The surface salinity is restored using a 15-day relaxation period. To realistically mimic cross-basin flow, the shallow and congested Palk Strait between India and Sri Lanka is shut in this configuration (Chatterjee et al., 2013, 2017). Temperature and salinity fields from NIOA climatology are used to initialise the physical model with a state of rest (Chatterjee et al., 2012). The model was spun for 35 years intially. Tropflux surface fluxes were used to force the model to run from 1990 to 2020 during this interannual run.

4.1.2 Model Sensitivity Experiments

To address our objectives, two sensitivity experiments have been carried out. These experiments differ from the final year of the climatological run only in terms of wind forcing. That is the climatological winds have been replaced by the real winds, derived from Tropflux, of a particular year and keeping the other forcing fields as climatological values.

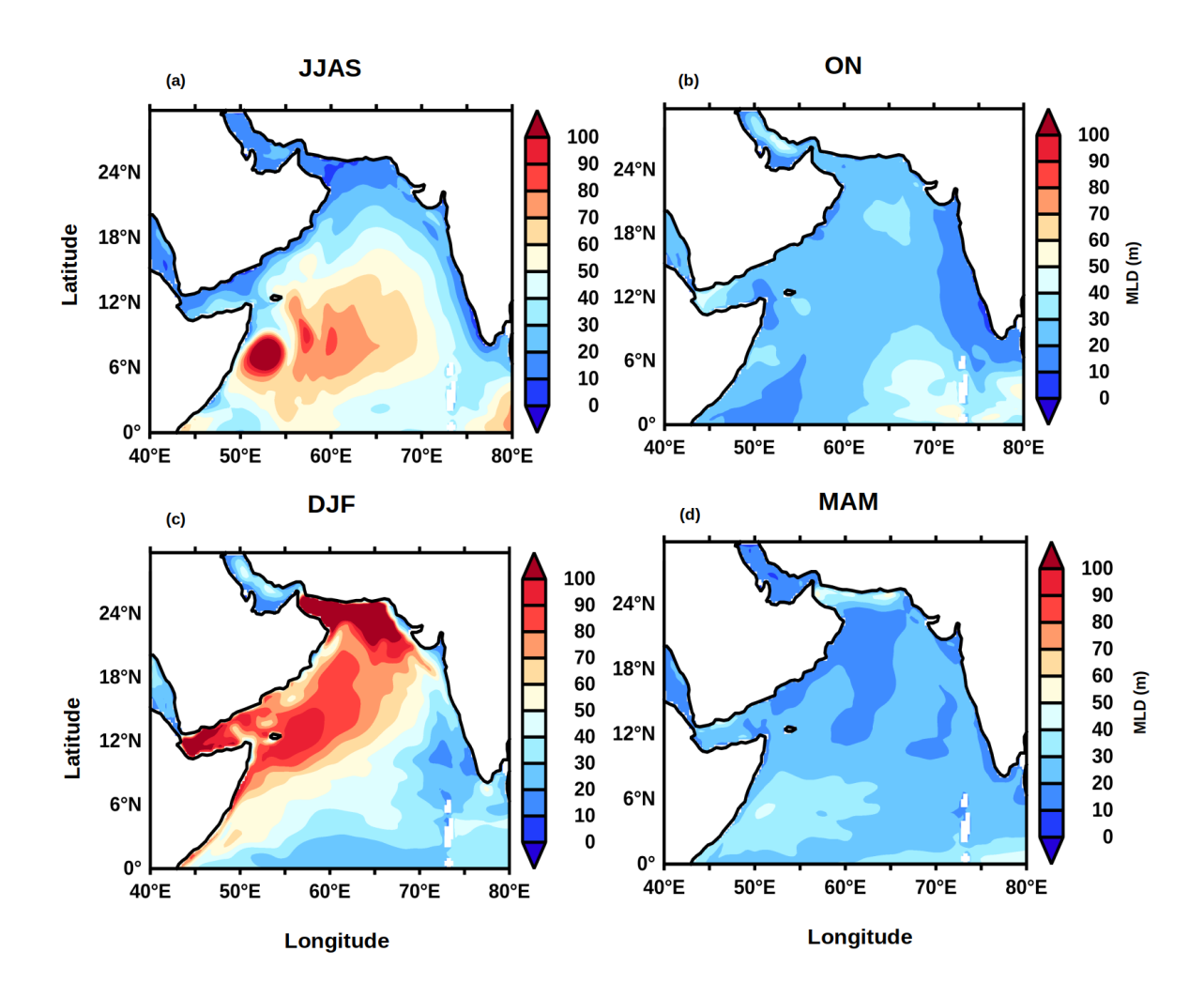


Figure 4.1: Climatology of mixed layer depth in MOM5 model simulations in the Arabian sea during (a) JJAS, (b) ON, (c) DJF and (d) MAM.

For our experiments, we consider two examples of good and bad monsoon years based on IMD criteria. The first sensitivity experiment pertains to 1988, a good monsoon year (IMD, 1943; Ashok et al., 2001). We imposed the 1988 real winds over the Indian Ocean to drive the ocean model while prescribing the climatological values to the other parameters. In the second sensitivity experiment, we take the year 2002, well known as a bad monsoon year (Ashok et al., 2009). Analogous to the 'good monsoon' experiment, we imposed the 2002 real winds to drive the ocean model while keeping climatological values for the other parameters. The winds are imposed from April of the said year till May of the following year, that is, each experiment runs for continuous 14 months.

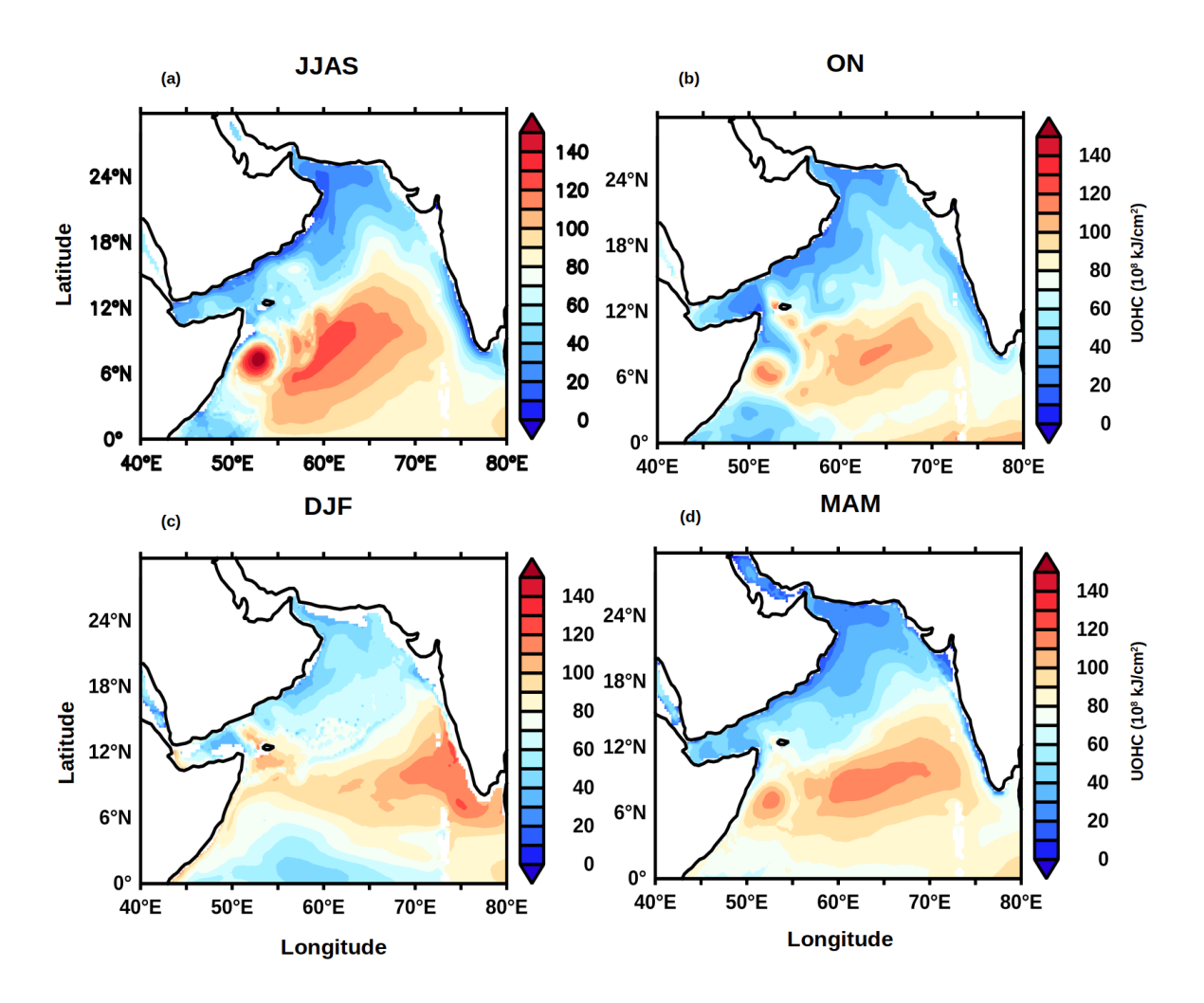


Figure 4.2: Climatology of upper ocean heat content in MOM5 model simulations the Arabian sea during (a) JJAS, (b) ON, (c) DJF and (d) MAM.

4.2 Validation of MOM5 output

At the outset, we validated all the MOM5 model climatological simulations with the available reanalysis datasets. The climatological seasonal evolutions of the mixed layer depth (MLD), and upper ocean heat content (UOHC) from the model simulation are validated by comparing the corresponding parameters from the SODA datasets (shown in Figures 4.1, 4.2, 4.3 and 4.4).

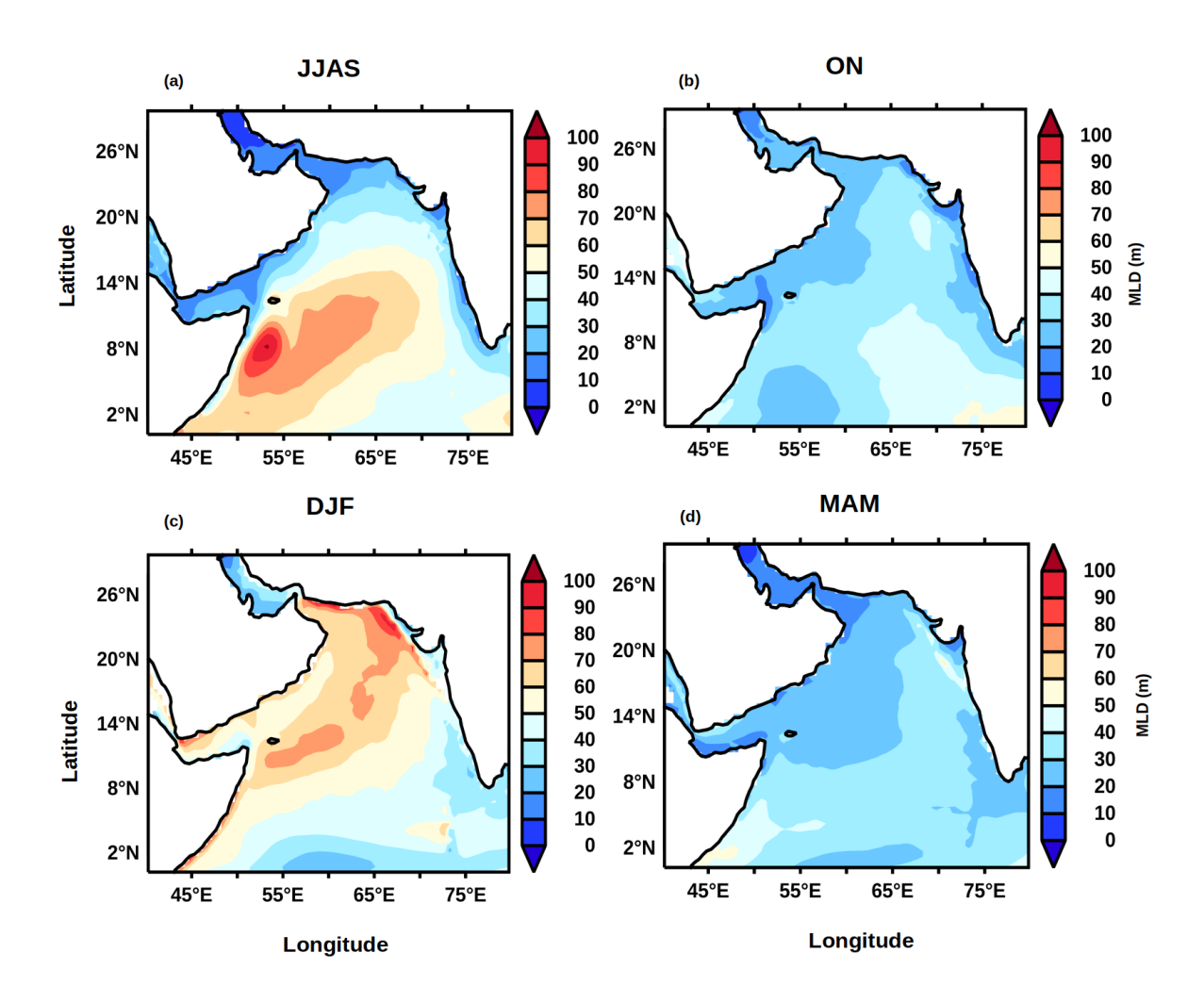


Figure 4.3: Climatology of mixed layer depth in SODA 3.3..1 reanalysis datasets in the Arabian sea during (a) JJAS, (b) ON, (c) DJF and (d) MAM.

The simulated seasonal evolutions of the MLD and UOHC across the AS are comparable with those from the SODA. Thus, we ascertain that the model is able to capture the seasonal cycle and the evolution of the various oceanographic features in the AS.

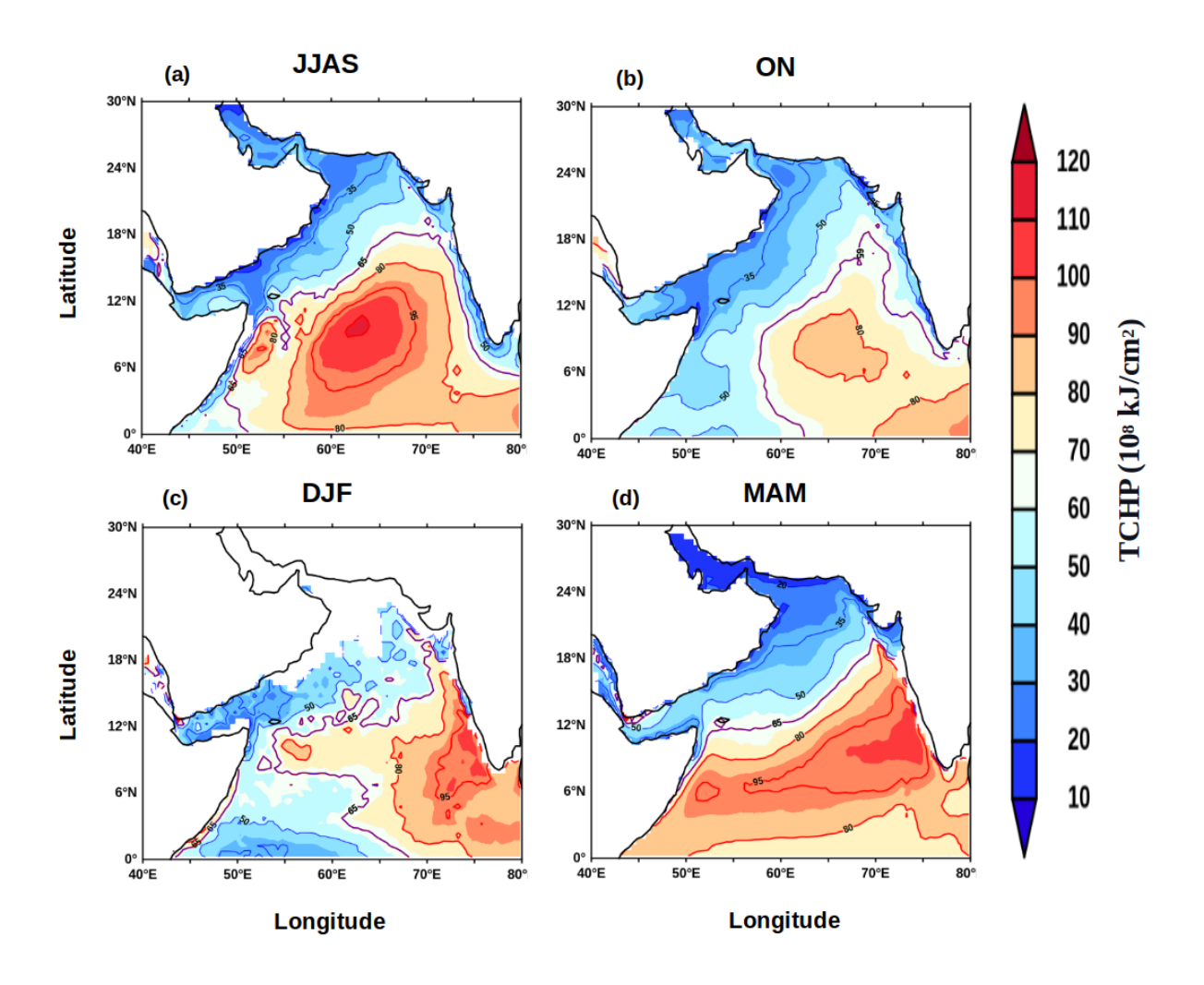


Figure 4.4: Climatology of upper ocean heat content in SODA 3.3..1 reanalysis datasets in the Arabian sea during (a) JJAS, (b) ON, (c) DJF and (d) MAM.

4.3 Wind Forcing during ISM in two distinct years

The winds during the ISM over the AS are used as the upper boundary condition to drive the model in the two sensitivity experiments for the years 1988 and 2002, as shown in Figure 5.1. The axis of the FJ can be easily discerned by noting the zero contour of the wind stress curl over the AS (Note, figure shows the wind stress vector not the wind), and the colour shading indicates the magnitude of the WSC in the AS. A contrasting feature of positive and negative WSC in the northern and southern AS respectively is clearly visible during the good monsoon season of JJAS in 1988 (Figure 4.5a). This wind structure leads to positive Ekman pumping the southern AS, which favours

downwelling surface waters. On the other hand, the wind structure in the northern AS favours upwelling of the deeper waters due to the effect of Ekman suction associated with the negative WSC. The transition from negative to positive WSC has a strong gradient in 1988 and is clearly observable, whereas, in 2002, the gradient is not clearly visible (Figure 4.5b). The distinct dipolar pattern of the wind stress curl seen during 1988 in the AS is not clearly discernible in 2002. The magnitude of the WSC in most part of the northern AS is weakly negative, while it is slightly positive in the southern AS. This leads to a rather weakened Ekman dynamics in the AS in 2002 in comparison to 1988.

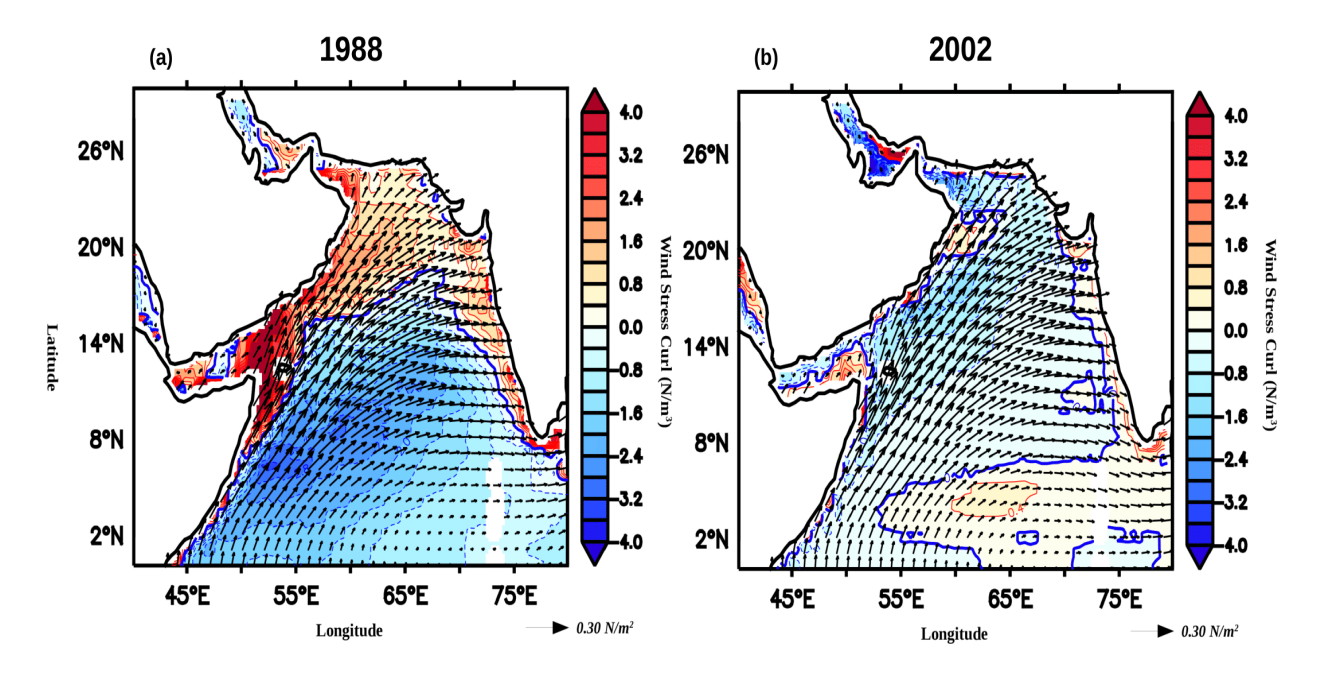


Figure 4.5: (a) Good monsoon year (1988) mean wind stress vector overlaid on windstress curl (N/m3) during June to September (JJAS) in the Arabian Sea.

(b) Bad monsoon year (2002) mean wind stress vector overlaid on windstress curl (N/m3) during JJAS in the Arabian Sea.

4.4 Mixed Layer Depth during ISM in two distinct years

In order to understand the sensitivity of the mixed layer in the AS to interannual variations in the concurrent summer monsoonal wind forcing across the good and bad monsoon years, the simulated MLD during the ISM is calculated. During the good monsoon years, the MLD spatial distribution across the FJ axis is quite a contrast. For example, the strong simulated Ekman suction due to the strong WSC during good monsoon season of 1988 leads to a relatively shallower mixed layer in Northern AS, compared to the deeper MLD in the southern AS. These results are consistent with Kushwaha et al. (2022) (Chapter 3 of this thesis) and the earlier observational studies based on the mooring and shipboard (Bauer et al., 1991, Prasanna Kumar et al., 2001). In bad monsoon year, the spatial distribution of the MLD is similar but weaker in magnitude, which is consistent with the WSC feature during the ISM.

4.5 Difference of oceanic parameters between two distinct years

As shown in this section, our model results shows that variations in the FJ modulate the MLD and, evidently, also the UOHC in the AS during the ISM. In fact, our earlier study, K22 proposed, based on an analysis of the annual cycle, that the FJ modulates UOHC during the ISM through Ekman dynamics, and its associated heat signals in the form of UOHC persist until the following spring.

To understand the role of FJ strength in preserving the signal in the AS in the following months after ISM, we calculate the change in the magnitudes of MLD and UOHC between the good and bad monsoon years.

4.5.1 Mixed layer depth

The seasonal difference of the simulated MLD between the good monsoon and bad monsoon years (dMLD, the difference between 1988 MLD and 2002 MLD) is calculated and shown in Figure 4.6.

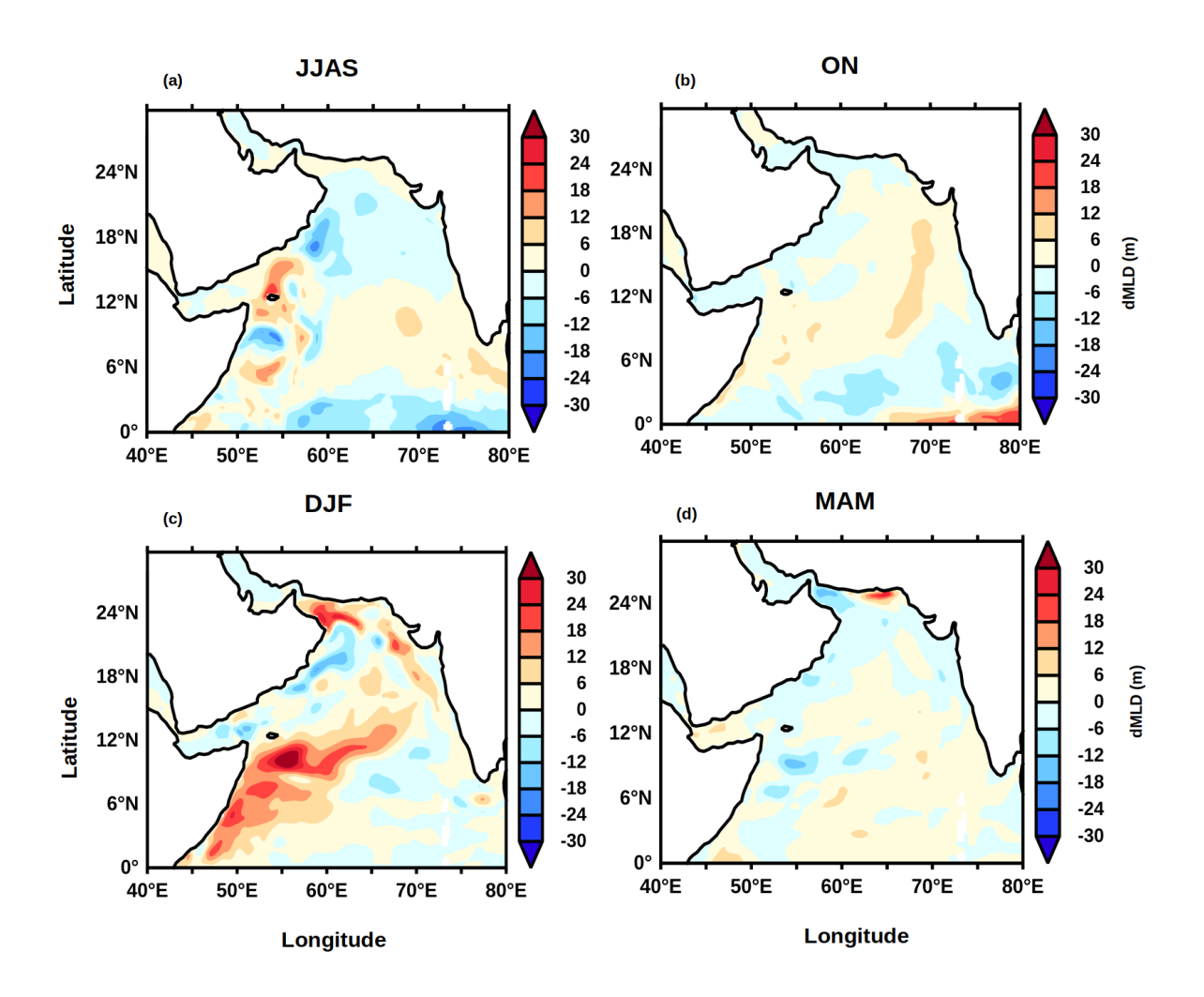


Figure 4.6: Difference of MLD (dMLD) of flood year (1988) - of drought year (2002) for (a)

JJAS, (b) ON, (c) DJF and (d) MAM

During the ISM, the dMLD is positive in the southern AS and negative in the northern AS (Figure 4.6a), indicating a relative deepening of the MLD in the south AS during good monsoon years and shoaling during weak monsoon years. After the ISM, in the months of October- November (ON), the dMLD was positive in the southern AS in 1988 (Figure 4.6b), indicating a relatively deeper MLD in good monsoon years; elsewhere in the AS, the dMLD is negative. This result confirms the hypothesis proposed by K22 that the FJ has an effect on the MLD that persists through with boreal fall with relatively deep (shallow) MLD in a strong (weak) monsoon year. The model experiments also confirm the leading impact of the FJ on the UOHC in the following seasons; the dMLD is still

positive in the south of the FJ core during the winter season (DJF) and negative elsewhere in the AS (Figure 4.6c). In the following spring, the dMLD yet shows positive in the most parts of the southern AS (Figure 4.6d). Overall, this result signifies that the MLD during a good monsoon year, such as 1988, is much deeper in the subsequent two post-monsoon seasons relative to those after a weak summer monsoon season, such as in the year 2002.

4.5.2 Upper ocean heat content

As the MLD modulates the UOHC, we calculate the simulated difference in the simulated UOHC between the weak and strong monsoon years (dUOHC) in the AS (Figure 4.7). During a strong ISM season, the UOHC shows a higher positive value in the south of the FJ core and lower to the north, as can be inferred from the dUOHC (Figure 4.7a). The high negative WSC induced by the strong FJ pushes the surface waters down in the southern AS, causing a relative downwelling of warm waters into the upper thermocline. Meanwhile, a relative upwelling of the deeper water in the northern AS occurs due to the positive WSC (Figure 4.7a). The water that downwells to the subsurface levels in the southern AS contains the heat signal of the ISM. Furthermore, in the post-monsoon (ON), the dUOHC is positive in the southern AS and negative in the northern AS (Figure 4.7b). The positive value of dUOHC spreads throughout the entire basin of southern AS, while it is primarily negative in northern AS (Figure 4.7c). Finally, in the next spring, the dUOHC shows a slightly positive value in the southern AS and negative elsewhere in AS (Figure 4.7d).

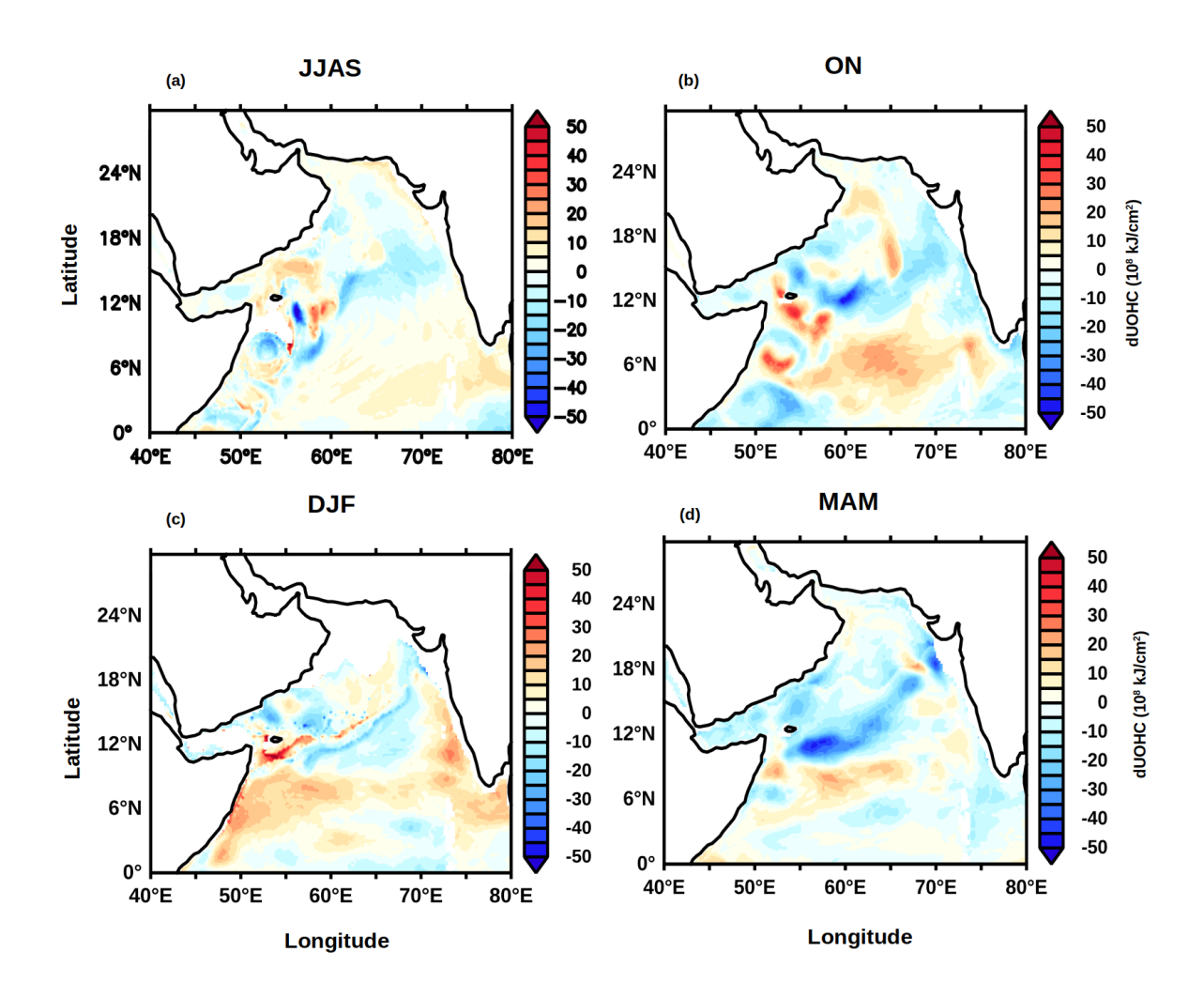


Figure 4.7: Difference of UOHC (dUOHC) of flood year (1988)- of drought year (2002) for (a)

JJAS, (b) ON, (c) DJF and (d) MAM.

We have also calculated the simulated annual cycle of area-averaged dUOHC (Figure 4.8) area-averaged over 50 °E: 70 °E; 4 °N:12 °N, the same region where we computed the dMLD, starting from April to the following year, May. Figure 4.8 shows a higher UOHC from the summer monsoon season to the following spring during the good monsoon years.

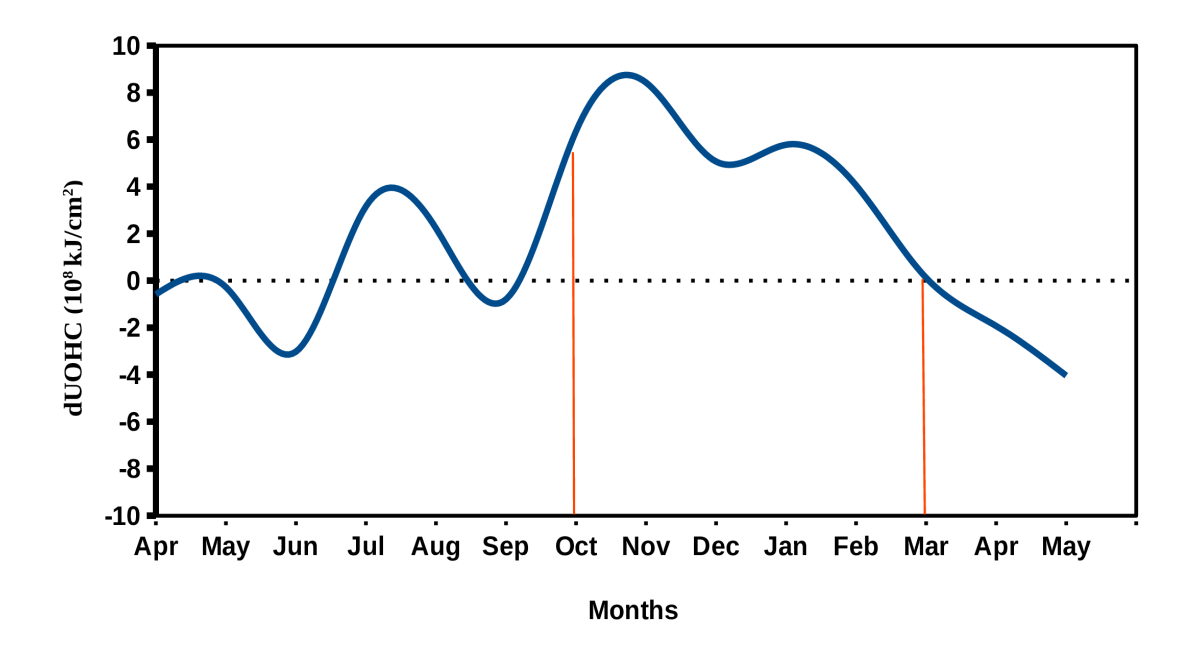


Figure 4.8: Time Series of dUOHC averaged over the box (50 °E: 70 °E; 4 °N: 12 °N)

4.5.3 Rossby wave

To decipher the role of downwelling Rossby waves in the modulation of the heat signal in the AS in the model, we present two Hovmöller plots of the depth of the $20\,^{\circ}$ C isotherm (D_{20}) averaged over the latitudes 4° to 12° N for the years 1988 and 2002, respectively (Figure 4.9). The D_{20} is commonly used to represent the variations in the thermocline in the tropical region and used in the present study to infer the signature of propagation of Rossby waves (Brandt et al., 2002; Jury et al., 2004; Rao et al., 2002; Prasanna Kumar et al., 2005). Figures 4.9a and 4.9b show that the westward propagation of deeper values of D_{20} isotherm during December to March period. This represents the signature of the Rossby waves in the model, which is consistent with K22. Furthermore, the model is able to capture the thermocline variations between the two years. In 1988, the depth of the thermocline is deeper as compared to 2002.

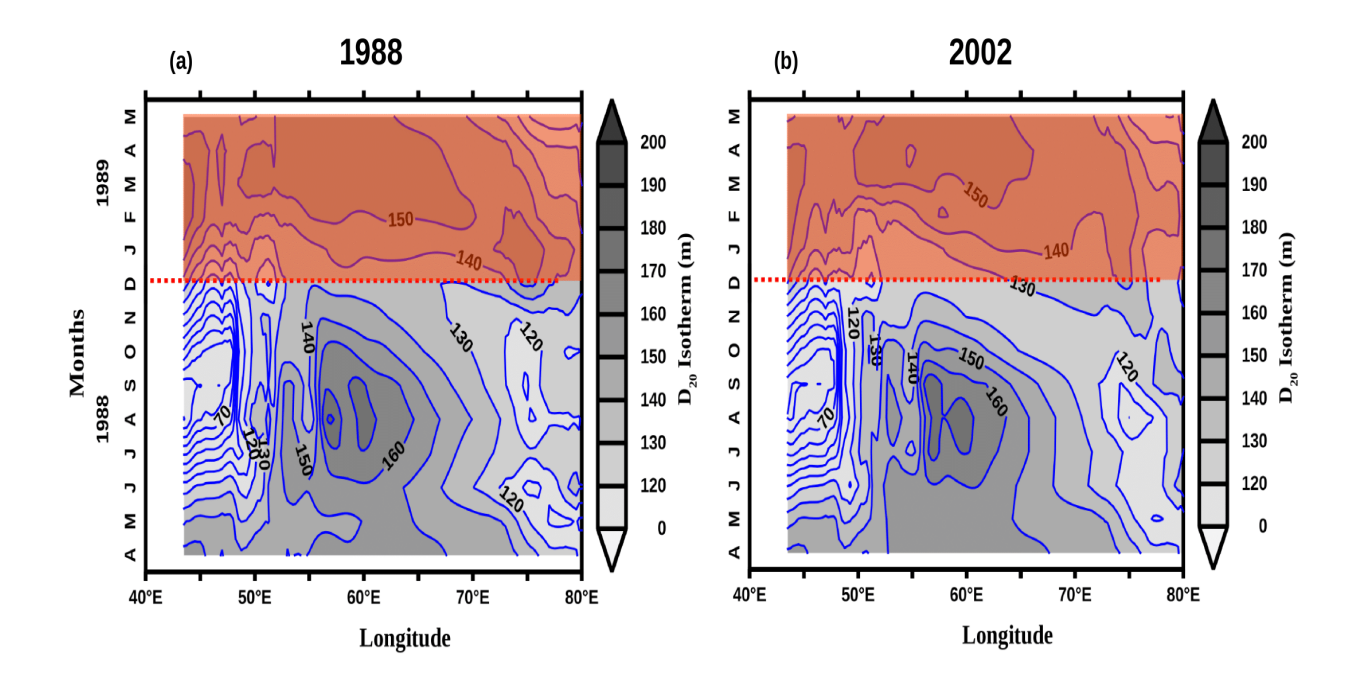


Figure 4.9: Hovmöller plot of depth of 20 $^{\circ}$ C isotherm (D₂₀ , m) (a) 1988 and (b) 2002 averaged over the latitudes from 4 $^{\circ}$ N to 12 $^{\circ}$ N in the Arabian Sea.

To validate our model results during 1988 and 2002 the SODA reanalysis data was used (Figure 4.10). The spatial and temporal structure of dUOHC in the AS during the seasons subsequent to the ISM are similar and consistent with our model results.

To further support our inferences from the model about the role of FJ in regulating the ISM rainfall through modulations in the MLD and UOHC during good and bad monsoons, a similar analysis was carried out for the years 1994, a good monsoon year, and 2014 a poor summer monsoon year. The spatial structure of dMLD and dUOHC between good (1994) and bad (2014) monsoon years are shown in Figure 4.11. These figures show a similar structure as shown in Figure 4.7. Hence, we conclude that our inferences on the good and band monsoon are robust and also consistent with K22.

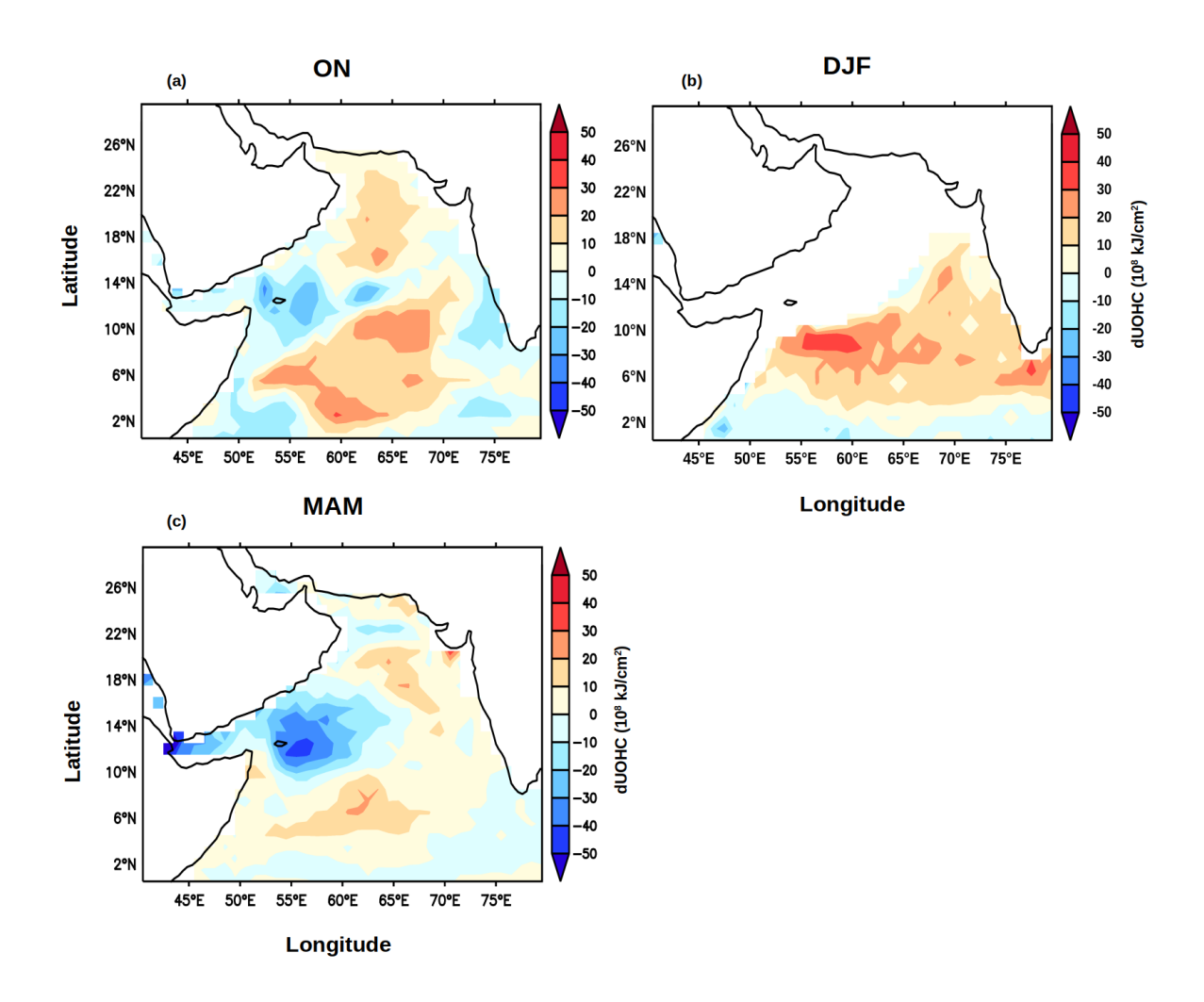


Figure 4.10: Difference of UOHC (dUOHC) of flood year (1988) - drought year(2002) for (a)

ON, (b) DJF and (c) MAM from SODA 3.3.1 reanalysis datasets.

Therefore, the model experiments demonstrate that (i) the FJ signal is stored through the boreal spring through various mechanisms in agreement with K22 and (ii) there are interannual variations in the lagged UOHC commensurate with the strength of the FJ over the AS during summer monsoon.

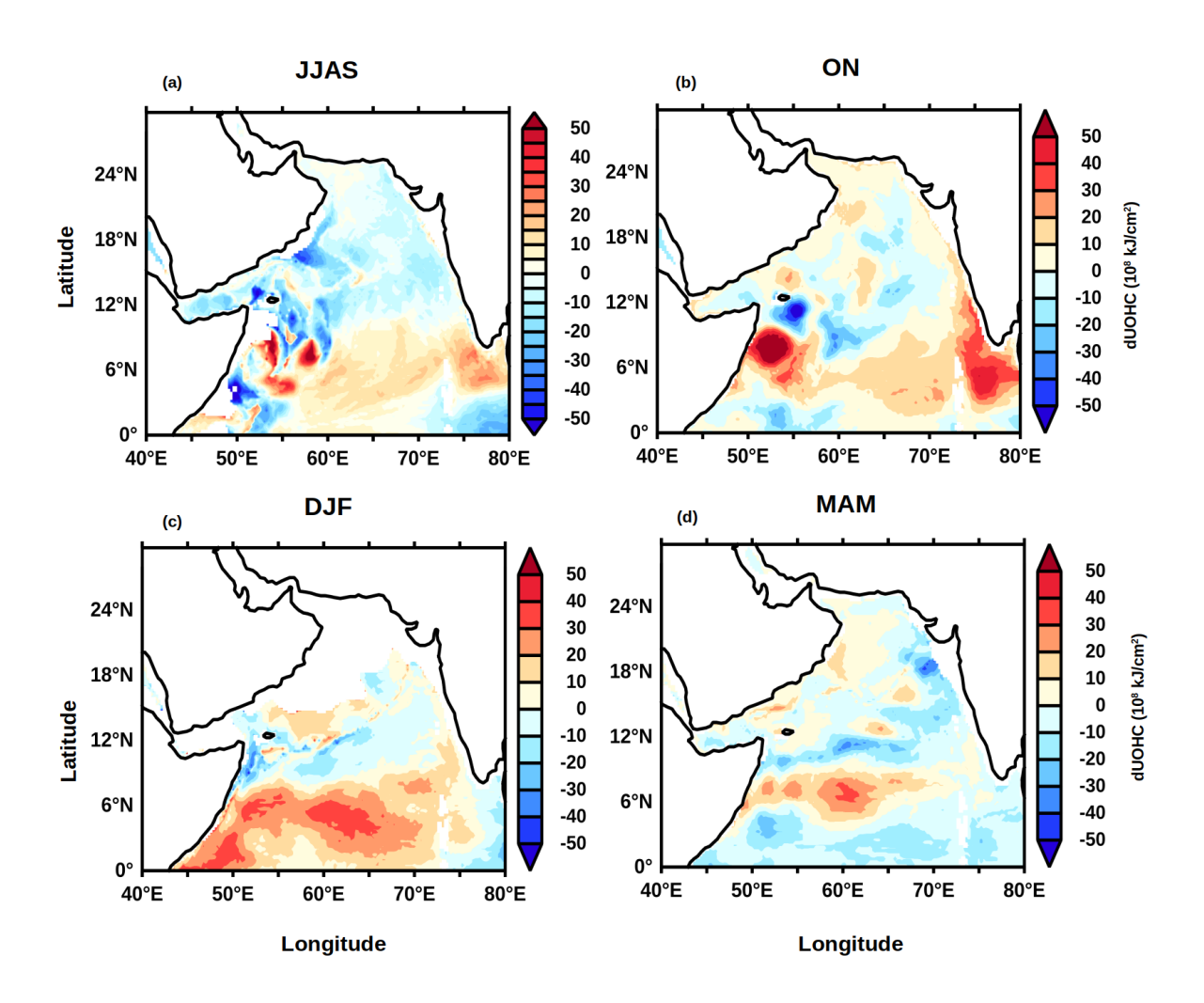


Figure 4.11: Difference of UOHC (dUOHC) of flood year (1994) - of drought year (2014) for (a) JJAS, (b) ON, (c) DJF and (d) MAM.

4.6 Conclusion

In this study, using an Indian ocean regional version of the MOM5 model, we have explored the impact of FJ strength on the subsurface AS during the good monsoon year of 1988 and a weak monsoon year of 2002, and for verification, during the good and bad summer monsoon years of 1994 and 2014, respectively. Comparisons with our analysis of SODA 3.3.1 reanalysis datasets for the period 1980-2015 show that the model faithfully simulates the seasonal cycle of the oceanic variables (e.g., MLD, UOHC) of the AS.

Chapter 3 (published as Kushwaha et al., 2022) based on observational and reanalysis datasets investigated the effect of FJ on the heat content in the AS, and hypothesized that the FJ-induced heat signal during the ISM is preserved in the UOHC of the AS till the following winter season. Our model study, carried out to confirm the hypothesis and also to understand the implications of the interannual variability of the ISM, shows that the dMLD values are positive during the following fall through spring seasons (i.e., ON, DJF, and MAM) in the southern AS. Also, the dUOHC values are positive during the subsequent seasons. This dUOHC signature ascertains the increase of UOHC for the three consecutive seasons after a good monsoon (1988 and 1994) with a strong FJ. Results from our sensitivity simulations strongly suggest that the observed increase in UOHC of the AS following the good monsoon years is due to an increase in the strength of overlying FJ.

Chapter 5

Impact of Indian summer monsoon on the frequency of post-monsoon tropical cyclones in the north Indian ocean

In this chapter, I explore the potential relevance of the Indian Summer Monsoon on the post-monsoon tropical cyclone (TCs) frequency in the northern Indian Ocean (NIO). To this end, I explore the Gray-Sikka cyclogenesis conditions and find that the monsoon and cyclonic frequency in the Bay of Bengal are in phase, with heavier monsoons followed by higher tropical cyclone frequency. Meanwhile, for the Arabian Sea, the cyclonic frequency has been increasing irrespective of the monsoon.

5.1 Tropical Cyclone frequency of the post-monsoon season in the NIO

From our analysis of the TCs frequency data for 130 years from 1891 to 2021 in the NIO, we find that the average frequency of TCs in the BoB during the post-monsoon season of October-November, the peak TCs period (Subbaramayya & Rao, 1984) is 1.64 cyclones per year (Table 5.1). The frequency increases slightly by about 0.6% to 1.65 cyclones per year in the post-monsoon season of flood years. Whereas for the drought years, the post-monsoon cyclone frequency significantly decreases to 1.36 cyclones per year, a decrease of about 17%. In December, the average cyclone frequency in the BoB is 0.4 cyclones per year. Furthermore, the frequency

increases to 0.52 cyclones per year for the drought years, a 30% increase. Meanwhile, for the AS, the cyclone frequencies during ON increase for both the flood years (0.53) and the drought years (0.44) when compared to normal monsoon years (0.4). This is an increase of 32.5% for flood years and 10% for drought years. In December, during all the listed flood years, the BoB witnessed only one cyclone, and similarly, the AS saw only one cyclone each during flood and drought years. These statistics are in qualitative agreement with pioneering studies such as Subbaramayya and Rao (1984). Therefore, I focus only on the cyclone frequencies of ON in both seas. Note that when I mention about drought (flood) years, I essentially refer to anomalously dry (wet) conditions in the summer monsoon that immediately precedes the October-November.

		Normal Years	Flood years		Drought years	
		Frequency	Frequency	Difference (%)	Frequency	Difference (%)
BoB	ON	1.64	1.65	0.6	1.36	-17.1
	D	0.40	*	*	0.52	30
AS	ON	0.40	0.53	32.5	0.44	10
	D	0.05	*	*	*	*

Table 5.1: The frequency of TCs in the North Indian Ocean during ON over the period 130 years from 1891 to 2021. Periods with occurence of only one cyclone has been marked as *.

5.2 The cyclogenesis parameters in the NIO

To understand the cause of the observed changing frequencies of cyclones in drought/flood years, we look at the various parameters for tropical cyclogenesis. Gray (1968, 1975) and Sikka (1977) define six conditions for tropical cyclogenesis, 1) The Coriolis parameter, 2) Low vertical shear of

winds from surface to upper troposphere, 3) High ocean thermal energy, 4) High low-level vorticity, 5) High values of surface to the mid-atmospheric equivalent potential temperature gradient 6) High mid-tropospheric relative humidity. As the Coriolis parameter remains the same for BoB or AS, we explore the other five conditions..

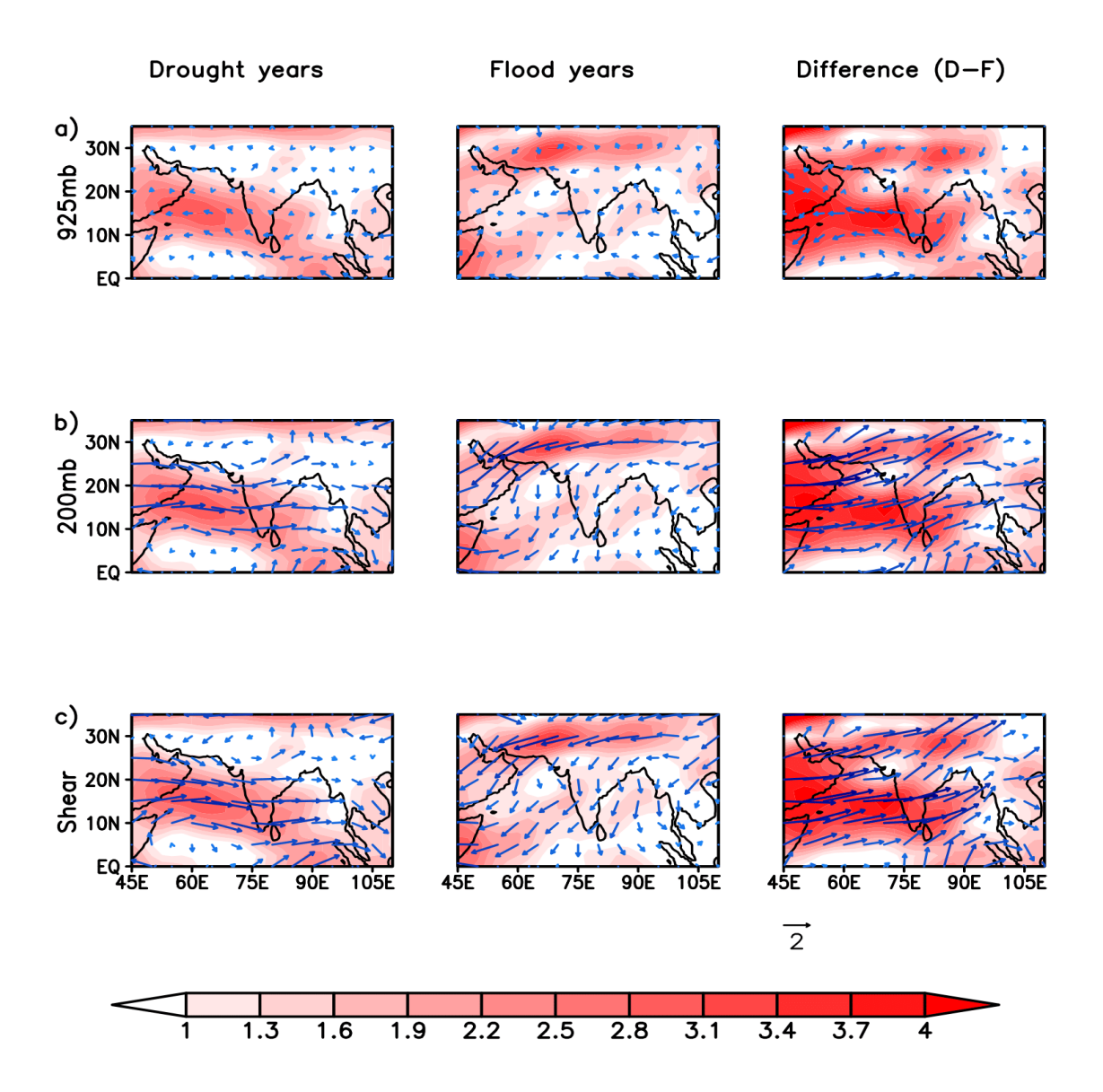


Figure 5.1: A Composites of vertical shear of winds during ON for drought years, flood years and their differences in columns respectively. The rows show winds at a) 925 hpa b) 200hpa c) the shear (200mb-925mb). The wind shear vector magnitudes are shaded.

Figure 5.1 shows the composites of vertical shear of winds during ON for dry monsoonal drought years, flood years and their differences. A low wind shear is conducive for cyclogenesis (DeMaria, 1996; Gray, 1966; Ramage, 1959; Riehl and Shafer, 1944). The wind shear is low in flood years over both the BoB and the AS explaining the increased frequencies of cyclones in flood years. The increased wind shear during drought years over BoB causes a decrease of 17% in its cyclone frequency. But as for the AS, the cyclone frequency shows an increase in drought years though the wind shear remains high except in latitudes below 10°N.

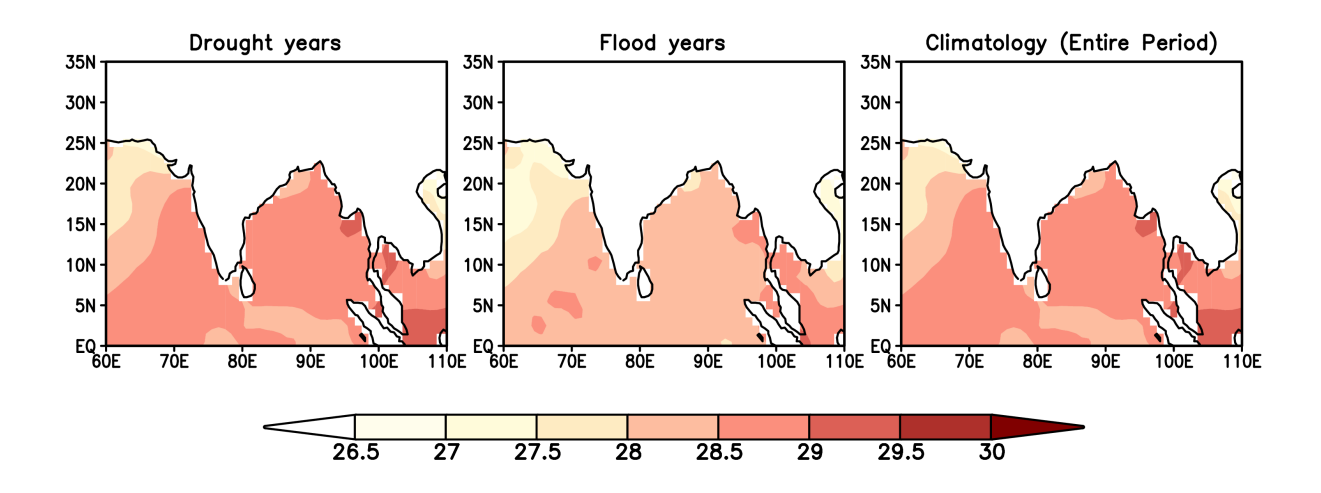


Figure 5.2: Composites of SST climatology during a) drought years and b) flood years and c) All years.

The ocean heat is the source of energy for tropical cyclogenesis and cyclone intensification (Rao et al., 1999; 2000; Singh and Roxy, 2022 and the references therein). Palmen (1948) states that the minimum SST required for cyclogenesis is 26 °C. Moreover, the energy source is not limited to the SST, and the TCHP also play a significant part in TCs activity (Shay et al., 2000; Ali et al., 2004; Ghetiya and Nayak et al., 2020; Girishkumar et al., 2015; Sharma and Ali, 2004). Maneesha et al. (2015) stresses on the importance of TCHP, referred to as the upper ocean heat content, and set a threshold value of 40 kJ/cm² as necessary for cyclogenesis and intensification in the Bay of Bengal.

Figure 5.2 and Figure 5.3 shows the SST and TCHP composites over NIO during flood and drought years. Though the SST is slightly lower (~0.5°C) during flood years, the average SST does not fall below 28°C, a surplus of 2°C from the prerequisite 26°C necessary for cyclogenesis. Similarly, TCHP over the NIO shows that irrespective of the monsoon, the TCHP remains higher than 40 kJ/cm² during ON over the entire NIO, with most of NIO having values higher than 80 kJ/cm².

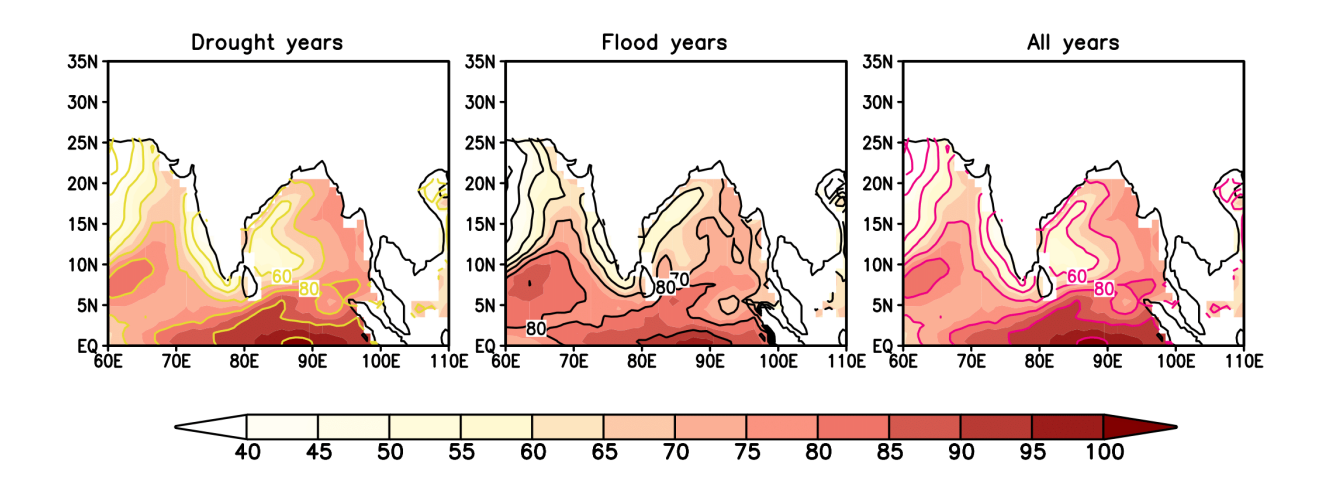


Figure 5.3: Composites of TCHP climatology during a) drought years and b) flood years and c) All years.

Cyclogenesis requires large values of low-level vorticity at ~925Mb height (Gray, 1968; Prajeesh & Ashok, 2013; Riehl, 1954). The low-level vorticity remains low over most of the NIO during drought years and higher in flood years. The difference plot (Figure 5.4) shows that the vorticity is lesser over most of BoB during drought years except at the head of the bay. Also, the vorticity shows higher values in drought years over the south-eastern AS.

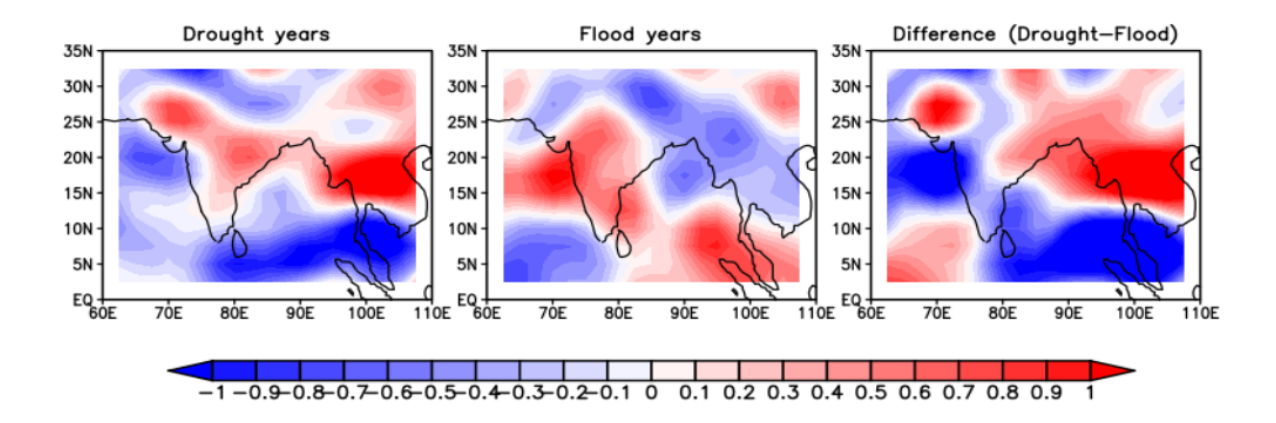


Figure 5.4: Composites of anomalous vorticity at 925 hPa during a) drought years b) flood years c) the difference between drought and flood years.

Our analysis of the mid-tropospheric humidity (RH; averaged over 500hpa to 700hpa, Figure 5.5) shows that the flood years are more humid than drought years, which again is favourable for cyclogenesis and cyclone intensification. The increase in humidity is observed over both the seas in the NIO.

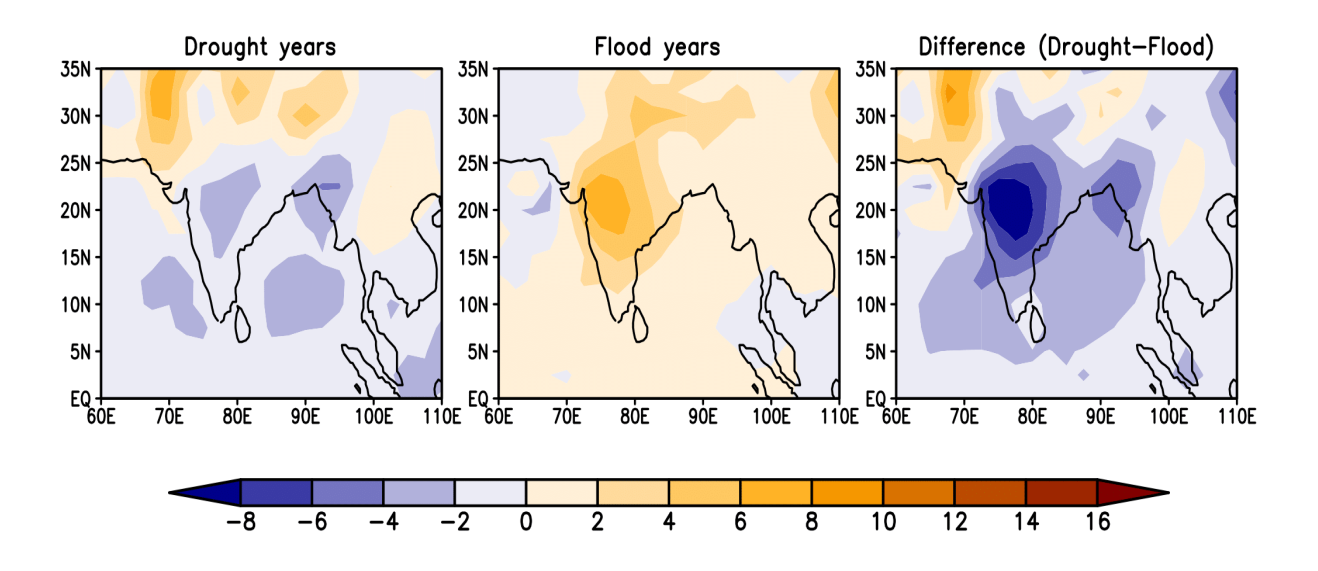


Figure 5.5: Composites of the mid-tropospheric humidity (RH; averaged over 500hpa to 700hpa) during a) drought years b) flood years c) the difference between drought and flood years.

Meanwhile, the potential temperature from the surface to the mid-troposphere (averaged over 500hpa to 1000hpa; Figure 5.6) shows higher values during drought years and lower values during flood years. This is to be expected as precipitation can cool surface temperatures (Boudreau, 1965; Flament & Sawyer, 1995; Ramos et al., 2022).

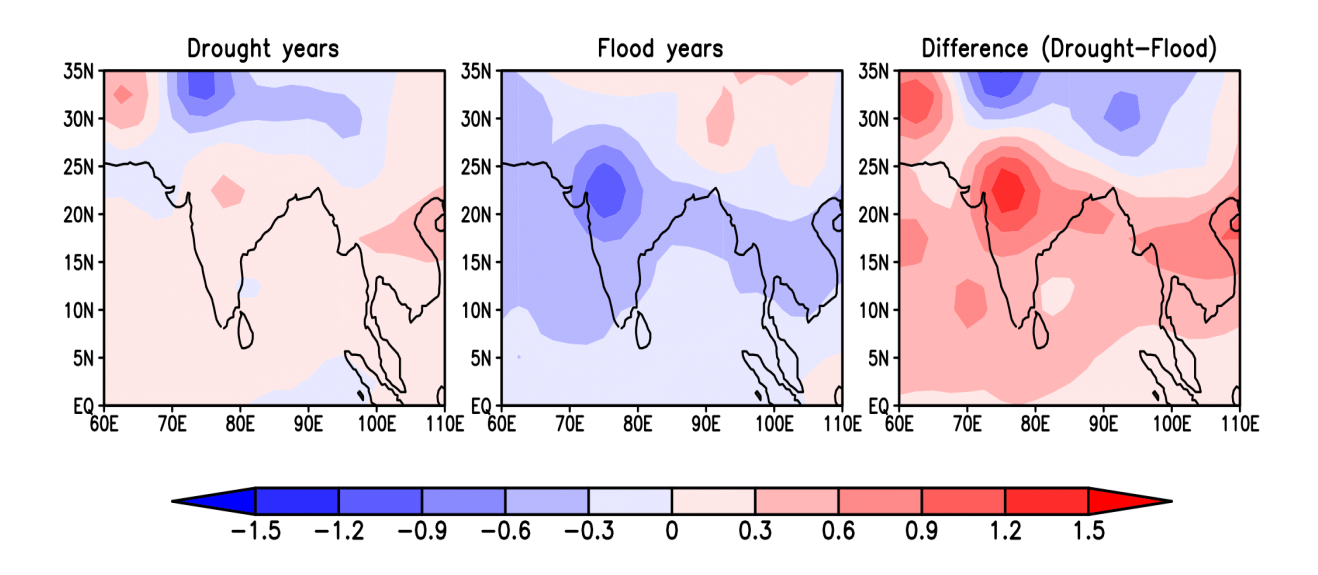


Figure 5.6: Composites of the potential temperature from the surface to mid-troposphere (averaged over 500hpa to 1000hpa) during a) drought years b) flood years c) the difference between drought and flood years.

5.3 Cyclogenesis Potential in the Bay of Bengal

The above analysis shows that the influence of ISM on the TCs frequency is potentially more prominent for BoB than for AS, where the relationship is slightly ambiguous. In order to understand how the summer monsoon season conditions influence the TCs that occur in the NIO in the next season, We then calculated the Cyclogenesis potential parameter (GPP, Kotal et al., 2009) in the BoB during the post-monsoon season for both flood and drought years. As seen in Figure 5.7, the

GPP value is higher during flood years over most of BoB, confirming our findings in the previous section and providing. A connection between the summer monsoon variations and the post-monsoon TCs, except in the southeastern region. The southeastern region could be influenced by the Indonesian throughflow, and probably hence the weak association. As for AS, the GPP shows a large variation, and the impact of ISM on cyclogenesis is unclear, though the frequency remains affected.

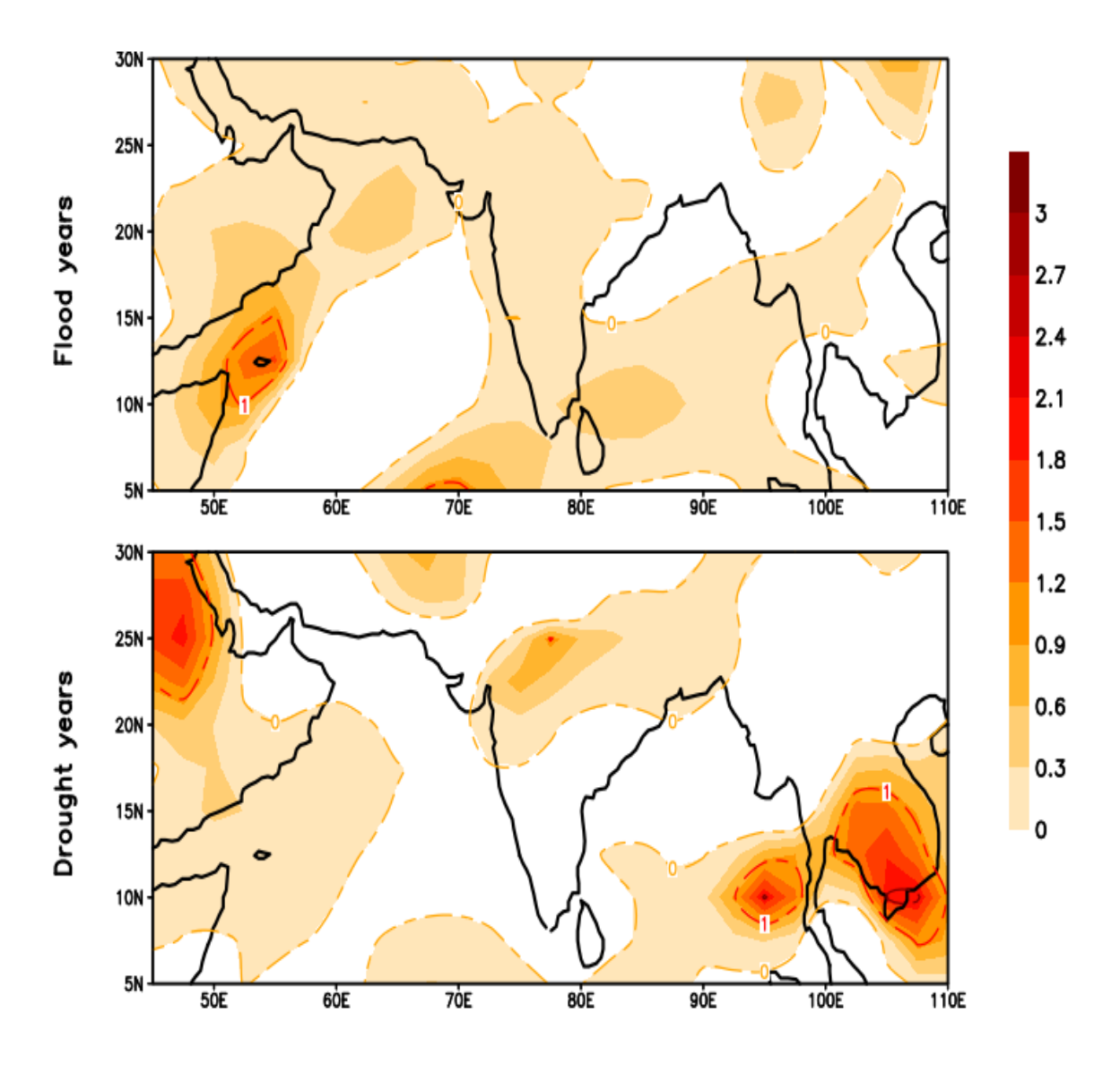


Figure 5.7: Cyclogenesis Potential Parameter (GPP) over NIO during flood and drought years.

5.4 Conclusion

Our study shows that the frequency of post-monsoon cyclones is likely connected to the preceding monsoon. A good monsoon season with greater than normal rainfall is followed by increased cyclonic activity in BoB and AS. The AS shows a very strong increase of 32.5%. After a monsoon with deficit rainfall, the cyclone frequency falls in the BoB by 17.1% but increases slightly in the AS. Our analysis of Gray's parameters for cyclogenesis shows that after a deficit monsoon, the humidity in the mid-troposphere, vorticity in the low- level, and TCHP are lower than in normal years, and the vertical shear is higher over most of the NIO. All of these factors contribute to the reduced cyclonic frequency in the BoB. Whereas, for the AS, the TCHP and low-level vorticity are slightly higher in the south-eastern AS, contributing to a slight increase of cyclones even in the drought years. The calculation of GPP ascertains that flood years show a higher potential for cyclogenesis over the BoB.

The frequency of flood years has considerably decreased in recent decades. The most recent flood year, 2019, comes after a gap of 25 years, the second recent year being 1994. Interestingly, both these years are positive IOD years (e.g., Ashok et al., 2001; Ratna et al., GRL, 2020?), which are known to cause anomalously high rainfall over India (e.g., Ashok et al., 2001, 2004; Ashok and Saji et al., 2007). Meanwhile, recent years show an increase in droughts, with the flood-less 25 years having 6 drought years. This non-linear change in frequencies of flood and drought years might have caused a skewness in the results of the flood year cyclone frequency. This could be further explored. Nevertheless, this study shows that the TCs frequency during post-monsoon season can be conjectured at least a season ahead.

Chapter 6

Conclusions and Future Scope

Over a billion people depend on the Indian summer monsoon (ISM) for their livelihood. Therefore, any new scientific knowledge that advances our comprehension of the ISM and its effects on different air-sea interaction processes is of incalculable value. This thesis aims to investigate and comprehend the effects of the Indian Summer Monsoon on numerous ocean atmospheric interaction systems in the NIO on a interannual time sacles.

6.1 Summary

In Chapter 1, I describe the Indian Summer Monsoon, its characteristics, such as the Findlater jet (FJ), and the variables that determine the variability of the ISM through a study of the literature that is currently accessible. I give a thorough explanation of the Findlater jet and the connections between it and the ISM rainfall. I also discuss the frequency of TCs in the NIO and how they relate to ISM. Finally, I discuss the connection between tropical cyclones (TCs) in the north Indian ocean and the heat content of the upper ocean. From the review, I arrive at various existing gaps. The impact of FJ on the subsurface heat content in the AS during the subsequent seasons is not fully understood. Also, the influence of ISM rainfall on the post-monsoon TCs in the NIO needs to be further studied. Based on these gaps, I define the objectives of my thesis as follows:

1 To study the response of the Arabian sea to the Findlater Jet and understand the dynamics behind the influence of Findlater jet to the Arabian Sea.

- A modeling approach to ascertain the response of the Arabian Sea due to the influence of the Findlater Jet.
- To study the impact of the Indian summer monsoon on the tropical cyclones during the postmonsoon in the north Indian ocean.

The rest of the chapters document my research achieve the objectives.

Chapter 2 describes all data sources (observations, reanalyses) used in this study. The data processing techniques performed on the model outputs have also been detailed. All the mathematical expressions used in computing relevant dynamical and physical parameters are also provided. All the statistical techniques used in this thesis are clearly presented and explained.

In Chapter 3, I briefly present the ISM mean circulation in the Arabian Sea and examine how the related oceanic fields ensure the preservation of heat-induced during the summer monsoon months till the subsequent winter months. I also bring out the contiguous chain of inherent seasonal processes in the AS from boreal summer through spring in the following year. My findings, based on the analysis of observational and reanalyses datasets, suggest that the signature of the FJ is stored in the southern AS as upper ocean heat content (UOHC), a form of heat energy, for three consecutive seasons. I then proceed to give a comprehensive explanation of the processes involved in storing the signature during the subsequent seasons. This chapter fulfills the first objective of the thesis.

Chapter 4, I introduce the ocean model and its setup and elaborate upon the required sensitivity experiments and the results from them. The experiments essentially involve forcing the MOM5 model with (a) good summer monsoon real winds (1988, 1994) and (b) bad summer monsoon real winds (2002, 2014) over the north Indian ocean while keeping the other forcing fields climatological. Our model studies were carried out to confirm the hypothesis proposed in chapter 2 about the links between the ISM and subsurface heat content from a seasonal cycle perspective and also to understand the implications of the interannual variability of the ISM (chapter 3). Our results ascertain the relationship between the ISM and UOHC and the mechanisms we proposed. Furthermore, our results show that the distribution of the difference in the seasonal mixed layer depth (dMLD) in the AS between a good summer monsoon and a bad summer monsoon is mostly positive in the southern AS during the following fall through spring seasons. Also, the dUOHC values are positive during the subsequent seasons. The simulated dUOHC signature ascertains higher o UOHC for three consecutive seasons after a good summer monsoon with strong FJ, such as in the years of 1988 and 1994, relative to a weak summer monsoon in the years of 1988 and 2002. Results from our sensitivity simulations strongly suggest that the increase in UOHC following a good summer monsoon is indeed due to an increase in the strength of FJ in the Arabian Sea, with a subsequent amplification of the associated seasonal processes described in Chapter 2. This chapter comprehensively addresses and fulfills the second objective.

In chapter 5, I analyze the frequency of post-monsoon TCs in the north Indian ocean for the period 1871-2021 and how they are affected by the ISM rainfall. We find that the frequency of post-monsoon cyclones is strongly associated with the preceding monsoon. A good summer monsoon season with greater than normal rainfall is followed by anomalously increased cyclonic activity in BoB and AS. We then explore the factors responsible for this increase. Our analysis of Gray-Sikka parameters for tropical cyclogenesis shows that after a deficit monsoon, the humidity in the mid-

troposphere, vorticity in the low- level, and TCHP are lower than in normal years, and the vertical shear is higher over most of the NIO. All of these factors contribute to the reduced cyclonic frequency in the BoB. Whereas, for the AS, the TCHP and low-level vorticity are slightly higher in the south-eastern AS, contributing to the slight increase of cyclones even in the drought years. The genisis potential parameter (GPP) calculation ascertains that flood years show a higher potential for cyclogenesis over the BoB. This chapter addresses and fulfills the third objective.

6.2 Future Scope

As we know, no study is ever fully finished since each completed study develops some new queries, and the cycle keeps going. In the following, we present ideas for further research which is beyond the scope of this thesis.

The aspect of the variability of Findlater jet-induced heat in the Arabian sea highlighted in Chapters 3 & 4 needs to be further explored. For example, the interaction of heat induced by the Findlater jet to the subsequent Indian summer monsoon rainfall and whether the knowledge contributes to any improvements in the prediction skills of ISM rainfall needs attention. Also, the impact of this anomalous heat on the biogeochemistry of the AS in the subsequent seasons after the ISM would be another interesting issue to explore. The interannual variability of the UOHC and its interaction with the tropical climate drivers (e.g., ENSO, IOD) can be looked at further through observational and reanalyzed data analysis and through sensitivity experiments with a global circulation model.

The TCs frequency during the drought years increases in the AS, as mentioned in Chapter 5. The non-linear change in the frequencies of flood and drought years in recent decades may have caused a skewness in the results of the flood year cyclone frequency. This aspect needs to be explored further. Also, the dynamical processes responsible for the increase in the TCs frequency during the

post-monsoon season have to be explored in future studies using ocean general circulation models and coupled models. Further, the analysis carried out in chapter 5 is statistical in nature. The proposed mechanism through which the summer monsoon affects the TCs in the following season through storage of heat content needs to be further explored, and the details of the process need a mechanistic assertion. In this context, Given the lack of oceanic observations in the NIO in the past, we plan to conduct sensitivity experiments with a global climate model in the future.

List of References

- Akhil, V.P., Durand, F., Lengaigne, M., et al., 2014. A modeling study of the processes of surface salinity seasonal cycle in the Bay of Bengal. J. Geophys. Res. Ocean 119, 3926–3947. https://doi.org/10.1002/2013JC009632.
- Alam, M.M., Hossain, M.A., Shafee, S., 2003. Frequency of Bay of Bengal cyclonic storms and depressions crossing different coastal zones. Int. J. Climatol. 23, 1119–1125. https://doi.org/10.1002/joc.927.
- Ali, A., 1999. Climate change impacts and adaptation assessment in Bangladesh. Clim. Res. 12.
- Ali, M. M., D. Swain, and R. A. Weller (2004), Estimation of ocean subsurface thermal structure from surface parameters: A neural network approach, Geophys. Res. Lett., 31, L20308, doi:10.1029/2004GL021192.
- Altabet, M., M. J. Higginson, and D. W. Murray (2002), The effect of millennial-scale changes in Arabian Sea denitrification on atmospheric CO2, Nature, 415, 159 162.
- Anderson, D. L. T. The low-level jet as a western boundary current. Mon. Weather. Rev. 104, 907–921 (1976)
- Anderson, D. M., J. T. Overpeck, and A. K. Gupta (2002), Increase in the Asian southwest monsoon during the past four centuries, Science, 297, 596 599.
- Annamalai, H., and R. Murtugudde (2004), Role of the Indian Ocean in regional climate variability, in Earth Climate: The Ocean-Atmosphere Interaction, Geophys. Monogr. Ser., vol. 147, edited by C. Wang, S.-P. Xie and J. A. Carton, pp. 213 246, AGU, Washington, D. C.
- Archer, C. & Caldeira, K. Historical trends in the jet streams. Geophys. Res. Lett. 35, L08803.
- Ardanuy, P. On the observed diurnal oscillation of the Somali jet. Mon. Weather Rev. 107, 1694-

- 1700 (1979)
- Ashok, K., Guan, Z., Saji, N. H. and Yamagata, T., 2004, "Individual and combined influences of the ENSO and Indian Ocean Dipole on the Indian summer monsoon", J. Climate, 17, 3141-3155.
- Ashok, K., Guan, Z., and Yamagata, T. (2003), Influence of the Indian Ocean Dipole on the Australian winter rainfall, Geophys. Res. Lett., 30, 1821, doi:10.1029/2003GL017926, 15.
- Ashok, K., Guan, Z. and Yamagata, T. (2001). Impact of the Indian Ocean dipole on the relationship between the Indian monsoon rainfall and ENSO. Geophysical Research Letters 28: doi: 10.1029/2001GL013294. Issn: 0094-8276.
- Ashok, K., Soman, M. & Satyan, V. Simulation of Monsoon Disturbances in a GCM . Pure appl. geophys. 157, 1509–1539 (2000). https://doi.org/10.1007/PL00001131
- Babu, K.N., Sharma, R., Agarwal, N., et al., 2004. Study of the mixed layer depth variations within the north Indian Ocean using a 1-D model. J. Geophys. Res. Ocean 109. https://doi.org/10.1029/2003JC002024.
- Balaguru, K., Ruby Leung, L., Yoon, J.H., 2013. Oceanic control of Northeast Pacific hurricane activity at interannual timescales. Environ. Res. Lett. 8, 44009. https://doi.org/10.1088/1748-9326/8/4/044009
- Balmaseda, M. A., Mogensen, K. and Weaver, A. T. (2013), Evaluation of the ECMWF ocean reanalysis system ORAS4. Q.J.R. Meteorol. Soc., 139: 1132–1161. doi: 10.1002/qj.2063.
- Barber RT, Marra J, Bidigare RC et al (2001) Primary productivity and its regulation in the Arabian Sea during 1995. Deep-Sea Res II 48:1127–1172. doi:10.1016/S0967-0645(00)00134-X
- Bauer, S., Hitchcock, G. & Olson, D. Influence of monsoonally-forced Ekman dynamics upon surface layer depth and plankton biomass distribution in the Arabian Sea. Deep Sea Res. Part A. 38, 531–553 (1991)

- Beal, L.M., Vialard, J., Roxy, M.K., et al., 2020. A roadmap to IndOOS-2: Better observations of the rapidly-warming Indian Ocean. Bull. Am. Meteorol. Soc. 1–50 https://doi.org/10.1175/bams-d-19-0209.1
- Behera, S. K., and T. Yamagata, 2003: Influence of the Indian Ocean Dipole on the Southern Oscillation. J. Meteor. Soc. Japan, 81, 169–177.
- Bhardwaj, P., Pattanaik, D.R., Singh, O., 2019. Tropical cyclone activity over Bay of Bengal in relation to El Niño-Southern Oscillation. Int. J. Climatol. 39, 5452–5469. https://doi.org/10.1002/joc.6165.
- Bhaskar Rao, D. V. & Ashok, K. Simulation of Tropical Cyclone Circulation over Bay of Bengal Using the Arakawa-Schubert Cumulus Parametrization. Part I -- Description of the Model, Initial Data and Results of the Control Experiment. Pure and Applied Geophysics 156, 525–542 (1999).
- Bhaskar Rao, D. V. & Ashok, K. Simulation of Tropical Cyclone Circulation Over the Bay of Bengal Using the Arakawa-Schubert Cumulus Parameterization. Part II: Some Sensitivity Experiments. Pure and Applied Geophysics 158, 1017–1046 (2001)
- Boudreau, R. D., 1965: Skin temperature of the sea as determined by radiometer. Ref. 65-15T, A and M proj 286, Texas Bull. Amer. Meteor. Soc., 78, 197–208.
- Boos, W. R. & Emanuel, K. A. Annual intensification of the Somali jet in a quasi equilibrium framework: Observational composites. Q. J. R. Meteorol. Soc. 135, 319–335
- Brandt, P. et al. Annual Rossby waves in the Arabian Sea from TOPEX/POSEIDON altimeter and in situ data. Deep-Sea Res. Part II 49, 1197–1210 (2002).
- Carton, J. A., Chepurin, G. A. & Chen, L. SODA3: A new ocean climate reanalysis. J. Clim. 31, 6967–6983 (2018)
- Chaitanya, A.V.S., Lengaigne, M., Vialard, J., et al., 2014. Salinity measurements collected by

- fishermen reveal a "river in the sea" flowing along the eastern coast of India. Bull. Am. Meteorol. Soc. 95, 1897–1908. https://doi.org/10.1175/BAMS-D-12-00243.1.
- Chatterjee, A., Shankar, D., McCreary, J., & Vinayachandran, P. (2013). Yanai waves in the western equatorial Indian Ocean. Journal of Geophysical Research: Oceans, 118, 1556–1570. https://doi.org/0.1002/jgrc.20121
- Chatterjee, A., Kumar, B. P., Prakash, S., & Singh, P. (2019). Annihilation of the Somali upwelling system during summer monsoon. Scientific reports, 9(1), 7598. https://doi.org/10.1038/s41598-019-44099-1
- Chatterjee, A., Shankar, D., Shenoi, S., Reddy, G., Michael, G., Ravichandran, M., et al. (2012). A new atlas of temperature and salinity for the North Indian Ocean. Journal of Earth System Science, 121(3), 559–593.
- Chatterjee, A., Shankar, D., McCreary, J., Vinayachandran, P., & Mukherjee, A. (2017). Dynamics of Andaman Sea circulation and its role in connecting the equatorial Indian Ocean to the Bay of Bengal. Journal of Geophysical Research: Oceans, 122, 3200–3218. https://doi.org/10.1002/2016JC012300
- Charles, C. D., D. E. Hunter, and R. G. Fairbanks (1997), Interaction between the ENSO and the Asian monsoon in a coral record of tropical climate, Science, 277, 925 927.
- Chen, S., Campbell, T.J., Jin, H., et al., 2010. Effect of two-way air-sea coupling in high and low wind speed regimes. Mon. Weather Rev. 138, 3579–3602. https://doi.org/10.1175/2009MWR3119.1.
- Chirokova, G., and P. J. Webster (2006), Interannual variability of Indian Ocean heat transport, J. Clim., 19(6), 1013–1031.
- Chowdhury, R.R., Prasanna Kumar, S., Narvekar, J., Chakraborty, A., 2020b. Back-to-back occurrence of tropical cyclones in the Arabian Sea During October–November 2015: causes

- and responses. J. Geophys. Res. Ocean 125, 1–23. https://doi.org/10.1029/2019JC015836.
- Cione, J.J., Uhlhorn, E.W., 2003. Sea surface temperature variability in hurricanes: Implications with respect to intensity change. Mon. Weather Rev. 131, 1783–1796. https://doi.org/10.1175//2562.1.
- Clark CO, Cole JE, Webster PJ (2000) Indian Ocean SST and Indian summer rainfall: predictive relationships and their decadal variability. J Clim. doi:10.1175/1520-0442(2000)013<2503:IOSAIS>2.0.CO;2
- Dimri AP, Niyogi D, Barros AP et al (2015) Western disturbances: a review. Rev Geophys 53:225–246. doi:10.1002/2014RG000460
- Dimri AP (2013) Intraseasonal oscillation associated with the Indian winter monsoon. J Geophys Res Atmos 118:1189–1198. doi:10.1002/jgrd.50144
- Duing, W., and A. Leetma (1980), Arabian Sea cooling: A preliminary heat budget, J. Phys. Oceanogr., 10, 307–312.
- Emanuel, K.A., 1986. An air-sea interaction theory for tropical cyclones. Part I: steady state maintenance. J. Atmos. Sci. 43, 585–604.
- Felton, C.S., Subrahmanyam, B., Murty, V.S.N., 2013. ENSO-modulated cyclogenesis over the Bay of Bengal. J. Clim. 26, 9806–9818. https://doi.org/10.1175/JCLI-D-13-00134.1.
- Findlater, J. Interhemispheric transport of air in the lower troposphere over the western Indian Ocean. Quart. J. R. Meteorol. Soc. 95, 400–403 (1969).
- Flament, P. and Sawyer, M., 1995: Observations of the effect of rain temperature on the surface heat flux in the intertropical convergence zone. J. Phys. Oceanogr., 25:3, 413-419
- Gadgil, S., 2018: The monsoon system: Land–sea breeze or the ITCZ? Journal of Earth System Science, 127 (1), 1.

- Gao, S., Chiu, L.S., 2010. Surface latent heat flux and rainfall associated with rapidly intensifying tropical cyclones over the western North Pacific. Int. J. Remote Sens. 31, 4699–4710. https://doi.org/10.1080/01431161.2010.485149.
- Gao, S., Jia, S., Wan, Y., et al., 2019. The role of latent heat flux in tropical cyclogenesis over the Western North Pacific: Comparison of developing versus non-developing disturbances. J. Mar. Sci. Eng. 7 https://doi.org/10.3390/jmse7020028.
- Gao, S., Zhai, S., Chiu, L.S., Xia, D., 2016. Satellite air-sea enthalpy flux and intensity change of tropical cyclones over the western North Pacific. J. Appl. Meteorol. Climatol. 55, 425–444. https://doi.org/10.1175/JAMC-D-15-0171.1.
- Ghetiya, Satyeshkumar & R.K. Nayak (2020) Genesis potential parameter using satellite derived daily tropical cyclone heat potential for North Indian ocean, International Journal of Remote Sensing, 41:23, 8934-8947, DOI: 10.1080/01431161.2020.1795299
- Giannini, A., R. Saravanan, and P. Chang (2003), Oceanic forcing of Sahel rainfall on interannual to interdecadal time scales, Science, 302, 1027 1030.
- Gill, A. E. Atmosphere-Ocean Dynamics (Academic Press, 1982)
- Girishkumar, M.S., Ravichandran, M., 2012. The influences of ENSO on tropical cyclone activity in the Bay of Bengal during October-December. J. Geophys. Res. Ocean 117, 1–13. https://doi.org/10.1029/2011JC007417.
- Girishkumar, M.S., Suprit, K., Chiranjivi, J., et al., 2014. Observed oceanic response to tropical cyclone Jal from a moored buoy in the south-western Bay of Bengal. Ocean Dyn. 64, 325–335. https://doi.org/10.1007/s10236-014-0689-6.
- Goswami, B., & Chakravorty, S. Dynamics of the Indian Summer Monsoon Climate. Oxford

 Research Encyclopedia of Climate Science.

 https://oxfordre.com/climatescience/view/10.1093/acrefore/9780190228620.001.0001/

acrefore-9780190228620-e-613

- Gray, W. M., 1968. Global view of the origin of tropical disturbances and storms. Mon. Weather Rev. 96 (10), 669–700.
- Gray, W. M. Tropical cyclone genesis. (Department of Atmospheric Science, Colorado State University, 1975).
- Gray, M. Hurricanes: Their formation, structure, and likely role in the tropical circulation.

 Meteorol. Over Trop. Oceans 155, 218 (1979).
- Griffies, S. M. (2012). Elements of the modular ocean model (MOM). GFDL Ocean Group Tech. Rep, 7, 620.
- Griffies, S. M., & Hallberg, R. W. (2000). Biharmonic friction with a Smagorinsky-like viscosity for use in large-scale eddy-permitting ocean models. Monthly Weather Review, 128(8), 2935–2946.
- Hallam, S., Guishard, M., Josey, S.A., et al., 2021. Increasing tropical cyclone intensity and potential intensity in the subtropical Atlantic around Bermuda from an ocean heat content perspective 1955-2019. Environ. Res. Lett. 16, 34052.
- Hoerling, M., and A. Kumar (2003), The perfect ocean for drought, Science, 299, 691 694.
- Hoskins, B. J. & Rodwell, M. J. A model of the Asian summer monsoon. Part I: The global scale. J. Atmos. Sci. 52, 1329–2134 (1995).
- Hsiung, J. (1985), Estimates of global oceanic meridional heat transport, J. Phys. Oceanogr., 15(11), 1405–1413.
- Indian Meteorological Department, 1943, "Climatological Atlas for Airmen".
- Iqbal, W. et al. Mean climate and representation of jet streams in the CORDEX South Asia simulations by the regional climate model RCA4. Theor. Appl. Climatol. 129, 1–19 (2017).

- Ivanochko, T., R. Ganeshram, G.-J. Brummer, G. Ganssen, S. Jung, S. Moreton, and D. Kroon (2005), Variations in tropical convection as an amplifier of global climate change at the millennial-scale, Earth. Planet. Sci. Lett., 235, 302 314.
- Jaimes, B., Shay, L.K., Uhlhorn, E.W., 2015. Enthalpy and momentum fluxes during hurricane earl relative to underlying ocean features. Mon. Weather Rev. 143, 111–131. https://doi.org/10.1175/MWR-D-13-00277.1.
- Joseph PV, Eishcheid JK, Pyle RJ. 1994. Interannual variability of the onset of the Indian summer monsoon and its association with atmospheric features, El Nino and sea surface temperature anomalies. ~ Journal of Climate 7: 81–105.
- Joseph, P. V. & Raman, P. L. Existence of low level westerly jet-stream over peninsular India during July. India J. Meteor. Geophys. 17, 407–410 (1966).
- Joseph, P. V. & Sijikumar, S. Intraseasonal variability of the low-level jet stream of the Asian summer monsoon. J. Clim. 17, 1449–1458 (2004).
- Jullien, S., Marchesiello, P., Menkes, C.E., et al., 2014. Ocean feedback to tropical cyclones: climatology and processes. Clim. Dyn. 43, 2831–2854. https://doi.org/10.1007/s00382-014-2096-6.
- Jung, S. J. A., G. R. Davies, G. Ganssen, and D. Kroon (2002), Decadal-centennial scale monsoon variations in the Arabian Sea during the early Holocene, Geochem. Geophys. Geosyst., 3 (10), 1060, doi:10.1029/2002GC000348.
- Jury, M. & Huang, B. The Rossby wave as a key mechanism of Indian Ocean climate variability.

 Deep Sea Res. I(51), 2123–2136 (2004)
- Kalnay, E., Kanamitsu, M., Kistler, R., Collins, W., Deaven, D., Gandin, L., et al., 1996. The NCEP/NCAR 40-year reanalysis project. B. Am. Meteorol. Soc. 77, 437–471. doi:10.1175/1520-0477(1996)077<0437:TNYRP>2.0.CO;2.

- Kaplan, J., DeMaria, M., 2003. Large-scale characteristics of rapidly intensifying tropical cyclones in the North Atlantic basin. Weather Forecast. 18, 1093–1108. https://doi.org/10.1175/1520-0434(2003)018<1093:LCORIT>2.0.CO;2.
- Kaplan, A., Y. Kushnir, M. A. Cane, and M. B. Blumenthal (1997), Reduced space optimal analysis for historical data sets: 136 years of Atlantic Sea surface temperatures, J. Geophys. Res., 102(D13), 27,835–27,860.
- Kotal, S.D., Kundu, P.D., Bhowmik, S.K.R., 2009. Analysis of cyclogeneis parameter for developing and nondeveloping low-pressure systems over the Indian Sea. Nat. Hazards 50, 389–402. https://doi.org/10.1007/s11069-009-9348-5.
- Kushwaha, V.K., Kumar, S.P., Feba, F. et al. Findlater jet induced summer monsoon memory in the Arabian Sea. Sci Rep 12, 13037 (2022). https://doi.org/10.1038/s41598-022-17025-1
- Large, W. G., McWilliams, J. C., & Doney, S. C. (1994). Oceanic vertical mixing: A review and a model with a nonlocal boundary layer parameterization. Reviews of Geophysics, 32(4), 363–403.
- Leipper, D. F. & Volgenau, D. Hurricane heat potential of the Gulf of Mexico. J. Phys. Oceanogr. 2, 218–224 (1972)
- Levitus, S., J. I. Antonov, T. P. Boyer, and C. Stephens (2000), Warming of the world ocean, Science, 287, 2225 2229.
- Lighthill, M. J. (1969), Dynamic response of the Indian Ocean to the onset of the southwest monsoon, Philos. Trans. R. Soc. London, Ser. A, 265, 45 92.
- Li, Z., Li, T., Yu, W., et al., 2016. What controls the interannual variation of tropical cyclone genesis frequency over Bay of Bengal in the post-monsoon peak season? Atmos. Sci. Lett. 17, 148–154. https://doi.org/10.1002/asl.636.
- Lin, I.I., Pun, I.F., Lien, C.C., 2014. "category-6" supertyphoon Haiyan in global warming hiatus:

- Contribution from subsurface ocean warming. Geophys. Res. Lett. 41, 8547–8553. https://doi.org/10.1002/2014GL061281.
- Lloyd, I.D., Vecchi, G.A., 2011. Observational evidence for oceanic controls on hurricane intensity.

 J. Clim. 24, 1138–1153. https://doi.org/10.1175/2010JCLI3763.1.
- Ma, Z., Fei, J., Liu, L., et al., 2013. Effects of the cold core eddy on tropical cyclone intensity and structure under idealized air-sea interaction conditions. Mon. Weather Rev. 141, 1285–1303. https://doi.org/10.1175/MWR-D-12-00123.1.
- Mahala, B.K., Nayak, B.K., Mohanty, P.K., 2015. Impacts of ENSO and IOD on tropical cyclone activity in the Bay of Bengal. Nat. Hazards 75, 1105–1125. https://doi.org/10.1007/s11069-014-1360-8.
- Maneesha K, Y. Sadhuram & K.V.S.R. Prasad (2015) Role of upper ocean parameters in the genesis, intensification and tracks of cyclones over the Bay of Bengal, Journal of Operational Oceanography, 8:2, 133-146, DOI: 10.1080/1755876X.2015.1087185
- Marathe, Shamal & Ashok, Karumuri. (2021). Chapter- The El Niño Modoki. In book: Tropical and Extratropical Air-Sea Interactions (pp.93-114). 10.1016/B978-0-12-818156-0.00009-5.
- Marathe, S., Ashok, K., Panickal, S. and Sabin, T. P., 2015, "Revisiting El Niño Modokis", Climate Dynamics, 45, 11-12, 3527-3545.
- McCreary, J. P., K. E. Kohler, R. R. Hood, and D. B. Olson (1996), A four-component ecosystem model of biological activity in the Arabian Sea, Prog. Oceanogr., 37, 117 165.
- McCreary, J. P., Kundu, P. K. & Molinari, R. L. A numerical investigation of dynamics, thermodynamics and mixed-layer processes in the Indian Ocean. Prog. Oceanogr. 31, 181–244 (1993).
- McCreary, J. P., and P. K. Kundu (1989), A numerical investigation of the sea surface temperature variability in the Arabian Sea, J. Geophys. Res., 94, 16,097–16,114.

- Miyama, T., J. P. McCreary, T. G. Jensen, J. Loschnigg, S. Godfrey, and A. Ishida (2003), Structure and dynamics of the Indian-Ocean cross-equatorial cell, Deep Sea Res., Part I, 50(12), 2023–2047.
- Molinari, R. L., J. Swallow, and J. F. Festa (1986), Evolution of the near-surface thermal structure in the western Indian Ocean during FGGE, J. Mar. Res., 44, 739–763.
- Murtugudde, R., Seager, R., and Thoppil, P. (2007), Arabian Sea response to monsoon variations, Paleoceanography, 22, PA4217, doi:10.1029/2007PA001467
- Nagura, M., and M. J. McPhaden (2008), The dynamics of zonal current variations in the central equatorial Indian Ocean, Geophys. Res. Lett., 35, L23603, doi:10.1029/2008GL035961
- Nagura, M., and M. J. McPhaden (2010a), Wyrtki jet dynamics: Seasonal variability, J. Geophys. Res., 115, C07009, doi:10.1029/2009JC005922.
- Nagura, M., and M. J. McPhaden (2010b), Dynamics of zonal current variations associated with the Indian Ocean dipole, J. Geophys. Res., 115, C11026, doi:10.1029/2010JC006423.
- Nair, S. K. et al. Diurnal variations of the low-level jet over peninsular India during the onset of Asian summer monsoon. Theor. Appl. Climatol. 120, 287–298 (2014).
- Narayanan, S., Kottayil, A. & Mohanakumar, K. Monsoon low-level jet over the gateway of Indian summer monsoon: A comparative study for two distinct monsoon years. Meteorol. Atmos. Phys. 128, 689–696 (2016).
- Narvekar, J., Prasanna Kumar, S., 2006. Seasonal variability of the mixed layer in the central Bay of Bengal and associated changes in nutrients and chlorophyll. Deep Res I Oceanogr Res Pap. 53, 820–835. https://doi.org/10.1016/j.dsr.2006.01.012.
- Ng, E.K.W., Chan, J.C.L., 2012. Interannual variations of tropical cyclone activity over the north Indian Ocean. Int. J. Climatol. 32, 819–830. https://doi.org/10.1002/joc.2304.

- Nicholls, N., Sea surface temperatures and Australian winter rainfall, J. Climate, 2, 965–973, 1989.
- Ogata, T., Mizuta, R., Adachi, Y., et al., 2015. Effect of air-sea coupling on the frequency distribution of intense tropical cyclones over the northwestern Pacific. Geophys. Res. Lett. 42, 10415–10421. https://doi.org/10.1002/2015GL066774.
- Ooyama, K.V., 1969. Numerical simulation of the life cycle of tropical cyclones. J. Atmos. Sci. 26, 3–40.
- Pai, D. S. et al. Development of a new high spatial resolution (0.25° × 0.25°) long period (1901–2010) daily gridded rainfall data set over India and its comparison with existing data sets over the region. Mausam 65, 1–18 (2014).
- Palmen, E. "On the Formation and Structure of Tropical Cyclones," Geophysica, Vol. 3, 1948, pp. 26-38.
- Papa, F., Durand, F., Rossow, W. B., Rahman, A., & Bala, S. K. (2010). Satellite altimeter-derived monthly discharge of the Ganga-Brahmaputra River and its seasonal to interannual variations from 1993 to 2008. Journal of Geophysical Research, 115, C12013. https://doi.org/10.1029/2009JC006075
- Parthasarathy, B., A. Munot, and D. Kothawale, 1994: All-India monthly and seasonal rainfall series: 1871–1993. Theoretical and Applied Climatology, 49 (4), 217–224.
- Pérez-Hernández, M. D., A. Hernández-Guerra, T. M. Joyce, and P. Vélez-Belchí (2012), Wind-driven cross-equatorial flow in the Indian Ocean, J. Phys. Oceanogr., 42(12), 2234–2253.
- Pushpanjali, B., Subrahmanyam, M. V. & Murty, K. P. R. V. Findlater jet intensity and characteristics in relation to Indian summer monsoon. In Monsoons: Formation, Environmental Monitoring and Impact Assessment (eds Leal, M. D. & Levins, M. B.) 47–63 (Environmental Science, Engineering and Technology, Nova Science Publishers, Inc., 2013)
- Pushpanjali, B., Subrahmanyam, V. M. & Murty, K. Relation between outgoing longwave radiation

- and findlater jet over Arabian Sea during summer monsoon and influence on Indian monsoon rainfall. Indian J. Geo-Mar. Sci. 49, 428–435 (2020)
- Prajeesh, A., Ashok, K. & Rao, D. Falling monsoon depression frequency: A Gray-Sikka conditions perspective. Sci Rep 3, 2989 (2013). https://doi.org/10.1038/srep02989
- Prasad, T.G., 2004. A comparison of mixed-layer dynamics between the Arabian Sea and Bay of Bengal: One-dimensional model results. J. Geophys. Res. Ocean 109. https://doi.org/10.1029/2003jc002000.
- Prasanna Kumar, S. et al. High biological productivity in the central Arabian Sea during the summer monsoon driven by Ekman pumping and lateral advection. Curr. Sci. 81, 1633–1638 (2001)
- Prasanna Kumar, S. & Narvekar, J. Seasonal variability of the mixed layer in the central Arabian Sea and its implication on nutrients and primary productivity. Deep-Sea Res. II 52, 1848–1861 (2005).
- Prasanna Kumar, S., Narvekar, J., Nuncio, M., Gauns, M. & Sardesai, S. What drives the biological productivity of the northern Indian Ocean? In Indian Ocean Biogeochemical Processes and Ecological Variability (eds Wiggert, J. D. et al.), AGU Geophysical Monograph Series. Vol. 185, 33–56 (2009).
- Prasanna Kumar S, Prasad TG (1999) Formation and spreading of Arabian Sea high-salinity water mass. J Geophys Res 104:1455–1464. doi:10.1029/1998JC900022
- Prasanna Kumar, S. & Prasad, T. G. Winter cooling in the northern Arabian Sea. Curr. Sci. 71, 834–841 (1996).
- Praveen, K. B., Vialard, J., Lengaigne, M., Murty, V., & Mcphaden, M. J. (2012). TropFlux: Airsea fluxes for the global tropical oceans-description and evaluation. Climate Dynamics, 38(7-8), 1521–1543.

- Praveen, K. B., Vialard, J., Lengaigne, M., Murty, V., Mcphaden, M. J., Cronin, M., et al. (2013). TropFlux wind stresses over the tropical oceans: Evaluation and comparison with other products. Climate Dynamics, 40(7-8), 2049–2071.
- Rao, Y., 1976: Southwest monsoon (meteorological monograph, synoptic meteorology no. 1).

 Indian Meteorological Department, New Delhi, 367pp.
- Rao, R.R., Sivakumar, R., 2003. Seasonal variability of sea surface salinity and salt budget of the mixed layer of the north Indian Ocean. J. Geophys. Res. Ocean 108. https://doi.org/10.1029/2001jc000907.
- Rao, R. R., T. Horii, Y. Masumoto, and K. Mizuno (2016), Observed variability in the upper layers at the Equator, 90°E in the Indian Ocean during 2001–2008, 2: Meridional currents, Clim. Dyn., doi:10.1007/s00382-016-2979-9.
- Ramage C.S. 1959: Hurricane Development. Journal Meteor., 16, 227-237.
- Ramage, C., 1971: [Monsoon Meteorology]. Academic Press.
- Ramos, C. G. M., Tan, H., Ray, P., & Dudhia, J. (2022). Estimates of the sensible heat of rainfall in the tropics from reanalysis and observations. International Journal of Climatology, 42(4), 2246–2259. https://doi.org/10.1002/joc.7363
- Rani, S. I. et al. IMDAA: High resolution satellite-era reanalysis for the Indian monsoon region. J. Clim. 34, 5109–5133 (2021)
- Rawlinson, H. G. (1916). Intercourse between India and the Western World. Cambridge University Press.
- Rayner, N., D. E. Parker, E. Horton, C. K. Folland, L. V. Alexander, D. Rowell, E. Kent, and A. Kaplan, 2003: Global analyses of sea surface temperature, sea ice, and night marine air temperature since the late nineteenth century. Journal of Geophysical Research: Atmospheres, 108 (D14).

- Riehl, h. (1954), Variations Of Energy Exchange Between Sea And Air In The Trades. Weather, 9: 335-340. https://doi.org/10.1002/j.1477-8696.1954.tb01706.x.
- Riehl, H., and R. J. Shafer, 1944: The recurvature of tropical storms. J. Meteor., 1, 42–54
- Ross SM (2020) Introduction to probability and statistics for engineers and scientists. Academic Press, Cambridge
- Roose, S., Ajayamohan, R.S., Ray, P. et al. ENSO influence on Bay of Bengal cyclogenesis confined to low latitudes. npj Clim Atmos Sci 5, 31 (2022). https://doi.org/10.1038/s41612-022-00252-8.
- Saji, N. H., B. N. Goswami, P. N. Vinayachandran, and T. Yamagata,1999: A dipole mode in the tropical Indian Ocean. Nature, 401, 360–363.
- Schott, F., and J. P. McCreary (2001), The monsoon circulation of the Indian Ocean, Prog. Oceanogr., 51, 1-123.
- Schott, F. A., J. P. McCreary, and G. C. Johnson (2004), Shallow overturning circulations of the tropical-subtropical oceans, in Earth's Climate, edited by C. Wang, S. P. Xie, and J. A. Carton, pp. 261–304, AGU, Washington, D. C., doi:10.1029/147GM15.
- Schott, F. A., M. Dengler, and R. Schoenefeldt (2002), The shallow overturning circulation of the Indian Ocean, Prog. Oceanogr., 53(1), 57–103.
- Schott, F. A., S. P. Xie, and J. P. McCreary (2009), Indian Ocean circulation and climate variability, Rev. Geophys., 47, RG1002, doi:10.1029/2007RG000245.
- Sengupta, D., Bharath Raj, G.N., Shenoi, S.S.C., 2006. Surface freshwater from Bay of Bengal runoff and Indonesian Throughflow in the tropical Indian Ocean. Geophys. Res. Lett. 33, 1–5. https://doi.org/10.1029/2006GL027573.
- Shay, L.K., Goni, G.J., Black, P.G., 2000. Effects of a warm oceanic feature on Hurricane Opal.

- Mon. Weather Rev. 128, 1366–1383. https://doi.org/10.1175/1520-0493(2000)128<1366:eoawof 2.0.co; 2.
- Shankar, D., Remya, R., Anil, A., & Vijith, V. (2019). Role of physical processes in determining the nature of fisheries in the eastern Arabian Sea. Progress in Oceanography, 172, 124–158.
- Shankar, D., Remya, R., Vinayachandran, P., Chatterjee, A., & Behera, A. (2016). Inhibition of mixed-layer deepening during winter in the northeastern Arabian Sea by the West India Coastal Current. Climate Dynamics, 47(3-4), 1049–1072.
- Sharma N, Ali MM (2014) Importance of Ocean Heat Content for Cyclone Studies. Oceanography 2: 124. doi:10.4172/2332-2632.1000124
- Shay LK, Goni GJ, Black PG (2000) Effects of a Warm Oceanic Feature on Hurricane Opal. Mon Weather Rev 128:1366–1383. doi: 10.1175/1520-0493(2000)128<1366:eoawof>2.0.co;2
- Shukla, J., and M. Misra (1977), Relationship between sea surface temperature and wind speed over the central Arabian Sea and monsoon rainfall over India, Mon. Weather Rev., 105, 998 1002.
- Shenoi, S.S.C., 2002. Differences in heat budgets of the near-surface Arabian Sea and Bay of Bengal: Implications for the summer monsoon. J. Geophys. Res. 107, 1–14. https://doi.org/10.1029/2000jc000679.
- Shenoy, L. R., Chatterjee, A., Prakash, S., & Mathew, T. (2020). Biophysical interactions in driving the summer monsoon chlorophyll bloom off the Somalia coast. Journal of Geophysical Research: Oceans, 125, e2019JC015549. https://doi.org/10.1029/2019JC015549
- Shepard. Donald, 1968. A two-dimensional interpolation function for irregularly-spaced data. In Proceedings of the 1968 23rd ACM national conference (ACM '68). Association for Computing Machinery, New York, NY, USA, 517–524. DOI:https://doi.org/10.1145/800186.810616

- Shetye, S.R., Gouveia, A.D., Shankar, D., et al., 1996. Hydrography and circulation in the western Bay of Bengal during the northeast monsoon. J. Geophys. Res. C Ocean 101, 14011–14025. https://doi.org/10.1029/95JC03307.
- Shetye, S. R. & Gouveia, A. D. Coastal circulation in the north Indian Ocean: Coastal segment (14, S-W). In The Sea, Vol. 11, 523–556 (Wiley, 1998)
- Sikka, D. (1977). Some aspects of the life history, structure and movement of monsoon depressions. Pure and Applied Geophysics, 115(5), 1501–1529.
- Sindhu, B., Suresh, I., Unnikrishnan, A., Bhatkar, N., Neetu, S., & Michael, G. (2007). Improved bathymetric datasets for the shallow water regions in the Indian Ocean. Journal of Earth System Science, 116(3), 261–274.
- Singh V, Roxy M (2022) A review of the ocean-atmosphere interactions during tropical cyclones in the north Indian Ocean. Earth-Sci Rev 226:103967.
- Subbaramayya, I., & Rao, S. R. M. (1984). Frequency of Bay of Bengal Cyclones in the Post-Monsoon Season, Monthly Weather Review, 112(8), 1640-1642.
- Subrahmanyam, B., Murty, V.S.N., Sharp, R.J., O'Brien, J.J., 2005. Air-sea coupling during the tropical cyclones in the Indian Ocean: A case study using satellite observations. Pure Appl. Geophys. 162, 1643–1672. https://doi.org/10.1007/s00024-005-2687-6.
- Tejavath CT, Ashok K, Chakraborty S, Ramesh R (2018) The ENSO teleconnections to the Indian summer monsoon climate through the Last Millennium as simulated by the PMIP3. Clim Past Discuss. https://doi.org/10.5194/cp-2018-7
- Trenberth, K.E., Cheng, L., Jacobs, P., et al., 2018. Hurricane harvey links to ocean heat content and climate change adaptation. Earth's Futur 6, 730–744. https://doi.org/10.1029/2018EF000825.
- Venugopal, T. et al. Statistical evidence for the role of southwestern Indian Ocean heat content in

- the Indian summer monsoon rainfall. Sci. Rep. 8, 12092
- Vinayachandran, P. N. (2004), Summer cooling of the Arabian Sea during contrasting monsoons, Geophys. Res. Lett., 31, L13306, doi:10.1029/2004GL019961.
- Vinod, K.K., Soumya, M., Tkalich, P., Vethamony, P., 2014. Ocean Atmosphere interaction during thane cyclone: A numerical study using WRF. Indian J Geo-Marine Sci 43, 1230–1235.
- Vissa, N.K., Satyanarayana, A.N.V., Prasad Kumar, B., 2013a. Intensity of tropical cyclones during pre- and post-monsoon seasons in relation to accumulated tropical cyclone heat potential over Bay of Bengal. Nat. Hazards 68, 351–371. https://doi.org/10.1007/s11069-013-0625-y.
- Vizy, E. K. & Cook, K. H. Interannual variability of East African rainfall: Role of seasonal transitions of the low-level cross-equatorial flow. Clim. Dyn. 54, 4563–4587 (2020)
- Von Storch, H., and F. W. Zwiers, 1999: Statistical analysis in climate research. Cambridge university press.
- Vörösmarty, C., Fekete, B., & Tucker, B. (1996). River discharge database, Version 1.0 (RivDIS v1. 0), Volumes 0 through 6. A contribution to IHP-V Theme: 1. Technical documents in hydrology series. Paris: UNESCO.
- Wada, A., Usui, N., 2007. Importance of tropical cyclone heat potential for tropical cyclone intensity and intensification in the Western North Pacific. J. Oceanogr. 63, 427–447. https://doi.org/10.1007/s10872-007-0039-0.
- Wang B, Clemens SC, Liu P (2003) Contrasting the Indian and East Asian monsoons: implications on geologic timescales. Mar Geol 201:5–21. doi:10.1016/S0025-3227(03)00196-8
- Wang L, Li J, Lu H et al (2012) The East Asian winter monsoon over the last 15,000 years: its links to high-latitudes and tropical climate systems and complex correlation to the summer monsoon. Quat Sci Rev 32:131–142. doi:10.1016/j.quascirev.2011.11.003

- Weare, B. C. (1979), A statistical study of the relationship between ocean surface temperatures and the Indian monsoon, J. Atmos. Sci., 36, 2279 2291.
- Webster, P. J., V. O. Magana, T. Palmer, J. Shukla, R. Tomas, M. Yanai, and T. Yasunari, 1998:

 Monsoons: Processes, predictability, and the prospects for prediction. Journal of
 Geophysical Research: Oceans, 103 (C7), 14 451–14 510.
- Weller, R. A. et al. Moored observations of upper-ocean response to the monsoons in the Arabian Sea during 1994–1995. Deep-Sea Res. Part II 49, 2195–2230 (2002).
- Wiggert, J. D., R. Murtugudde, and C. R. McClain (2002), Processes controlling interannual variations in wintertime (northeast monsoon) primary productivity in the central Arabian Sea, Deep Sea Res., Part II, 47, 2319 2343.
- Winguth, A. M. E., M. Heimann, K. D. Kurz, E. Maier-Reimer, U. Mikolajewicz, and J. Segschneider (1994), El Niño Southern Oscillation related fluctuations of the marine carbon cycle, Global Biogeochem. Cycles, 8, 39 64.
- Yu, B., G. J. Boer, F. Zwiers, and W. Merryfield (2009), Covariability of SST and surface heat fluxes in reanalyses and CMIP3 climate models, Clim. Dyn., doi:10.1007/s00382-009-0669-6
- Yuan, J.P., Cao, J., 2013. North Indian Ocean tropical cyclone activities influenced by the Indian Ocean Dipole mode. Sci. China Earth Sci. 56, 855–865. https://doi.org/10.1007/s11430-012-4559-0.
- Zhu, H., Ulrich, W., Smith, R.K., 2004. Ocean effects on tropical cyclone intensification and inner-core asymmetries. J. Atmos. Sci. 61, 1245–1258. https://doi.org/10.1175/1520-0469(2004)061<1245:OEOTCI>2.0.CO;2.

Implications of Indian Summer Monsoon on various coupled air-sea processes in the North Indian Ocean

by Vikas Kumar Kushwaha

Prof. KARUMURI ASHOK

Prof. KARUMURI

Prof. KARU

Submission date: 21-Feb-2023 12:22PM (UTC+0530)

Submission ID: 2019461716

File name: Vikas_Kumar_Kushwaha.pdf (8.05M)

Word count: 15056 Character count: 74928

Librarian

Indira Gandhi Memorial Library UNIVERSITY OF HYDERABAD

Central University P.O. HYDERABAD-500 046.

Implications of Indian Summer Monsoon on various coupled air-sea processes in the North Indian Ocean

ORIGINALITY REPORT SIMILARITY INDEX INTERNET SOURCES **PUBLICATIONS** STUDENT PAPERS **PRIMARY SOURCES** www.ncbi.nlm.nih.gov Internet Source Vikas Kumar Kushwaha, S. Prasanna Kumar, F Feba, Karumuri Ashok. "Findlater jet induced summer monsoon memory in the Arabian Sea", Scientific Reports, 2022 Publication PROFILE RUMURI ASHOK Vineet Kumar Singh, M.K. Roxy. "A review of Centre for Carto Acean & Atmospheric Sciences University of Hyderabad ocean-atmosphere interactions during Hyderabad-500 046, INDIA. tropical cyclones in the north Indian Ocean", Earth-Science Reviews, 2022 Publication os.copernicus.org Internet Source Kad Pratik, Anant Parekh, Ananya Karmakar, Jasti S. Chowdary, C. Gnanaseelan. "Recent changes in the summer monsoon circulation and their impact on dynamics and thermodynamics of the Arabian Sea", The opetical and Applied Climatology, 2018 2121/23 Prof. KARUMURI ASHOK Centre for Earth, Ocean & Atmospheric Sciences

University of Hyderabad Hyderabad-500 046, INDIA.

	and to their week
12	Internet Source
13	www.researchgate.net Internet Source Prof. KARUMURI ASHOK Prof. KARUMURI ASHOK Prof. KARUMURI ASHOK Prof. KARUMURI ASHOK Internet Source Prof. KARUMURI ASHOK Prof. KARUMURI ASHOK Prof. KARUMURI ASHOK Internet Source Prof. KARUMURI ASHOK Prof. KARUMURI ASHOK Internet Source Prof. KARUMURI ASHOK Prof. KARUMURI ASHOK Internet Source Internet Source Internet Source Internet Source Prof. KARUMURI ASHOK Internet Source Interne
14	Monitoring and Prediction of Tropical Cyclones in the Indian Ocean and Climate Change, 2014. Publication Change August 15
15	www.nature.com Internet Source Row Man (1 %)
16	Internet Source d-nb.info Internet Source Prof. KARUMURI ASHOK Prof. KARUMURI & Mimospherit Scientes Prof. KARUMURI & Mimospherit Scientes University of Hyderabad-500 046, MO A-96 Hyderabad-500 046, MO A-96
17	hdl.handle.net Internet Source Hyderaba 41 %
18	Submitted to University of Hyderabad, Hyderabad Student Paper herald.uohyd.ac.in Submitted to University of Hyderabad, All the submitted to University of Hyderabad
19	Internet Source \\ \\ \\ \\ \\ \\ \\ \\ \\ \\ \\ \\ \\
20	Springer Climate, 2016. Publication Prof. KARUMURI ASHOK Prof.
21	Springer Climate, 2016. Publication Prof. KARUMURI ASHON Prof. KARUMUR
Your 21	Prof. KARUMURI ASHOK Centre for Earth, Ocean & Atmospheric Sciences University of Hyderabad Hyderabad-500 046, INDIA.

over the Bay of Bengal", Journal of Operational Oceanography, 2015 Publication

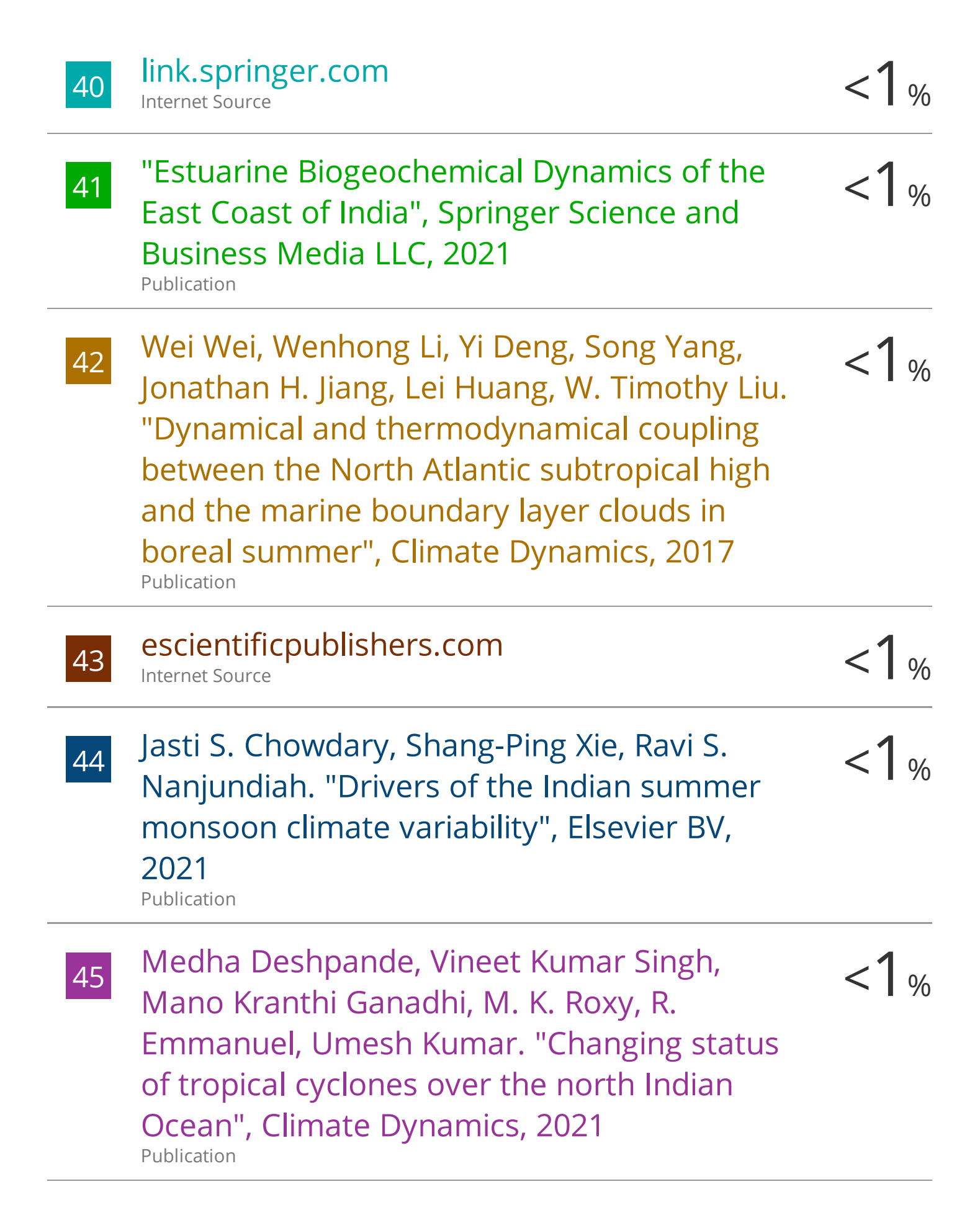
22	"El Niño Southern Oscillation in a Changing Climate", Wiley, 2020 Publication	<1%
23	mseas.mit.edu Internet Source	<1%
24	Naresh Krishna Vissa, A. N. V. Satyanarayana, B. Prasad Kumar. "Intensity of tropical cyclones during pre- and post-monsoon seasons in relation to accumulated tropical cyclone heat potential over Bay of Bengal", Natural Hazards, 2013 Publication	<1%
25	Yi Wang, Michael J. McPhaden. "Seasonal cycle of cross-equatorial flow in the central Indian Ocean", Journal of Geophysical Research: Oceans, 2017 Publication	<1%
26	Submitted to Atlanta International High School Student Paper	<1%
27	Ines Wendler, Karin A. F. Zonneveld, Helmut Willems. "Calcareous cyst-producing dinoflagellates: ecology and aspects of cyst preservation in a highly productive oceanic	<1%

region", Geological Society, London, Special Publications, 2022

Publication

28	J. Narvekar, S. Prasanna Kumar. " Mixed layer variability and chlorophyll biomass in the Bay of Bengal ", Biogeosciences, 2014 Publication	<1%
29	R. S. Lakshmi, Abhisek Chatterjee, Satya Prakash, Teesha Mathew. "Biophysical Interactions in Driving the Summer Monsoon Chlorophyll Bloom Off the Somalia Coast", Journal of Geophysical Research: Oceans, 2020 Publication	<1%
30	William KM. Lau, Duane E. Waliser. "Intraseasonal Variability in the Atmosphere- Ocean Climate System", Springer Nature, 2012 Publication	<1%
31	eprints.soton.ac.uk Internet Source	<1%
32	"Intraseasonal Variability in the Atmosphere- Ocean Climate System", Springer Nature, 2005 Publication	<1%
33	Abhisek Chatterjee, Gouri Anil, Lakshmi R. Shenoy. "Marine heatwaves in the Arabian	<1%

P. N. Vinayachandran. "Summer cooling of the <1% 34 Arabian Sea during contrasting monsoons", Geophysical Research Letters, 2004 Publication Sourav Sil, Avijit Gangopadhyay, Glen <1% 35 Gawarkiewicz, Saikat Pramanik. "Shifting seasonality of cyclones and western boundary current interactions in Bay of Bengal as observed during Amphan and Fani", Scientific Reports, 2021 **Publication** eprints.utas.edu.au <1% 36 Internet Source <1% Kalpesh Patil, M. C. Deo. "Basin-Scale 37 Prediction of Sea Surface Temperature with Artificial Neural Networks", Journal of Atmospheric and Oceanic Technology, 2018 Publication mars.gmu.edu Internet Source <1_% D. Swain. "Comparison of NCEP turbulent heat fluxes with in situ observations over the south-eastern Arabian Sea", Meteorology and Atmospheric Physics, 04/30/2009 Publication



46

Soumya Mohan, P. Vethamony. "Interannual and long-term sea level variability in the eastern Indian Ocean and South China Sea", Climate Dynamics, 2017

<1%

Publication



core.ac.uk Internet Source

Exclude quotes Exclude bibliography Exclude matches

< 14 words

scientific reports



OPEN Findlater jet induced summer monsoon memory in the Arabian Sea

Vikas Kumar Kushwaha^{1⊠}, S. Prasanna Kumar^{1,2}, Feba F¹ & Karumuri Ashok¹

A cross-equatorial low-level wind, known as Findlater Jet (FJ), modulates the thermocline in the Arabian Sea (AS) during summer monsoon (June to September). By analysing ocean and atmospheric data, we show that the FJ signal gets 'trapped' in the AS in the form of upper ocean heat content till the following winter months (December to February). This memory is the consequence of the combined effect of FJ-induced wind stress curl and the annual downwelling Rossby waves in the AS. During the summer monsoon months, the strong low-level westerly winds cause a negative wind stress curl in the south of the FJ axis over the central AS, resulting in a deep thermocline and high magnitude of heat being trapped. In winter monsoon months, though the wind stress curl is positive over large parts of the AS and could potentially shoal the thermocline and reduce the upper ocean heat content in the central AS, this does not happen due to two reasons. Firstly, winds are weaker, and spread over a larger area over the AS making the magnitude of the wind stress curl low. Secondly, westward propagating downwelling Rossby wave radiated from the eastern AS deepens the thermocline and prevents ventilation of the trapped heat. During the following spring, the collapse of the Rossby waves leads to the shoaling and mixing of underlying waters with surface waters thereby resurfacing of the trapped heat. The resurfacing of the trapped heat makes the AS a memory bank of the FJ induced signal.

The Indian Summer Monsoon (ISM), also known as southwest monsoon, is a prominent ocean-atmospheric phenomenon characterized by organized south-westerly winds and enhanced rainfall that becomes active during June to September. It affects the livelihood of the people of the Indian subcontinent and also impacts the dynamics and biogeochemistry of the surrounding water bodies, the Arabian Sea (AS) and the Bay of Bengal (BoB), making their regional oceanography contrastingly different1. The ISM accounts for 70% of annual precipitation over India and 60% of agriculture sector jobs^{2,3}. Though the interannual variability in the ISM rainfall is small with a standard deviation of about 10%, it can severely affect the economy of this region which is largely based on rain-fed agriculture and industry based on agriculture. Understanding the effects of environmental change on ISM rainfall and its spatial patterns present a key research challenge4 with huge ramifications on the water resources and the management policies. Thus, a lead prediction of the ISM turns out to be exceptionally critical and important.

The AS has a strong seasonality wherein the atmospheric as well as the oceanic circulation switches directions semi-annually under the influence of seasonally reversing monsoon winds. During ISM the cross-equatorial atmospheric flow from the East African coast towards India, the south-westerly winds, develops by the end of May, intensifies into a low-level jet during July, and collapses by end of September^{5,6}. This low-level atmospheric jet, known as Findlater Jet? (FJ), attains a speed as high as 100 knots near the East African coast^{8,9}. The axis of the FJ is represented by the region of maximum wind speed at a height of 850 millibars (hPa) and extends from the Horn of Africa to the coast of Gujarat in India. The FJ plays an important role in the spatio-temporal variability of the ISM rainfall. For example, Webster et al.² and Pushpanjali et al.¹⁰ found that the SM rainfall is positively correlated with the strength of FJ. In general, strong FJs are associated with more active spells of ISM rainfall, while weak FJs are associated with breaks in the rainfall. The characteristics of the FJ and its variability ranging from diurnal^{11–13}, intraseasonal^{14,15}, and to interannual^{10,16,17} time scales has been well-researched. There are also studies on the long-term trends of FJ^{18,19}.

It is known that FJ has some influence on the upper ocean through wind stress. The cyclonic wind stress north of the axis of the FJ induces Ekman suction and open-ocean upwelling, while the anticyclone wind stress south of the axis leads to Ekman pumping and open ocean downwelling^{20,21}. This results in the modulation of mixed

¹Centre for Earth, Ocean and Atmospheric Science, University of Hyderabad, Hyderabad, India. ²CSIR-National Institute of Oceanography, Dona Paula, Goa 403002, India. [™]email: kushwaha.vikas@outlook.com

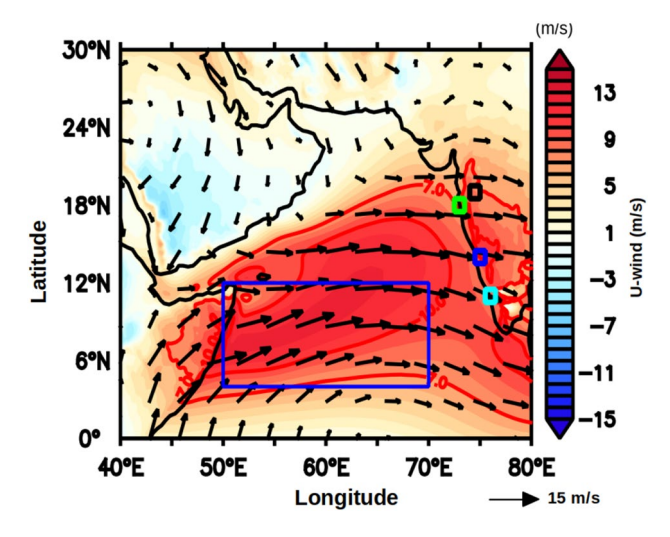


Figure 1. Climatological mean wind vector overlaid on zonal wind (u-wind, m/s) during June to September (JJAS) at 850 hPa in the Arabian Sea. The blue box (50–70°E and 4–12°N) represents the region within which parameters were averaged. Red solid lines indicate the zonal wind speed contours of 7 m/s and 10 m/s. The different colour small squares represent the location of sub-divisional stations, Madhya Maharashtra (black), Konkan (green), Coastal Karnataka (blue), and Kerala (cyan).

layer depth on either side of the axis of the FJ²²⁻²⁴. During the winter monsoon months (December to February; DJF), though the north-easterly winds are weak the convective cooling and associated mixing deepens the mixed layer in the northern AS^{23,25}. The other dominant factor influencing the upper ocean including the mixed layer in the AS is the annual Rossby waves^{24,26,27}. They are the dominating patterns of sea surface height (SSH) variability, especially all through the inter-monsoon period. The westward propagation of first—and second mode annual Rossby waves explains 87% of the seasonal, mid basin hydrographic variance below 100 m, along 8°N²⁶.

Though there had been various studies focused on understanding the dynamics of circulation in the north Indian Ocean during different seasons^{28,29} there are only a few studies that have focused on the impact of FJ on the modulation of the upper waters in the AS during the ISM months^{20,21}. However, no studies have examined the impact of the FJ on the subsurface heat content in the AS beyond the ISM months and its feedback on the ISM rainfall. Therefore, the main objective of the current study is to explore the response of the subsurface AS to the FJ and examine potential processes in regulating ISM rainfall through oceanic heat content changes.

Results and discussion

In order to understand the role of FJ in regulating the ISM rainfall, the climatological mean wind at 10 m above the sea surface for the study period was examined during JJAS (Fig. 1), which shows the signature of the FJ as a core of strong south-westerly winds. The presence of the FJ can be identified by the climatological south-westerly winds seen over the central AS with a zonal wind speed in excess of 10 m/s. Figure 2 shows the temporal and vertical structure of the wind vectors averaged over the box (Fig. 1) located in the core region of the FJ in the central AS. During the ISM, the maximum intensity of the FJ is seen at 850 hPa. These winds are mostly westerly up to the height of 600 hPa, and the winds reverse to easterlies at greater heights with an increase in their magnitude. Just after the JJAS, the ISM winds collapse, and the north-easterly winds start to prevail prominently between 1000 and 850 hPa indicating the winter monsoon conditions. Notice that the upper-level easterly winds between 200 to 300 hPa of the ISM also reverse to westerly during the winter monsoon.

To decipher the impact of FI on the upper ocean dynamics, the annual cycle of wind stress curl (WSC) (Fig. 3) and mixed layer depth (MLD) (Fig. 4) were examined in the AS. The axis of the FJ is denoted by the zero WSC in Fig. 3a during JJAS. North of the axis of the FJ the WSC was positive which would drive Ekman suction and support upwelling of subsurface waters. In contrast, south of the axis of the FJ the negative WSC would drive Ekman pumping and support downwelling of surface waters. The response of the wind forcing was seen clearly in the spatial distribution of MLD during JJAS (Fig. 4a) which showed shallow mixed layer north of the axis of FJ and deep mixed layer south of it. These results are consistent with earlier studies based on shipboard observation^{20,21} as well as mooring²³. As the season changes from ISM to post-monsoon (ON), the FJ collapses and disappears with weak WSC values over the entire AS (Fig. 3b). Accordingly, the MLD also showed a decrease of 20-30 m (Fig. 4b). In the winter season (DJF), under the prevailing easterly trade winds the WSC over the north-western AS was weak and negative, while in the eastern and most of the southern AS the WSC was weak and positive (Fig. 3c) suggesting a weak downwelling and upwelling respectively. Consistent with the wind forcing the basin-wide MLD in the AS was deep in the north and shallow in the south (Fig. 4c). However, the deepening of MLD by 30 m in the north in comparison to post-monsoon was not entirely driven by wind as the WSC, though negative, was weak. The winter cooling and convective mixing that prevails in this season in the northern AS contributed to the deepening of MLD²⁵. The basin-wide WSC in the AS further weakened during

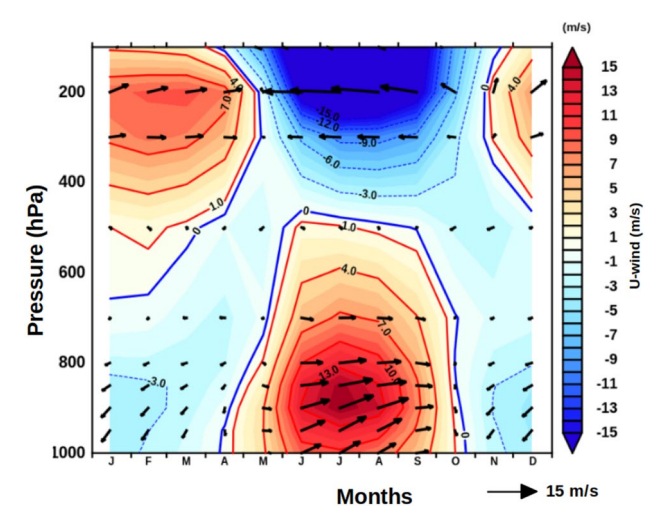


Figure 2. Vertical structure of monthly mean climatology of zonal wind (u-wind, m/s) averaged over the longitude 60°E to 70°E and latitude 6°N to 20°N overlaid with wind vectors.

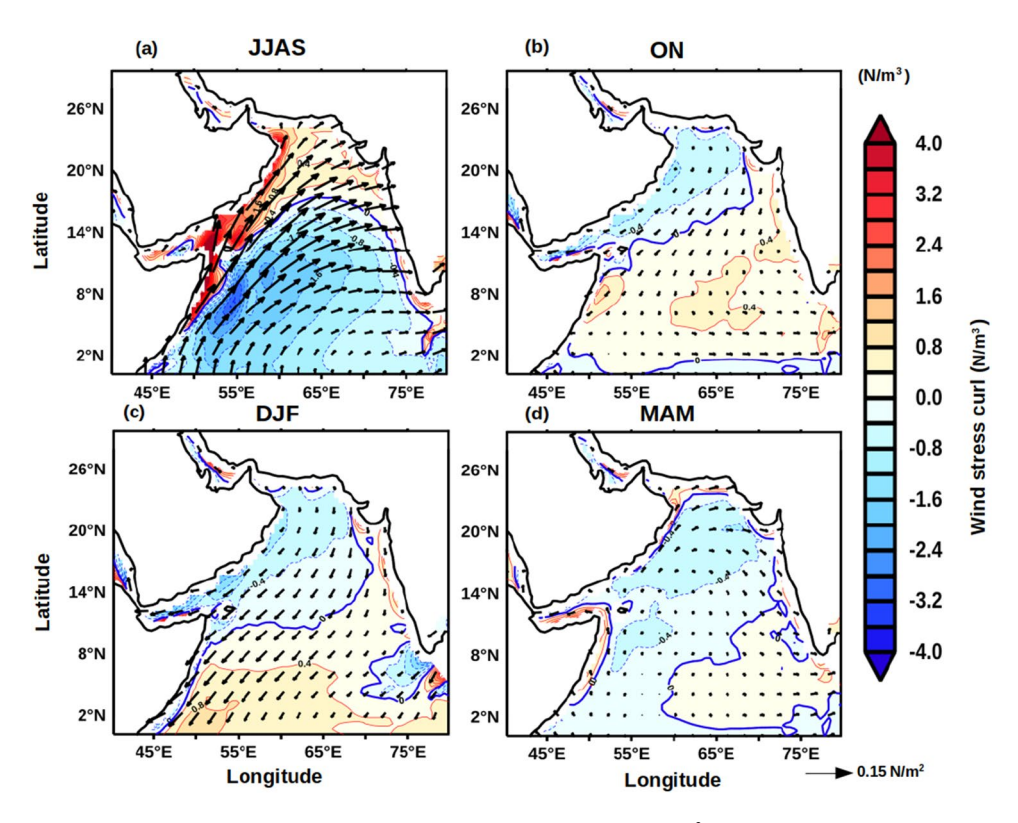


Figure 3. Annual cycle of climatology of wind stress curl (WSC, N/m³) during (a) JJAS, (b) ON, (c) DJF, and (d) MAM. Contour lines represent the magnitude of zero wind stress curl while the arrows represent the wind stress (N/m²) vector.

the pre-monsoon (MAM) season (Fig. 3d) as winds were weak and variable. This resulted in the occurrence of basin-wide shallow MLD (Fig. 4d).

Thus, FJ plays a crucial role in basin-scale modulation of mixed layer during ISM. As the FJ modulated the mixed layer it is expected that the upper ocean heat content also will be impacted. The upper ocean heat content plays important role in the generation of several atmospheric processes including tropical cyclone³⁰ and Indian summer monsoon³¹. The upper ocean thermal energy integrated from surface to the depth of 26 °C isotherm (D_{26}) is a commonly used metric for the Upper Ocean Heat Content (UOHC) and generally referred as the tropical cyclone heat potential³². The seasonal cycle of UOHC (Fig. 5) was examined to understand the role of FJ in modulating the upper ocean heat content. The basin-wide structure of UOHC during ISM (JJAS) showed that south of the axis of FJ the value was more than 65×10^8 kJ/cm² and increased to 100×10^8 kJ/cm² towards

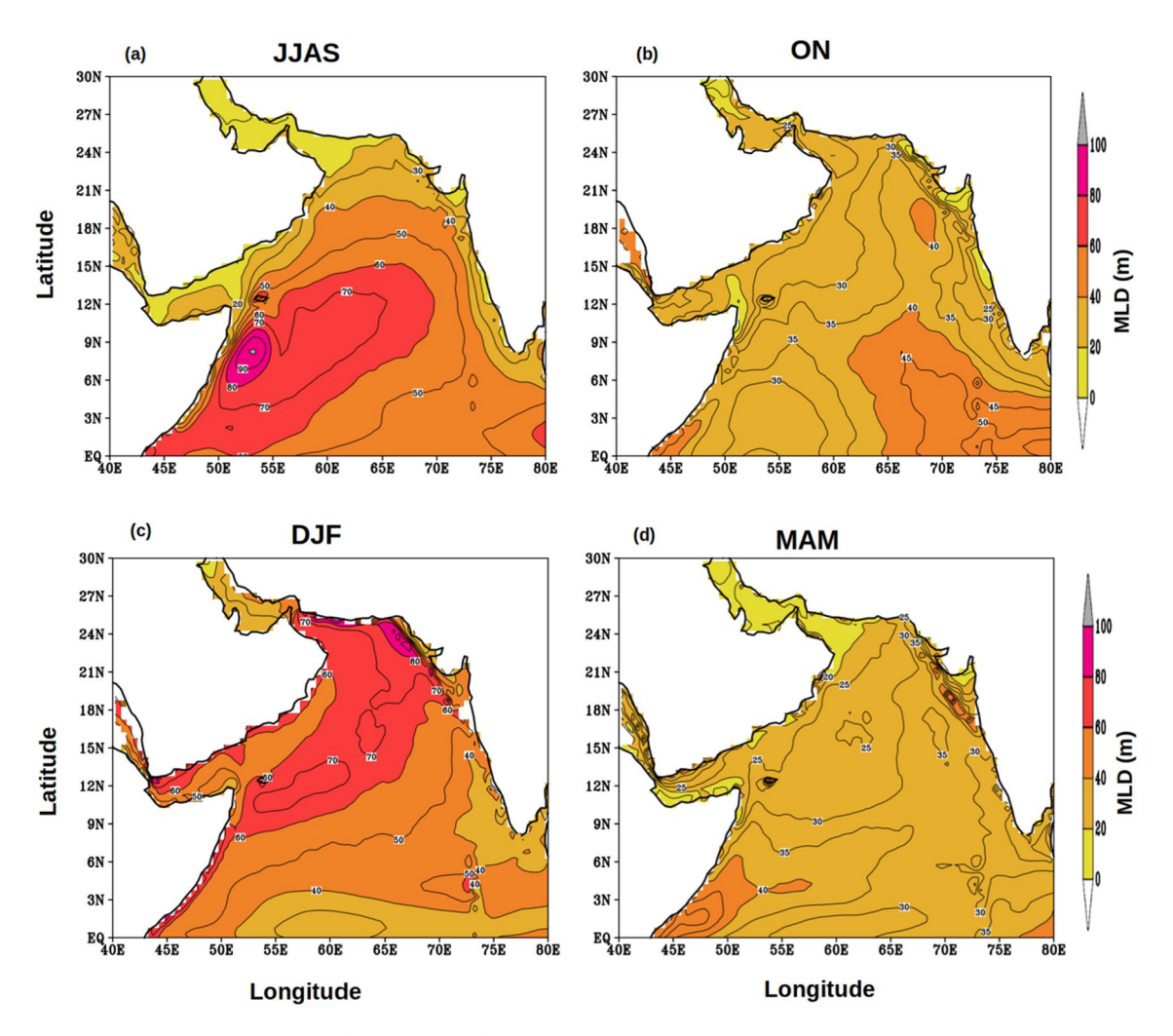


Figure 4. Annual cycle of climatology of mixed layer depth (MLD, m) during (a) JJAS, (b) ON, (c) DJF, and (d) MAM.

the central AS, while towards the northwest and eastern parts of the AS it progressively decreased reaching as low as 20×10^8 kJ/cm² (Fig. 5a). The spatial distribution of D_{26} during ISM showed a similar pattern similar to that of UOHC (figure not shown) with values increasing form 65 m to 100 m south of the axis of the FJ, while towards the north and east it decreased and the lowest value was 20 m. Thus, the high values of UOHC were closely coupled to the deepening of D₂₆. The spatial pattern of both UOHC and D26 was consistent with that of the WSC (Fig. 3). The region of high UOHC and D₂₆ showed a progressive shift towards the southeast in the post-monsoon (Fig. 5b) and winter (Fig. 5c) monsoons. However, the magnitude of both UOHC and D₂₆ showed a marginal decrease during post-monsoon, which was linked to the weakening of the WSC. In contrast, the magnitude of both UOHC and D₂₆ increased during winter (Fig. 4d), though the WSC was positive. In the premonsoon season, both UOHC and D₂₆ extend westward from their winter location and as a zonal band occupy the entire southern part of the AS. Interestingly, the WSC during this period was weak in the entire basin and positive over the southern and eastern parts. The increasing magnitudes of both D₂₆ and UOHC during winter and its westward expansion until the pre-monsoon were an anomaly. A potential mechanism that could explain this anomaly is the propagation of Rossby waves. It is known that downwelling Rossby wave propagates from the west coast of India towards the coast of Somalia during each winter which is generated by the coastally trapped Kelvin wave traveling along the eastern boundary of the AS²². To explore this Hovmöller plot of SLA averaged over the latitudes 4° to 12°N were prepared (Fig. 6) which clearly indicated zonally sloping bands of SLAs. This was the signature of a westward propagating downwelling Rossby wave. These Rossby waves are known to deepen the thermocline and in the present case it was manifested by the deepening of the D₂₆ and associated increase in the ocean heat content.

The above discussion leads to the understanding that due to the WSC associated with the FJ during ISM the southern part of the AS is able to store more thermal energy compared to the northern part of the AS. To further understand this association a box within the southern AS was selected (50–70°E and 4–12°N, Fig. 1), which essentially encompasses the region south of the axis of the FJ. A monthly spatial anomaly correlation was computed for the calendar months from October through May using the WSC within the box region with the UOHC in the AS during ISM to see how closely they were related. The monthly anomaly of WSC was calculated

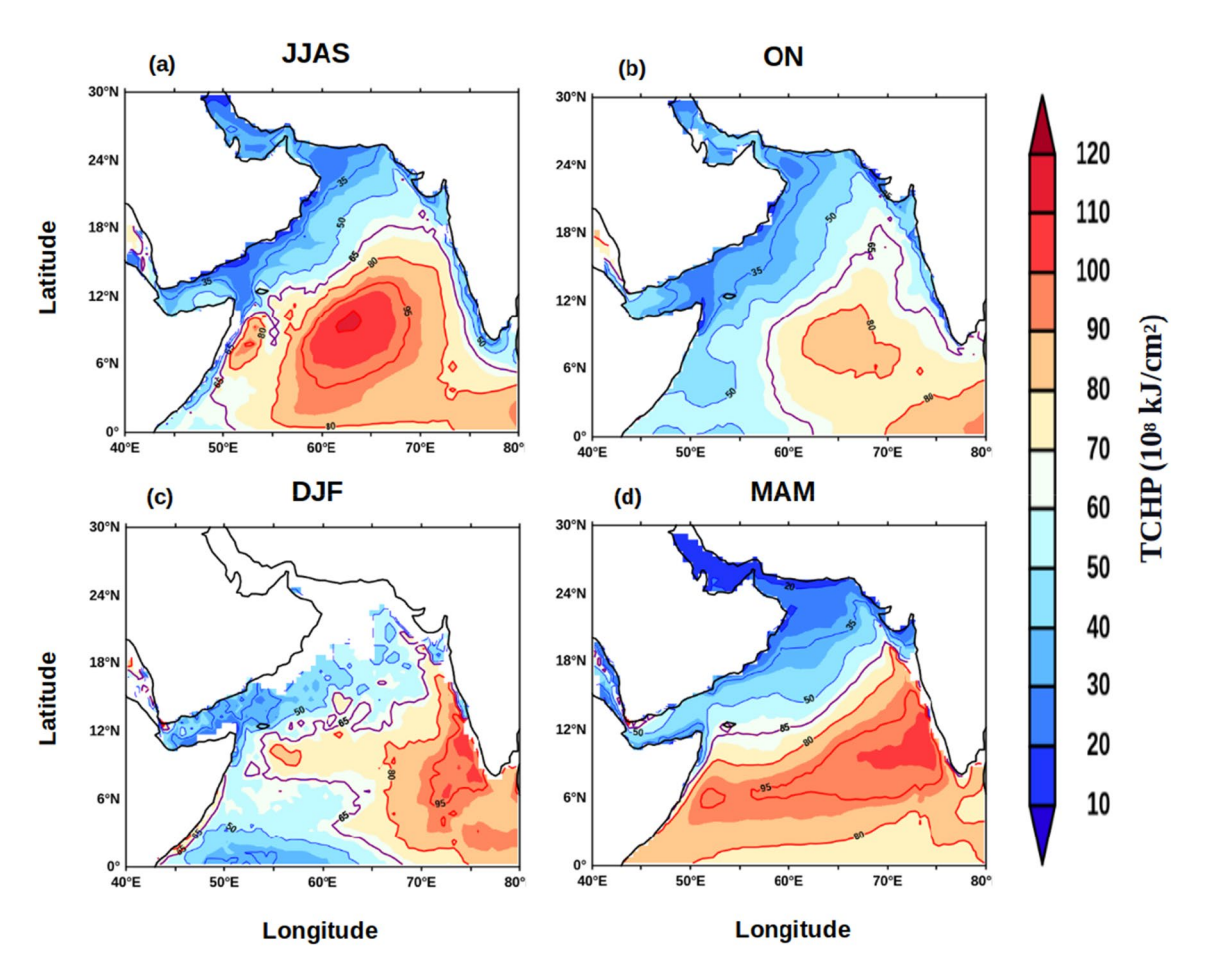


Figure 5. Annual cycle of climatology of UOHC (108 kJ/cm²) during (a) JJAS, (b) ON, (c) DJF and (d) MAM.

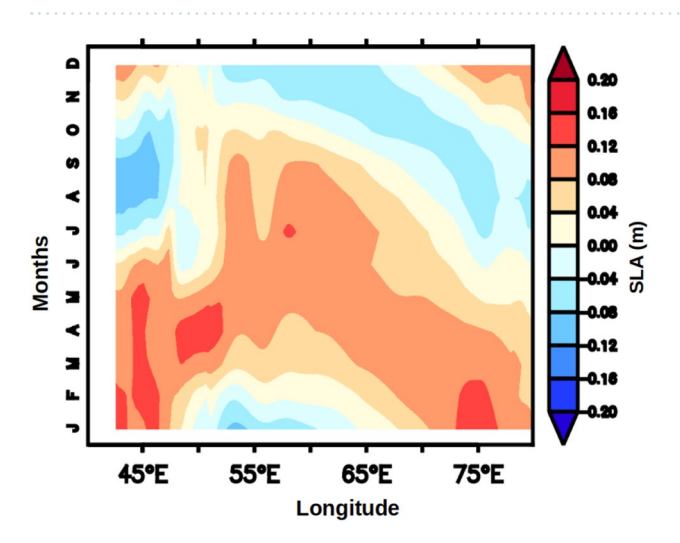


Figure 6. Hovmöller plot of climatology of monthly mean sea level anomaly (SLA, m) averaged over the latitudes from 4°N to 12°N in the Arabian Sea.

by subtracting the JJAS-averaged WSC within the box from each calendar month. Similarly the monthly anomaly of UOHC was calculated by subtracting the JJAS-averaged UOHC at each grid point from each calendar month. Figure 7 showed the monthly spatial anomaly correlation from October to May in the AS. The UOHC anomaly from October to December south of the FJ was positively correlated to the WSC at 95% confidence level. By the beginning of the subsequent year, i.e., during January and February, the region of significant positive correlations moved closer to the FJ axis. From March to May, the WSC and the UOHC anomaly in the southern AS were not significantly correlated at 95% confidence level. The result reiterates the role of FJ-induced Ekman dynamics in

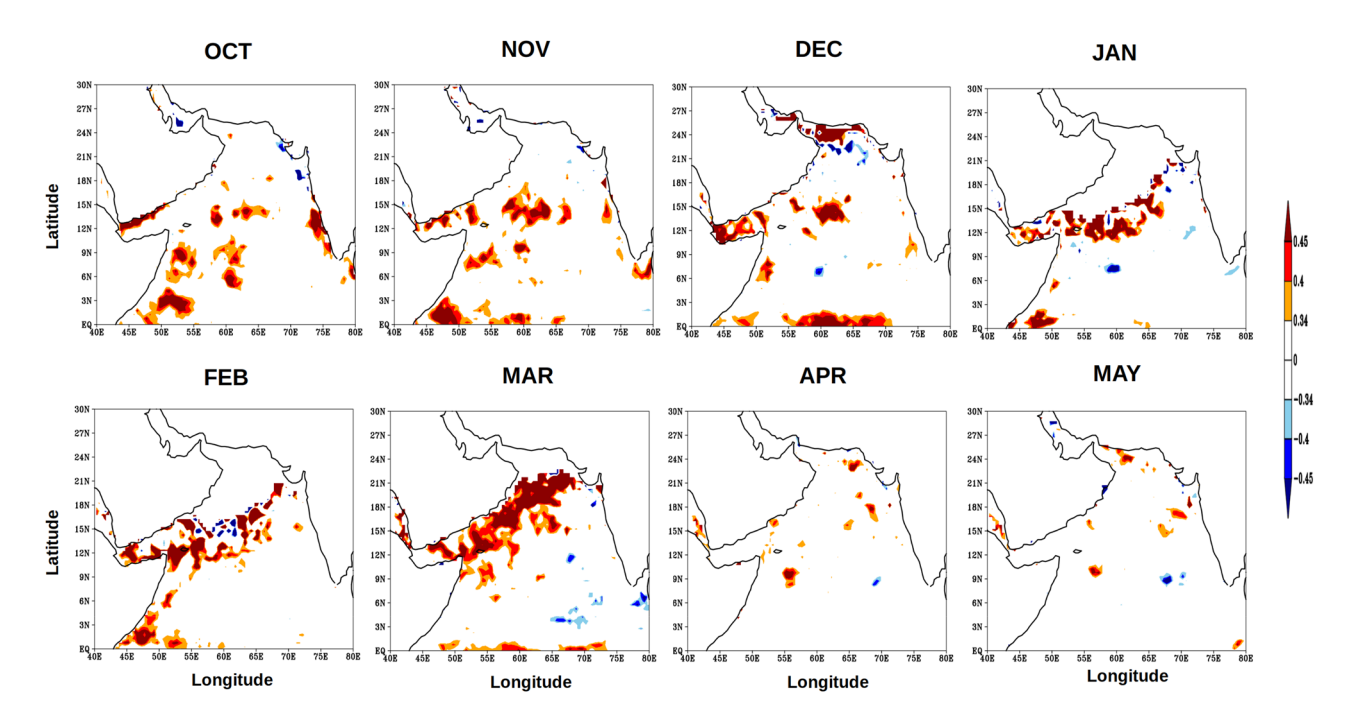


Figure 7. Monthly anomaly correlation of wind stress curl over the box region (50–70°E and 4–12°N, see Fig. 1) with UOHC of the Arabian Sea from October to May for the period of 1980–2015. The red colour represent the positive correlation value and the blue colour represents the negative correlation value, both significant at 95% confidence.

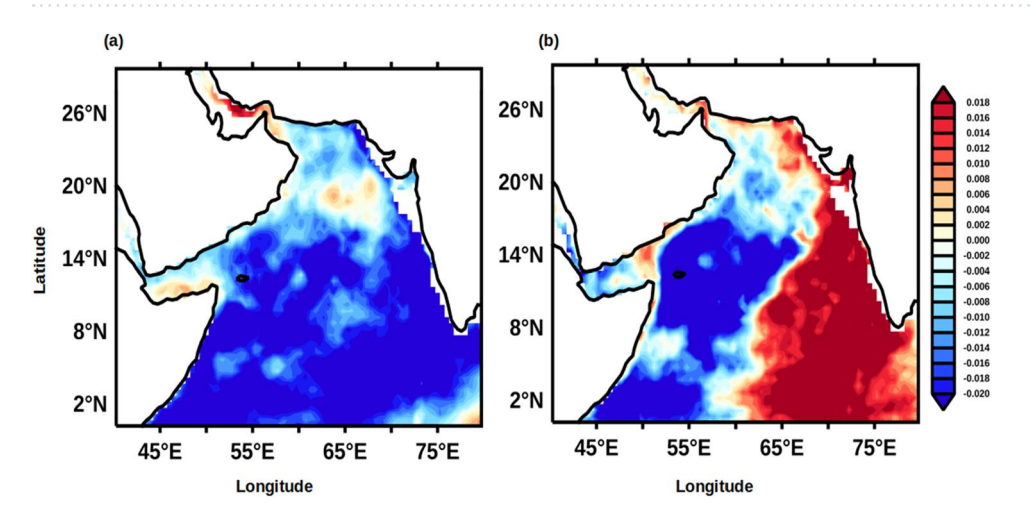


Figure 8. (a) The Principal Component 1 and (b) Principal component 2 of the EOF of the UOHC during ON.

regulating the upper ocean heat content in the region south of the axis of the FJ during the post-monsoon and the winter monsoon.

To ensure the robustness of the above results, we have computed the variability of Empirical Orthogonal Function (EOF) for UOHC during ON months. Figure 8a,b shows the first and second principal components (PC) of the EOF. The variance of the first and second PCs of EOF for UOHC during ON months is 23.6% and 9.3% respectively. The second mode of EOF clearly brings out the pattern of spatial variability in the UOHC which is similar to that of the basin-wide pattern of WSC induced by the Findlater jet during ISM months. The contrast between the northern and the southern sides of the FJ axis is quite distinctly visible in the second PC of EOF which is shown in Fig. 8b.

Having examined the relationship between the WSC within the box in the southern AS with UOHC over the AS, it is pertinent to see how the WSC within the box was related to the rainfall over the Indian sub-continent. Figure 9 presents the spatial correlation of WSC averaged within the box during June to September with rainfall averaged for the same period in the Indian sub-continent. The salient result is that the WSC over the box region is negatively correlated with rainfall along the western, central and northern parts of India at 95% confidence

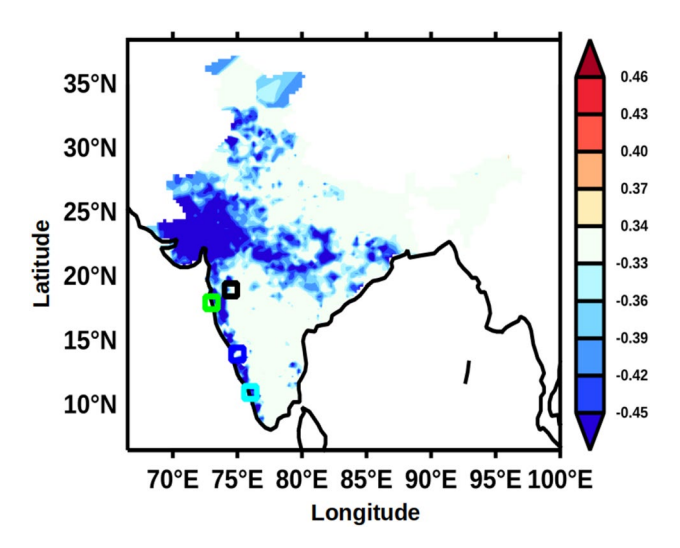


Figure 9. Anomaly correlation of WSC averaged during JJAS within the box region (50–70°E and 4–12°N, see Fig. 1) with rainfall averaged for the same months in the Indian sub-continent. The blue colour represents the significant negative correlation value at 95% confidence. The small squares of different colours represent the location of sub-divisonal stations, Madhya Maharashtra (black), Konkan (green), Coastal Karnataka (blue), and Kerala (cyan).

level. This implies that a higher negative WSC would lead to an increase in the ISM rainfall. Mechanistically, this happens through increase in the UOHC via deepened D_{26} .

Finally, to address how the upper ocean heat content was related to the Indian summer monsoon, the monthly mean climatology of rainfall data from four locations along the west coast of India (see Fig. 9 for locations) were averaged for June to September and designated as west Indian coastal rainfall (WICR). A lead correlation of WICR with UOHC in the AS were computed and presented in Fig. 10. In the post-monsoon period (Fig. 10a) the UOHC in the south-eastern part of the AS was positively and strongly correlated with WICR at 95% confidence level. During the winter monsoon period (Fig. 10b) the positive correlation of UOHC and WICR is spread over most part of the southern AS and along the west coast of India. The positive correlation of WICR and UOHC completely disappears in pre-monsoon period (Fig. 10c). The result from this lead correlation suggested that the UOHC in the southern part of the AS was anomalously higher during the subsequent seasons if the FJ strengthens and the rainfall over the WICR is more and vice versa. It emerges from the above results that the FJ signal was potentially 'memorized' in the sub-surface AS in the form of UOHC. It is intriguing why the heat-put by the summer monsoon into the subsurface layer of the southern AS was not reduced or dissipated by mixing in the subsequent two seasons. In the next paragraphs, based on the results from the present study and existing understanding of the regional oceanography of the AS, we propose a potential mechanism, which facilitates the observed 'memory' of the FJ to be preserved through the next two seasons.

During the ISM period the FJ produces a strong upper ocean convergence through the wind stress curl towards the south of its axis. The resultant Ekman pumping leads to the downwelling of water to the south of the FJ axis. The downwelling of warm surface waters during June to September eventually builds up the heat content in the upper thermocline. A stronger FJ would lead to an increased Ekman pumping and deeper downwelling. This in turn will deepen the D_{26} and results in the increase the upper ocean heat content during ISM. As the season changes from ISM to post-monsoon two processes co-occur in the AS: (1) the secondary heating and development of strong thermal stratification of the upper ocean, (2) the prevalence of weak and variable winds\(^1\). Both of these will curtail the mechanical mixing and results in retaining most of the heat in the subsurface layers in the upper thermocline.

Why does not the subsurface heat stored during post-monsoon come up in the winter under winter convection? In winter, surface waters of the northern AS experiences sensible heat loss by reduced incoming solar radiation and latent heat loss due to evaporative cooling under the prevailing dry north-easterly winds of continental origin both of which will deepens the mixed layer²⁴. In contrast, in the southern part of the AS, especially south of 15°N do not experience winter cooling and convection. As the convective mixing is absent the heat stored in the subsurface does not dissipate. In addition, the westward propagating downwelling Rossby waves radiated from the eastern boundary of the AS deepens the upper thermocline. This will help to retain the warm waters below the surface during winter as has been inferred from the UOHC and deep D_{26} during winter. As the inherent strength of the winter monsoon winds over the AS is substantially weaker compared to the ISM, the wind-driven entrainment has very little effect on the subsurface warmer waters. All this keeps the FJ-induced heat at a deeper level during the post-monsoon and winter monsoon. Once the propagation of Rossby wave from the eastern AS collapses towards the end of winter monsoon/beginning of the pre-monsoon the thermocline shoals and the heat that was stored in the previous seasons in the subsurface layer becomes available to the upper ocean for subsequent ocean–atmosphere interaction.

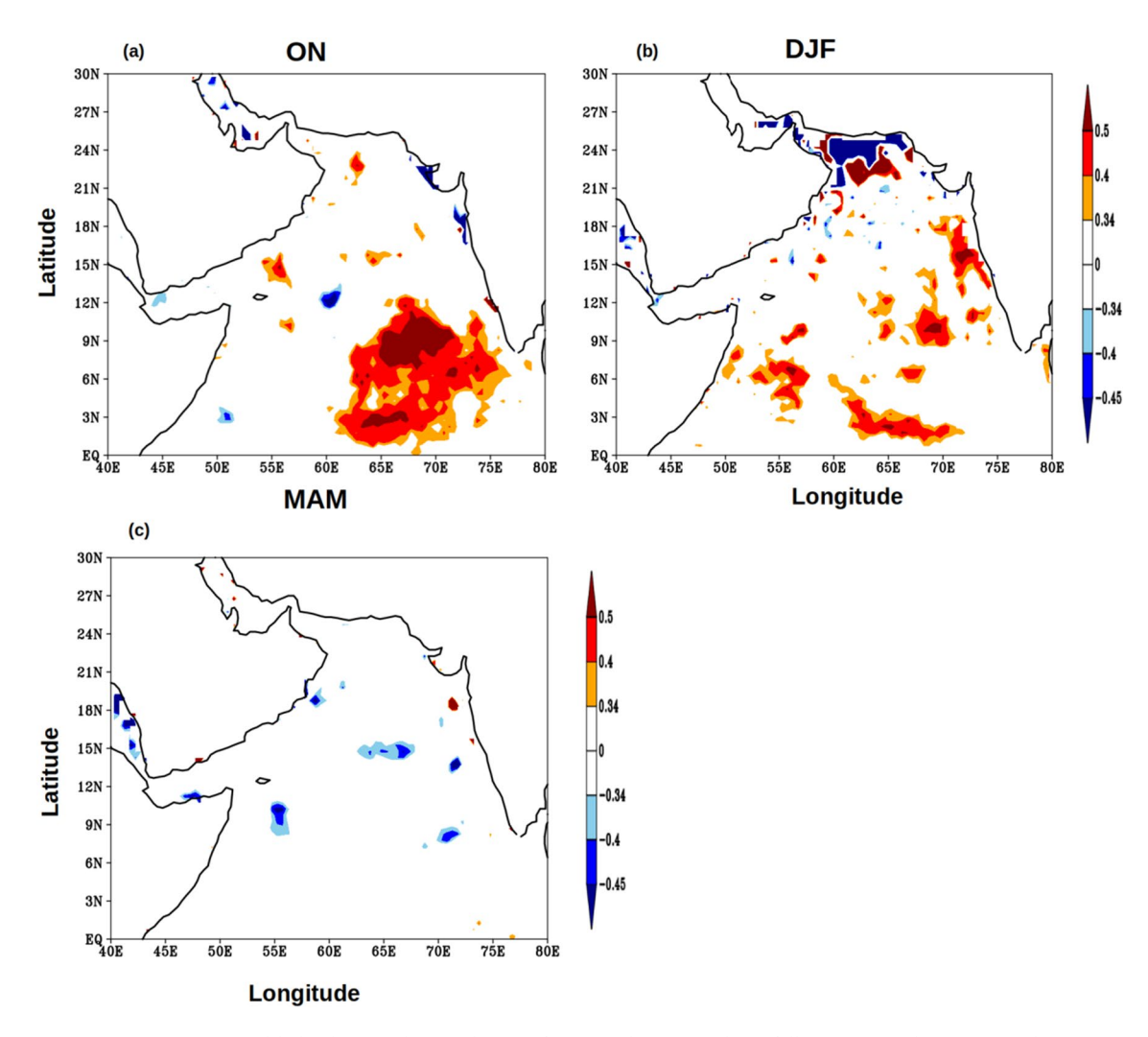


Figure 10. Monthly lead anomaly correlation of West Indian coastal rainfall (WICR) with UOHC in the Arabian Sea during (a) ON, (b) DJF, and (c) MAM for the period of 1980–2015. The red and blue colours represent the significant positive and negative correlation value respectively at 95% confidence.

Summary and concluding remarks

The seasonal cycle of the AS is a net response to the Ekman dynamics associated with the local southwest and succeeding northeast monsoons, associated air-sea fluxes, and annual Rossby waves. Through an examination of various reanalysis/observational datasets for the period 1980–2015, we document a contiguous chain of inherent seasonal processes in the AS from boreal summer through the following year spring, which showed storage of the signature of the FJ in the form of heat energy in the sub-surface, represented by the UOHC for three consecutive seasons. Our study ascertains that the UOHC in the southern part of the AS during the winter monsoon was positively correlated with the WSC of the summer monsoon. Further, during a strong monsoon with strong FJ the UOHC in the southern AS was not only anomalously high, as expected, but continues to be so even during the subsequent boreal winter season in such years.

This THCP signature of the previous year FJ stored in the AS is because of the seasonality of winds over the AS and the westward propagating Rossby wave radiated from the eastern boundary of AS. The modulation of the upper thermocline by the Rossby wave keeps the signal stored in the subsurface till the beginning of boreal spring and probably may pre-condition the local SST for the next monsoon. Exploring this aspect is beyond the scope of the present study. The proposed mechanism of subsurface storage of summer monsoon memory in our study is based only on the correlation analysis and needs further extensive modelling studies over the AS to further understand the interactions of FJ with the subsurface ocean. Nevertheless, findings from this study have great implications on the understanding of dynamics and thermodynamics of the upper ocean in the AS in the context of summer monsoon and its predictability.

Data and methodology

The zonal and meridional component of wind at different pressure levels having a horizontal resolution of 25 km was downloaded for the period 1980 to 2015 from the National Centre for Medium Range Weather Forecast (NCMWRF) monthly reanalysis data product³³ (https://rds.ncmrwf.gov.in/dashboard/download). This data was

used to calculate the climatological monthly mean wind at different pressure levels to characterize the FJ in the AS.

The subsurface temperature (°C) and wind stress ((N/m²) data were taken from the Simple Ocean Data Assimilation Ocean/sea ice reanalysis (SODA) Version 3.3.1³4 for the period 1980 to 2015 which has a spatial resolution of 0.25° × 0.25° longitude by latitude (https://www2.atmos.umd.edu/~ocean/index_files/soda3.3.1_mn_download.htm). The climatological monthly mean wind stress curl was calculated for the box 50°E to 70°E and 4°N to12°N in the central AS (see Fig. 1) following the equation³5

$$WSC = \frac{\partial \tau_y}{\partial x} - \frac{\partial \tau_x}{\partial y} \tag{1}$$

where τ_x and τ_y respectively denote the wind stress components along zonal and meridional directions.

The subsurface temperature data was used for the determination of the monthly mean climatology of depth of the 26 °C isotherm (D26) and further for the calculation of the monthly mean climatology of tropical cyclone heat potential referred as Upper Ocean Heat Content (UOHC)³² using the following equation

$$UOHC = \rho * Cp \int_{0}^{D26} [T(z) - 26] dz$$
 (2)

where T(z) is the temperature at depth z (m), ρ is the density (1024 kg/m³), and C_p is the specific heat (3850 J/kg C) of sea water.

The sea level anomaly (SLA, m) data having a spatial resolution of $0.25^{\circ} \times 0.25^{\circ}$ longitude by latitude for the period 1993–2019 was downloaded from the Copernicus Marine Environment Monitoring Services³⁶ (https://resources.marine.copernicus.eu/). Using this data the monthly mean climatology of SLA was computed for the preparation of Hovmöller plot.

The gridded rainfall data over India having a spatial resolution of $0.25^{\circ} \times 0.25^{\circ}$ longitude by latitude for the period 1980–2015 was obtained from India Meteorological Department (IMD)³⁷ (https://cccr.tropmet.res.in/home/data_portals.jsp). This data was used for calculating the climatology of average Indian summer monsoon rainfall during June to August (JJAS) at each of the grid point. Additionally, we have used the rainfall data from four sub-divisional stations from Madhya Maharashtra, Kerala, Konkan and Goa, and Coastal Karnataka (see Fig. 1 for location) for the same period. The rainfall data of the four sub-divisional stations were averaged for June to August (JJAS) for the period 1980–2015 and referred as West Indian coastal rainfall (WICR) for the present study.

We have de-trended the data for the study period to remove any linear trends present in the data. Furthermore, we used the linear anomaly correlation analysis and the statistical significance of the correlations was obtained through a 2-tailed Student's t-test.

Data availability

All the data used in the study were downloaded from the open source and the web site details are given under "Data and methodology".

Received: 30 March 2022; Accepted: 19 July 2022

Published online: 29 July 2022

References

- Prasanna Kumar, S., Narvekar, J., Nuncio, M., Gauns, M. & Sardesai, S. What drives the biological productivity of the northern Indian Ocean? In *Indian Ocean Biogeochemical Processes and Ecological Variability* (eds Wiggert, J. D. et al.), AGU Geophysical Monograph Series. Vol. 185, 33–56 (2009).
- Webster, P. J. et al. Monsoons: Processes, predictability, and the prospects for prediction. J. Geophys. Res. 103, 14451–14510. https://doi.org/10.1029/97JC02719 (1998).
- 3. Gadgil, S. & Gadgil, S. The Indian monsoon, GDP and agriculture. Econ. Pol. Wkly 41, 4887-4895 (2006).
- 4. Turner, A. G. & Annamalai, H. Climate change and the South Asian summer monsoon. *Nat. Clim. Change* 2, 587–595. https://doi.org/10.1038/nclimate1495 (2012).
- 5. Joseph, P. V. & Raman, P. L. Existence of low level westerly jet-stream over peninsular India during July. *India J. Meteor. Geophys.* 17, 407–410 (1966).
- 6. Anderson, D. L. T. The low-level jet as a western boundary current. Mon. Weather. Rev. 104, 907-921 (1976).
- 7. Findlater, J. Interhemispheric transport of air in the lower troposphere over the western Indian Ocean. *Quart. J. R. Meteorol. Soc.* **95.** 400–403 (1969)
- 8. Hoskins, B. J. & Rodwell, M. J. A model of the Asian summer monsoon. Part I: The global scale. J. Atmos. Sci. 52, 1329-2134 (1995).
- 9. Boos, W. R. & Emanuel, K. A. Annual intensification of the Somali jet in a quasi equilibrium framework: Observational composites. Q. J. R. Meteorol. Soc. 135, 319–335. https://doi.org/10.1002/qj.388 (2009).
- Pushpanjali, B., Subrahmanyam, M. V. & Murty, K. P. R. V. Findlater jet intensity and characteristics in relation to Indian summer monsoon. In Monsoons: Formation, Environmental Monitoring and Impact Assessment (eds Leal, M. D. & Levins, M. B.) 47–63 (Environmental Science, Engineering and Technology, Nova Science Publishers, Inc., 2013).
- 11. Ardanuy, P. On the observed diurnal oscillation of the Somali jet. Mon. Weather Rev. 107, 1694-1700 (1979).
- 12. Kalapureddy, M. C. R., Rao, D. N., Jain, A. R. & Ohno, Y. Wind profiler observations of a monsoon low-level jet over a tropical Indian station. *Ann. Geophys.* 25, 2125–2137 (2007).
- Nair, S. K. et al. Diurnal variations of the low-level jet over peninsular India during the onset of Asian summer monsoon. Theor. Appl. Climatol. 120, 287–298 (2014).
- 14. Joseph, P. V. & Sijikumar, S. Intraseasonal variability of the low-level jet stream of the Asian summer monsoon. *J. Clim.* 17, 1449–1458 (2004).
- 15. Pushpanjali, B., Subrahmanyam, V. M. & Murty, K. Relation between outgoing longwave radiation and findlater jet over Arabian Sea during summer monsoon and influence on Indian monsoon rainfall. *Indian J. Geo-Mar. Sci.* 49, 428–435 (2020).

- Narayanan, S., Kottayil, A. & Mohanakumar, K. Monsoon low-level jet over the gateway of Indian summer monsoon: A comparative study for two distinct monsoon years. *Meteorol. Atmos. Phys.* 128, 689–696 (2016).
- 17. Vizy, E. K. & Cook, K. H. Interannual variability of East African rainfall: Role of seasonal transitions of the low-level cross-equatorial flow. Clim. Dyn. 54, 4563–4587 (2020).
- 18. Archer, C. & Caldeira, K. Historical trends in the jet streams. Geophys. Res. Lett. 35, L08803. https://doi.org/10.1029/2008GL0336
- 19. Iqbal, W. et al. Mean climate and representation of jet streams in the CORDEX South Asia simulations by the regional climate model RCA4. *Theor. Appl. Climatol.* 129, 1–19 (2017).
- 20. Bauer, S., Hitchcock, G. & Olson, D. Influence of monsoonally-forced Ekman dynamics upon surface layer depth and plankton biomass distribution in the Arabian Sea. *Deep Sea Res. Part A.* 38, 531–553 (1991).
- 21. Prasanna Kumar, S. *et al.* High biological productivity in the central Arabian Sea during the summer monsoon driven by Ekman pumping and lateral advection. *Curr. Sci.* **81**, 1633–1638 (2001).
- 22. McCreary, J. P., Kundu, P. K. & Molinari, R. L. A numerical investigation of dynamics, thermodynamics and mixed-layer processes in the Indian Ocean. *Prog. Oceanogr.* 31, 181–244 (1993).
- 23. Weller, R. A. et al. Moored observations of upper-ocean response to the monsoons in the Arabian Sea during 1994–1995. Deep-Sea Res. Part II 49, 2195–2230 (2002).
- 24. Prasanna Kumar, S. & Narvekar, J. Seasonal variability of the mixed layer in the central Arabian Sea and its implication on nutrients and primary productivity. *Deep-Sea Res. II* 52, 1848–1861 (2005).
- 25. Prasanna Kumar, S. & Prasad, T. G. Winter cooling in the northern Arabian Sea. Curr. Sci. 71, 834-841 (1996).
- 26. Brandt, P. et al. Annual Rossby waves in the Arabian Sea from TOPEX/POSEIDON altimeter and in situ data. Deep-Sea Res. Part II 49, 1197–1210 (2002).
- 27. Jury, M. & Huang, B. The Rossby wave as a key mechanism of Indian Ocean climate variability. *Deep Sea Res.* I(51), 2123–2136 (2004).
- 28. Shetye, S. R. & Gouveia, A. D. Coastal circulation in the north Indian Ocean: Coastal segment (14, S-W). In *The Sea*, Vol. 11, 523–556 (Wiley, 1998).
- 29. Schott, F. A. & McCreary, J. P. The monsoon circulation of the Indian Ocean. Prog. Oceanogr. 51, 1-123 (2001).
- 30. Gray, M. Hurricanes: Their formation, structure, and likely role in the tropical circulation. *Meteorol. Over Trop. Oceans* **155**, 218 (1979).
- 31. Venugopal, T. et al. Statistical evidence for the role of southwestern Indian Ocean heat content in the Indian summer monsoon rainfall. Sci. Rep. 8, 12092. https://doi.org/10.1038/s41598-018-30552-0 (2018).
- 32. Leipper, D. F. & Volgenau, D. Hurricane heat potential of the Gulf of Mexico. J. Phys. Oceanogr. 2, 218-224 (1972).
- 33. Rani, S. I. et al. IMDAA: High resolution satellite-era reanalysis for the Indian monsoon region. J. Clim. 34, 5109-5133 (2021).
- 34. Carton, J. A., Chepurin, G. A. & Chen, L. SODA3: A new ocean climate reanalysis. J. Clim. 31, 6967-6983 (2018).
- 35. Gill, A. E. Atmosphere-Ocean Dynamics (Academic Press, 1982).
- 36. Lea, D. J. et al. Assessing a new coupled data assimilation system based on the Met Office coupled atmosphere-land-ocean-sea ice model. Mon. Weather. Rev. 143, 4678–4694 (2015).
- 37. Pai, D. S. *et al.* Development of a new high spatial resolution (0.25° × 0.25°) long period (1901–2010) daily gridded rainfall data set over India and its comparison with existing data sets over the region. *Mausam* **65**, 1–18 (2014).

Acknowledgements

The authors wish to acknowledge the use of the Ferret and Grads software for analysis and graphics (http://ferret.pmel.noaa.gov/Ferret/). VKK, KA and FF are grateful to Dr. Sathish Shetye for suggestions during the initial discussions of the study. VKK thanks Dr. Charan Teja Tejavath for his assistance in the data analysis and CSIR-UGC NET for providing the JRF fellowship. SPK acknowledges JN Chair Professorship of University of Hyderabad, CSIR Emeritus Scientist project ES84091 (RIO-CC-AMEF), and CSIR-NIO Goa (NIO contribution).

Author contributions

V.K.K., S.P.K., and K.A. conceived the idea and designed analysis. V.K.K. carried out the data analysis and visualisation. F.F. contributed towards data analysis. S.P.K. and V.K.K. interpreted the results. V.K.K., S.P.K., and F.F. wrote the paper. All authors reviewed the manuscript.

Competing interests

The authors declare no competing interests.

Additional information

Correspondence and requests for materials should be addressed to V.K.K.

Reprints and permissions information is available at www.nature.com/reprints.

Publisher's note Springer Nature remains neutral with regard to jurisdictional claims in published maps and institutional affiliations.

Open Access This article is licensed under a Creative Commons Attribution 4.0 International License, which permits use, sharing, adaptation, distribution and reproduction in any medium or format, as long as you give appropriate credit to the original author(s) and the source, provide a link to the Creative Commons licence, and indicate if changes were made. The images or other third party material in this article are included in the article's Creative Commons licence, unless indicated otherwise in a credit line to the material. If material is not included in the article's Creative Commons licence and your intended use is not permitted by statutory regulation or exceeds the permitted use, you will need to obtain permission directly from the copyright holder. To view a copy of this licence, visit http://creativecommons.org/licenses/by/4.0/.

© The Author(s) 2022